PROPER ENVIRONMENTAL REDUCTION FOR ATTENUATION IN MULTI-SECTOR SONARS

by

Rodrigo de Campos Carvalho

B.Sc.E Electronics, Naval Academy, Brazil, 1999

Post-grad Hydrography Cat. A (IHO), Directorate of Hydrography and Navigation, Brazil, 2003

A Thesis Submitted in Partial Fulfillment
of the Requirements for the Degree of

Master of Science in Engineering

in the Graduate Academic Unit of Geodesy and Geomatics Engineering

Supervisor: John E. Hughes Clarke, Ph.D., Geodesy and Geomatics Engineering, University of New Brunswick

Examining Board: Yun Zhang, Ph.D., Geodesy and Geomatics Engineering, University of New Brunswick

Jonathan Daniel Beaudoin, Ph.D., Center for Coastal and Ocean Mapping, University of New Hampshire

This thesis is accepted by the Dean of Graduate Studies

THE UNIVERSITY OF NEW BRUNSWICK

August, 2012

© Rodrigo de Campos Carvalho, 2012

DEDICATION

To my lovely wife Simone, for her never-ending support.

ABSTRACT

While an imperfect attenuation coefficient has no effect on bathymetry accuracy, it significantly reduces the value of the backscatter strength. As we move towards more precise calibration of backscatter strength to get additional information about the nature of the seafloor, such as bottom type or bottom micro roughness and their respective lateral and temporal homogeneity, the requirement for a precise attenuation coefficient is increasingly important. The need for better calibrated acoustic backscatter strength estimate is driven by operational needs in environmental monitoring, oil field development and defense applications, such as submarine and mine detection. A particular application used as an example is monitoring seasonal changes in backscatter on the floor of a fjord with active turbidity currents.

Most recently, multi-sector multibeam sonars have made the requirement for proper attenuation coefficients more pressing. These systems are capable of operating simultaneously on different frequencies, often use CW and FM chirp pulses and divide their transmit fan in multiple sectors and even in multiple swaths, with the purpose of allowing a sufficient sounding density alongtrack at reasonable vessel speeds, achieving longer range capability and thus reducing ship time surveying. However, as attenuation is a frequency, temperature, salinity and pressure dependent environmental control, the fidelity of the backscatter strength output from these new multi-sector systems potentially suffer by different wave absorption in their multiple sectors/swaths, if an incorrect attenuation is used.

This research reviews the role of attenuation and its proper application, and the sensitivity of attenuation variation. It then develops an extension to the UNB/OMG code to specifically correct any input multibeam data, accounting for the attenuation applied, and properly reapplies a new attenuation using a specific CTD and specific centre frequency.

ACKNOWLEDGEMENTS

Firstly, I would like to acknowledge the Brazilian Navy for the funds provided for this research and for trusting me with such a noble mission. Be assured that I tried to dedicate myself to the fullest to take advantage of this opportunity to enhance my knowledge.

I also would like to thank a number of people that helped me during these two years of research, without whom this thesis might not have been written, and to whom I am greatly indebted:

- My supervisor Dr. John Hughes Clarke from whom I have gained knowledge that will be largely applied in my future works in Navy. I am grateful for your constructive help throughout this research and essential software modifications to accommodate my proposed attenuation model. Congratulations for your contagious passion to teach and lead your students through the sciences of the sea;
- Dr. Yun Zhang and Dr. Jonathan Beaudoin who compose my examining board and provide me substantial suggestions that enriched my work;
- Dr. Marcelo Santos for providing intelligent advises during my work;
- LCmd. Aluizio for all support provided to me and my family since the beginning of the selection process for this mission. I hope to meet the expectations and assist you in the work at Navy Hydrographic Centre;

- Cmd. Izabel King, LCmd. Barroso, LCmd. Felipe Santos and LCmd Adriano Vieira (Navy Hydrographic Centre) for all technical information exchanged and data provided for my research;
- Capt. Alenquer (Directorate of Hydrography and Navigation) for all guidance during the selection process for this course and for the assistance throughout these two years;
- Capt. Marc Thibault (Canadian Coast Guard) and Keith Levesque (ArcticNet) for the opportunity to go onboard the CCGC Amundsen and take part in a hydrographic survey in the Arctic, collecting data for this thesis;
- Ian Church (Ocean Mapping Group) for all assistances with OMG software tools and your help in polishing my English and pointing out my grammatical errors in my several reports;
- Doug Cartwright and Steve Brucker (Ocean Mapping Group) for providing guidance of Linux and OMG software;
- Yun-ta Teng (Taiwan Navy) for all guidance since my first day at the University of New Brunswick and support with Matlab programming;
- Anand Hiroji, Danar Pratomo, Hesham Elhegazy, James Muggah and Travis Hamilton (Ocean Mapping Group) for our fruitful discussions; and
- Gordon Allison for his skill in piloting Heron during the surveys in Squamish.

I also thank the University of New Brunswick, especially the professors, secretaries and students of the Geodesy and Geomatics Department and the Ocean Mapping Group, for all friendship. It was an honor to me to be part of this team.

Special thanks to my friend Carlos Rubrio (Portuguese Navy) for never ending help, support and feedback. These two years studying together created a strong bond of friendship. Good luck and happiness in your return to your home country.

Thanks to my mother Maria Berenice, my father Francisco, my brother Breno, my sister Vanessa, my family and friends for never stopping to support me and cheering for my success from Brazil.

Special thanks to God, without whom this dream would not have been accomplished.

Finally, thanks for my lovely wife Simone, for whom I dedicate this thesis. Thanks for your happiness and love, tireless support and patience and for helping me in innumerable ways.

TABLE OF CONTENTS

DEDICATION ii
ABSTRACT iii
ACKNOWLEDGEMENTS v
TABLE OF CONTENTS viii
LIST OF TABLES x
LIST OF FIGURES xi
LIST OF ACRONYMS xx
Chapter 1: INTRODUCTION 1
Chapter 2: BOTTOM BACKSCATTER STRENGTH 7
Chapter 3: PROPAGATION OF SOUND IN THE WATER 11
3.1 Transmission loss, spherical spreading and attenuation itself 11
3.2 Environmental controls on attenuation 14
3.3 Example cases 17
3.4 Cumulative attenuation and its sensitivity analysis 29
3.4.1 Calculation of cumulative attenuation – Depth dependence 29
3.4.2 Example cases 33
3.4.3 Near-equivalence of refracted and straight line ray path 41
Chapter 4: BACKSCATTER DATA REDUCTION 46
4.1 Gain controls 46
4.2 Options to apply absorption coefficient in SIS 52
4.3 The problem of SIS SVP/CTD extrapolations 58
Chapter 5: PROPOSED METHODOLOGY TO REAPPLY ATTENUATION 60
5.1 Current and proposed methodology 64
5.2 Case study: Upper Howe Sound 70
5.2.1 EM3002 71
5.2.2 EM710 79

Chapter 6: THE NEW OMG ATTENUATION CORRECTION ALGORITHM... 91

6.1 Algorithms developed 92

Chapter 7: FUTURE APPLICATION IN BRAZILIAN NAVY 98

Chapter 8: CONCLUSIONS 102

8.1 Summary 102

8.2 Limitations and Recommendations 103

8.3 Future Work 104

REFERENCES 105

CURRICULUM VITAE

LIST OF TABLES

Table 3.1 – Layers A, B and C sampled in the water column used as an example in Figure 3.17 and their synthetic *in situ* attenuation coefficient values. 30

Table 3.2 – Layers A', B' and C' sampled in the water column used as an example in Figure 3.18 and their synthetic *in situ* attenuation coefficient values..... 31

Table 3.3 – Three different cases: same OWTT and launch angle, but different sound speed profiles. 43

Table 3.4 - Results for Z_1 and Z_2 (depth penetration in each layer), t_1 and t_2 (time spent in each layer), R_1, R_{1p}, R_2 and R_{2p}. 43

Table 3.5 - Difference in percentage between the actual ray trace and the Pythagoras distance in each layer 43

Table 5.1 – EM710 dual swath mode overview (from [Kongsberg, 2010b]). 79

Table 6.1 – The "raw range and angle 78" datagram for the new multibeam models. The red rectangle highlights the mean absorption coefficient provided by SIS for each sector centre frequency [Kongsberg Maritime, 2009b]. 93

LIST OF FIGURES

Figure 1.1 - New multi-sector sonars from Kongsberg Company: EM302 (left) and EM710 (right) (from [http://www.kongsberg.com/]). 1

Figure 1.2 - At the top, a high resolution bathymetric map, with 100% coverage and some detected boulders of different sizes. At the bottom, a backscatter image of the same area, able to provide information about the nature of the seafloor (from [Hughes Clarke, 2011c]). 2

Figure 1.3 - Old version of multibeam echo sounder (MBES) with only one sector one frequency (left) and new version of MBES with multi-sectors multi-frequencies dual swath (right). 3

Figure 1.4 - Multi-sector sonar EM302 operating in a Dual Swath Medium Mode (from [Hughes Clarke, 2011c]). 4

Figure 1.5 - Multi-sector sonar EM302 operating in a Dual Swath Deep Mode (from [Hughes Clarke, 2011c]). 4

Figure 2.1 - Bottom Backscatter Strength (edited from [deMoustier, 2011]). 7

Figure 2.2 - Backscatter strength signatures measured from MBES data collected by survey ship (edited from [Hughes Clarke et al., 1997]). 8

Figure 2.3 - Each different sediment type (clay, silt, sand, gravel, cobbles, rock etc) is going to present its own BS signature, also called angular response curve (edited from [Hughes Clarke et al., 1997 and Hughes Clarke, 2011c]). 9

Figure 2.4 - Seabed type prediction from BS signatures measured, after geometric and radiometric reduction (edited from [Hughes Clarke et al., 1997 and APL, 1994]). 10

Figure 3.1 - Attenuation coefficients in sea water and in distilled water (from [Urick, 1983]). 12

Figure 3.2 - Pure water (S= 0‰ and pH=7) and seawater (for S= 35‰ and pH=8) absorption for three temperatures (0, 10 and 20° C) for frequencies from 10 to 500 kHz, according to Francois and Garrison model [1982b]. In grey, the frequency

range of the new MBES: EM122, EM302, EM710 and EM2040 (edited from [Francois and Garrison, 1982b]). 16
Figure 3.3 - Hawaii profile collected during the summer 2008 (from [http://www.soest.hawaii.edu/HOT_WOCE/ctd.html]). 17
Figure 3.4 - Arctic profile collected during the summer 2011 (from [ArcticNet Program 2011]). 18
Figure 3.5 - Attenuation and its frequency and pressure dependence. 19
Figure 3.6 - Attenuation slightly decreases with pressure at low frequencies (12kHz, in that case). 20
Figure 3.7 - Attenuation and its pH dependence at low frequencies (12kHz). 21
Figure 3.8 - Attenuation and its pH dependence at medium frequencies (70kHz). 22
Figure 3.9 - Attenuation and its pH dependence at high frequencies (300kHz). 22
Figure 3.10 - Two different Hawaii profiles: summer profile represented in red and winter profile represented in blue. 23
Figure 3.11 - First 250 meters of Hawaii profiles shown in Figure 3.10. 24
Figure 3.12 - Attenuation results considering a hydrographic survey at 50 meters in the environmental presented in Figure 3.11, using a 300kHz system during the winter and the summer. 25
Figure 3.13 - Considering a 50m water deep, the attenuation fluctuation is about 1 dB (whole ray tracing) for nadir beams and about 2 dB for outer beams. 25
Figure 3.14 - Actual temperature and salinity Arctic profile (left and centre, respectively). In the right side, two close mean salinity values used for attenuation calculation: 33 and 35 ppt are represented. 26
Figure 3.15 - Attenuation and its salinity dependence at 32kHz. In green, attenuation coefficient results for salinity 33 ppt and in red, attenuation coefficient results for salinity 35 ppt. 27
Figure 3.16 - Considering a water depth of 2,500 meters, the total attenuation difference is about 2.5 dB (whole ray tracing) for nadir beams and about 5 dB for outer beams. 28

Figure 3.17 - Cumulative attenuation plot (right, in solid blue line) based on synthetic *in situ* attenuation coefficients (left, in solid red line) sampled throughout a water column. A, B and C (in green) represent the three different layers considered in this example. 30

Figure 3.18 - Cumulative attenuation plot (right, in dashed blue line) based on synthetic *in situ* attenuation coefficients (left, in dashed red line) sampled throughout a water column. A', B' and C' (in green) represent the three different layers considered in this new example. 32

Figure 3.19 – Compilation of examples shown in Figures 3.17 and 3.18. Solid and dashed lines represent data shown in Figures 3.17 and 3.18, respectively. 33

Figure 3.20 - Temperature and salinity profiles of shallower cast collected to 170 meters deep. 34

Figure 3.21 - Temperature and salinity profiles of deeper cast collected to 280 meters deep. 35

Figure 3.22 - Temperature and salinity profiles of shallower (in red) and deeper (in blue) casts represented at the same plots 36

Figure 3.23 - Zoom in the first 100 meters of shallower and deeper casts, where most significant variations in temperature and salinity occur. 37

Figure 3.24 - Absorption *in situ* and cumulative absorption for both casts (shallower cast in red and deeper in blue). Notice that, after 100 meters, for both casts, absorption *in situ* has almost the same values (red and blue solid lines) and the two cumulative absorptions curves converge (red and blue dashed lines). 38

Figure 3.25 Absorption *in situ* for both casts (shallower and deeper casts in red and blue solid lines, respectively). Notice that, after 100 meters, for both casts, absorption *in situ* has almost the same values (left hand). The plot in the right hand represents the absorption *in situ* difference by a solid green line. After about 100 meters, the difference is close to zero. 39

Figure 3.26 - Cumulative absorption for both casts (shallower and deeper casts in red and blue dashed lines, respectively). Notice that, after 100 meters, for both casts, the cumulative absorptions have almost the same values (left hand). The plot in the

right hand represents the cumulative absorption difference by a dashed green line. After about 100 meters, the difference is close to zero..... 40

Figure 3.27 - Two different ray paths: actual ray tracing (dashed red line) and Pythagoras distance (dotted purple line) (edited from [deMoustier, 2011]). 41

Figure 3.28 – A synthetic situation: in the left, a sound speed profile with two discrete values (V_1 and V_2) and, in the right, two different ray paths: Pythagoras distance (represented by R_{1p} and R_{2p}) and the actual ray tracing (represented by R_1 and R_2). 42

Figure 3.29 – Results show that the ratios for Z_1, Z_2, R_1, R_{1p}, R_2, R_{2p}, t_1 and t_2 are not exactly for the three cases considered earlier, but for typical sound speed variations (1490 to 1520 m/s) this is acceptable. 44

Figure 4.1 – 5 main components of gain corrections (axis Y) applied by Kongsberg in its MBES based on the time between transmission and reception (axis X). 48

Figure 4.2 – The beam pattern issues and attempts to address them, described in detail in Teng [2012]. This image represents three beam patterns BP_S, BP_C and BP_P (starboard, center and portside, respectively) and three points X, Y and Z, which represent three different times (also represented in Figure 4.1D). As each beam has a known angle relative to the transmitter centre (θ') and the system knows the steering angle of each received beam for each frequency, SIS is assumed to add a certain amount of correction for each beam for each sector centre frequency, represented by the blue and red arrows..... 49

Figure 4.3 – The flat seafloor assumption of Hammerstad [2000] based on the Minimum Slant Range (MSR), corresponding to point "A" on the seafloor..... 49

Figure 4.4 – SIS compensates the angular response effect: by estimating BS_N and BSo values from previous pings, Kongsberg model draws the dashed lines and considers they are the appropriate model for normalizing next pings to the crossover level. The model assumes a linear behavior for nadir region ($90° > \Theta >$ ($90° - CA$)) and a "Lambertian" behavior for the oblique incidence region (($90° -$ CA) $> \Theta > 0°$). However, next pings can present different shapes, such as the ones represented by curves (1) and (2). Therefore, corrections applied will under-

compensate or over-compensate backscatter curves (edited from [Oliveira Jr., 2007 and Hughes Clarke, 2011c]). 51
Figure 4.5 – The relationship of the range to the normal incident crossover angle (CA). 51
Figure 4.6 - Absorption coefficient window in SIS for an EM710 device. In that case, the Source selected was Salinity and the value inserted was 35 ppt, which is also the default value. If necessary, the user can correct that value. When the Source is set to Salinity or CTD, the frequency field is disabled (greyed), but it shows the current value of absorption coefficient in dB/km used for each one of those 5 frequencies (from [Kongsberg Maritime, 2010a]). 53
Figure 4.7 - Absorption coefficient profiles made by SIS while operating the EM302 onboard CCGS Amundsen. Notice that SIS creates one absorption profile for each one of the full range of required frequencies used by the echo sounders: 12, 32, 60, 70, 80, 90, 95, 100, 200, 250, 300, 350 and 400 kHz. 54
Figure 4.8 - Absorption coefficient profile "1102029_salinity_03500_32kHz.abs" made by SIS for 32kHz while operating the EM302 onboard CCGS Amundsen in the Arctic 2011. Notice that the file contains three columns: depth, which is already extended until 12,000 m, absorption coefficient *in situ* and cumulative absorption coefficient, respectively. 55
Figure 4.9 - Some printed parameters from the "raw range and angle 78" datagram for the first swath (three sectors, in that operating mode) of the EM710 mounted on CSL Heron. In blue is highlighted the mean absorption coefficient (expressed in 0.01dB/km) calculated by SIS for each one of the three sectors of first swath. ... 57
Figure 5.1 - Backscatter strength fluctuations observed between data collected by the first and second swaths of MBES EM302 surveying in the Arctic during the summer 2011 60
Figure 5.2 - All backscatter strength data projected to the same side of the axis X (in that case, right side). 61
Figure 5.3 - Backscatter strength fluctuations between two different sectors: 27.1kHz and 31.3kHz, each one belonging to a different swath. Notice that in some parts the backscatter strength difference is about 8 dB. 62

Figure 5.4 – Absorption coefficient windows in SIS for an EM302 (left) and an EM710 (right) (from [Kongsberg Maritime, 2006a and 2010a]). 64
Figure 5.5 – Multi-sector MBES operating in a regular seafloor geometry. Notice that the cumulative absorption in the boundaries of Sector 1 slightly varies, as represented by red circles in the plot in the right side. 65
Figure 5.6 – Multi-sector MBES operating in special seafloor geometry. Notice that inside the same sector (same centre frequency) the cumulative absorption varies with depth, as represented by red circles in the plot in the right side. 66
Figure 5.7 – Current model representing SIS approach. 68
Figure 5.8 – Proposed model. 69
Figure 5.9 – Howe Sound in British Columbia (from [http://www.britishcolumbia.com] (left) and [http://en.wikipedia.org/wiki/Howe_Sound] (right)). 70
Figure 5.10 – Howe Sound map (left), survey line collected from 8 to 140 m deep and the three closest CTD available in the WOD (right). 71
Figure 5.11 – EM3002 original BS image (left) and the gain correction in dB to be applied to the original BS image based on WOA (centre) and WOD (right) oceanographic data selected for the same period and location. 72
Figure 5.12 – *In situ* and cumulative absorption plots for 4 oceanographic profiles: one from WOA (in black) and the other three from WOD (in blue, green and magenta). The solid lines represent *in situ* absorption coefficients and dashed lines represent the cumulative absorptions. 74
Figure 5.13 - EM3002 corrections for nadir beams considering the WOD CTD profile number 0959. Red represents the mean absorption coefficient calculated by SIS and applied to the original BS image shown in Figure 5.11 (left); blue represents the cumulative absorption calculated by new methodology and green represents the difference between them. Magenta represents the nadir beam range and cyan shows the gain correction that should be applied to those beams 75
Figure 5.14 - EM3002 corrections for outer beams at 45° launch angle considering the WOD CTD profile number 0959. Red represents the mean absorption coefficient calculated by SIS and applied to the original BS image shown in Figure 5.11

(left); blue represents the cumulative absorption calculated by new methodology and green represents the difference between them. Magenta represents the outer beam range and cyan shows the gain correction that should be applied to those beams. 76

Figure 5.15 - Images A and C represent the original BS image in grayscale and in color, respectively; and images B and D represent the final BS image also in grayscale and in color, respectively. 77

Figure 5.16 - Angular response curves of the original and the corrected BS images represented in Figure 5.15, for the region bounded by the red rectangle (left). ... 78

Figure 5.17 – Howe Sound map and the survey line collected from 36 to 280m deep (left) and the zoom in (at right) in that same map representing the end of the survey line at 280m and the only CTD available in the WOD for this area in this period..... 80

Figure 5.18 - EM710 original BS image (left), the gain correction image in dB (centre) and the zoom in of the boundary where EM710 switches from shallow to medium mode (right). 81

Figure 5.19 - Cumulative absorption calculated by SIS (in red) and the one calculated using the proposed methodology (in blue) for detected centre frequencies: 77 and 85kHz (left); 79 and 89kHz (centre); 81 and 97kHz (right), considering only nadir beams. The dashed lines highlight the depth boundaries of three EM710 MBES modes: very shallow, shallow and medium. 83

Figure 5.20 - EM710 corrections for nadir beams for detected centre frequencies 77, 81 and 89 kHz. Red represents the original mean absorption coefficient calculated by SIS and applied to the original BS image shown in Figure 5.18 (left); blue represents the cumulative absorption calculated by new methodology and green represents the difference between them. Magenta represents the nadir beams range and cyan shows the gain correction that should be applied to them, also representing its range dependence. 84

Figure 5.21 - Cumulative absorption calculated by SIS (in red) and the one calculated using the proposed methodology (in blue) for detected outer beam frequencies: 73, 75 and 77 and 81 kHz considering only outer beams at 60° launch angle. The

dashed lines highlight the depth boundaries of three EM710 MBES modes: very shallow, shallow and medium. 85
Figure 5.22 - EM710 corrections for outer beams (launch angle 60°) and detected centre frequency 73 kHz. Red represents the mean absorption coefficient calculated by SIS and applied to the original BS image shown in Figure 5.18 (left); blue represents the cumulative absorption calculated by new methodology and green represents the difference between them. Magenta represents the outer beams range and cyan shows the gain correction that should be applied to them, also representing its range dependence. 86
Figure 5.23 - Images A and C represent the original BS image in grayscale and in color, respectively; and images B and D represent the final BS image also in grayscale and in color, respectively. 87
Figure 5.24 - Angular response curves of the original and the corrected BS images represented in Figure 5.23, for the region bounded by the red rectangle (left). ... 88
Figure 5.25 – Backscattering model for 70kHz developed by Applied Physics Laboratory (APL) at University of Washington, based on a compilation of calibrated BS observations, highlighting the medium sand ARC (modified from [APL, 1994]). 89
Figure 5.26 – Limits of medium sand ARC (represented by the solid green curves) if not applied the proper gain corrections: about 1dB for nadir beams and 2.5dB for outer beams. 89
Figure 5.27 – A family of curves that the seabed type can be on if not applied the proper gain corrections. 90
Figure 6.1 – EM3002 original BS image (left) and the cumulative attenuation image, calculated by the proposed model and based on CTD 0959 from WOD (right). . 95
Figure 6.2 - EM710 original BS image (left) and the cumulative attenuation image, calculated by the proposed model and based on CTD 1450 from WOD (right). Boxes indicate mode transitions where centre frequencies are changed. 96
Figure 7.1 – Brazilian Navy ships: NApOc "Barão de Teffé" (left), NapOc "Ary Rongel" (centre) and Polar Ship "Admiral Maximiano" (right). 98

Figure 7.2 – Annual transit (red solid line) of Brazilian polar ships from Rio de Janeiro (A) until Antarctic Station "Comandante Ferraz" (B), Keller Peninsula, Admiralty Bay, King George Island, South Shetland Islands. 99

LIST OF ACRONYMS

APL	Applied Physics Laboratory
AR	Angular Response
ARC	Angular Response Curve
BBS	Bottom Backscatter Strength
BS	Backscatter Strength
BTS	Bottom Target Strength
CA	Crossover Angle
CCGS	Canadian Coast Guard Ship
CSL	Canadian Survey Launch
CTD	Conductivity-Temperature-Depth
CW	Continuous Wave
FG	Fixed Gain
FM	Frequency Modulation
GA	Grazing Angle
GCI	Gain Correction Image
GDEM	Generalized Digital Environmental Model
GEBCO	General Bathymetric Chart of the Oceans
IHO	International Hydrographic Organization
MBES	Multibeam Echo Sounder
MSR	Minimum Slant Range
MVP	Moving Vessel Profiler

NIB	Normal Incidence Backscatter
NODC	National Oceanographic Data Centre
OB	Oblique Backscatter
OMG	Ocean Mapping Group
OWTT	One-Way Travel Time
ppt	Parts Per Thousand
PU	Processing Unit
SBES	Single Beam Echo Sounder
SIS	Seafloor Information System
SL	Source Level
SSP	Sound Speed Profile
SV	Sound Velocity
SVP	Sound Velocity Profile
TD	Transducer Depth
TL	Transmission Loss
TVG	Time-Varying Gain
TWTT	Two-Way Travel Time
UNB	University of New Brunswick
UW	University of Washington
VRIA	Vertically Referenced Incidence Angle
WOA	World Ocean Atlas
WOD	World Ocean Database

Chapter 1: INTRODUCTION

As electromagnetic waves such as light, radar and microwaves attenuate very rapidly in salt water, they are not able to propagate for significant distances in the ocean. On the other hand, as acoustic waves suffer a much lower attenuation than electromagnetic waves in that same environment, it has become the main tool for sensing, identifying and communicating under the ocean surface.

However, the internal structure of the sea and its peculiar upper and lower surface generate diverse effects upon the acoustic waves created underwater, making the sea a complex medium for the propagation and study of sound. The quality of the products generated by most underwater devices depends on a proper identification and compensation of these undesirable effects upon acoustic waves, such as in the new multi-sector sonars, shown in Figure 1.1.



Figure 1.1 - New multi-sector sonars from Kongsberg Company: EM302 (left) and EM710 (right) (from [http://www.kongsberg.com/]).

If properly compensated, multibeam backscatter data can provide valuable information about the nature of the seafloor, such as bottom type or bottom micro roughness and their respective spatial and temporal homogeneity. As part of that compensation, however, frequency and environment-dependent attenuation must be correctly applied.

Rapidly advancing technology has put at the service of contemporary Hydrography more modern equipment, including new multi-sector sonars. These systems can produce high resolution bathymetric contour charts, revealing, in detail, the shape of the seafloor features. Besides that, they can provide 100% seabed coverage, boulders detection and, if properly compensated, provide additional information about the nature of the seafloor from backscatter images, as shown in Figure 1.2.

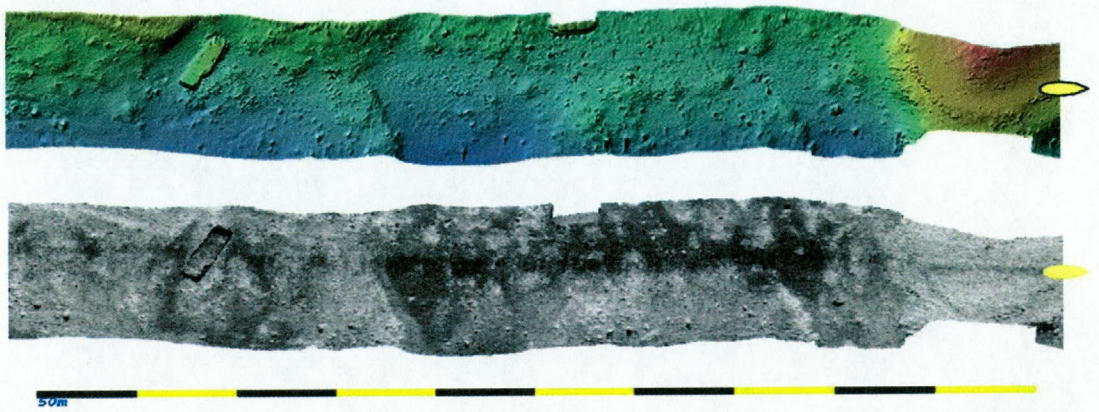

Figure 1.2 - At the top, a high resolution bathymetric map, with 100% coverage and some detected boulders of different sizes. At the bottom, a backscatter image of the same area, able to provide information about the nature of the seafloor (from [Hughes Clarke, 2011c]).

Unlike older single sector systems, these new devices are capable of operating simultaneously on different frequencies, dividing their transmit fan in multiple sectors

and even in multiple swaths (Figure 1.3), with the purpose of allowing a sufficient and uniform sounding density alongtrack at reasonable vessel speeds. This helps to ensure International Hydrographic Organization (IHO) compliant target detection. When combined with FM pulses, which provide longer range capability, it can reduce ship surveying time. Furthermore, the development of multi-sectors also provided yaw stabilization.

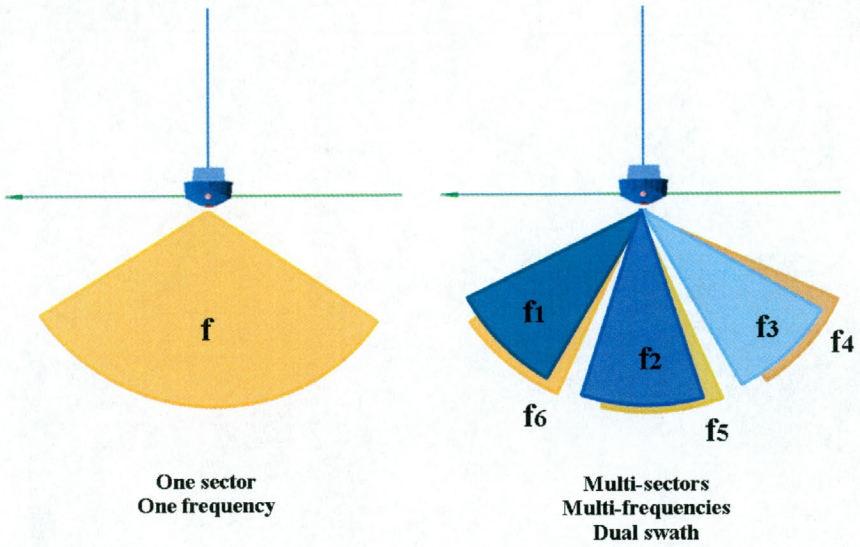

Figure 1.3 - Old version of multibeam echo sounder (MBES) with only one sector one frequency (left) and new version of MBES with multi-sectors multi-frequencies dual swath (right).

Figure 1.4 shows an example of EM302 operating in a Dual Swath Medium Mode. As we can notice, operating at that mode, the system generates 8 different sectors, each one with a different centre frequency, divided in two swaths.

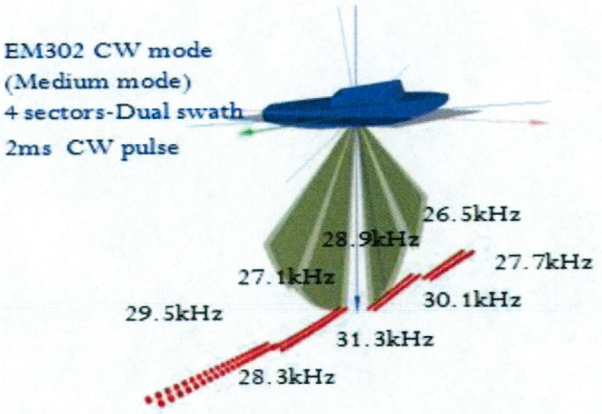

Figure 1.4 - Multi-sector sonar EM302 operating in a Dual Swath Medium Mode (from [Hughes Clarke, 2011c]).

However, as attenuation is frequency dependent (also depends on temperature, salinity, pH and pressure, as discussed in detail later), each sector suffers with different wave absorption, with an impact on the backscattered signals and their products. Attenuation issues can become worse in cases like the one presented in Figure 1.5: it is also an EM302, but operating in a Dual Swath, Deep Mode, with 16 different sectors and 16 different frequencies; thus 16 different attenuation values.

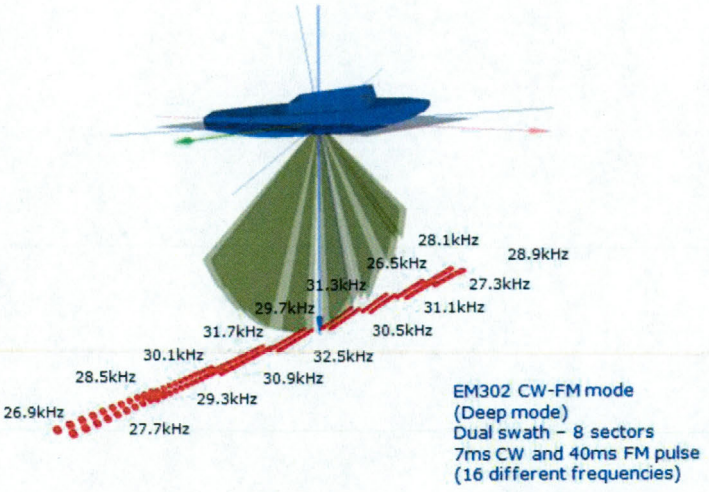

Figure 1.5 - Multi-sector sonar EM302 operating in a Dual Swath Deep Mode (from [Hughes Clarke, 2011c]).

While an imperfect attenuation coefficient has no effect on bathymetry accuracy, it significantly reduces the utility of the backscatter strength measurement. As we move towards more precise calibration of backscatter strength to get additional information about the nature of the seafloor, the requirement for precise attenuation coefficients becomes increasingly important.

Currently, the need for a better calibrated acoustic backscatter strength estimate is driven by operational needs in oil field development, environmental monitoring and defense applications. For an oil platform to sit on the bottom, we must know the geotechnical properties of the seafloor. Another application is in environmental monitoring of fishery habitats. Nowadays, as we mandate to preserve offshore resources, we must know the bottom substrate for certain species, to determine, for example, if it is a habitat where scallop will live or where clam will bury. In some particular cases, monitoring environmental changes is also mandated. Such change is likely to be very subtle, requiring very precise calibration.

Finally, two defense applications are with submarines and seabed mines. As submarines often sit on the bottom, it is critical to know the seabed classification to guarantee they are not going to damage the hull. Besides that, seafloor characterization is important to decide the place to launch seabed mines: if the bottom has too many boulders, we might not find the mines later; if the bottom has a substrate where a seabed mine can be buried, it should be avoided also. Thus, in a mine hunting operation, the fact of not visualizing any mine does not guarantee they do not exist: depending on the seafloor classification, they might be buried. It is important to highlight that maybe not all these applications have this discrete sensitivity (+/- 2dB).

Multibeam backscatter data represent a major seabed discrimination tool. For seafloor characterization, however, one of the most significant limitations is the absolute calibration. There are many components of this and environmental and frequency controls on the backscatter level are two of the most important ones. As many multibeam backscatter data are reduced imperfectly for attenuation, this thesis examines how important it is and how consequential it is. It introduces a precise and explicit method to properly compensate given a CTD (Conductivity-Temperature-Depth) and full knowledge of specific sector frequencies used, as long as the absorption coefficient already applied is preserved. Example cases are given for two different frequencies for historical data that were imperfectly compensated and the method is demonstrated.

Chapter 2: BOTTOM BACKSCATTER STRENGTH

Bottom backscatter strength (BBS) is defined as the ratio of the backscattered intensity I_B (taken 1 meter from the target) to the incident wave intensity I_I (per unit area per unit solid angle) on the seafloor. Normally, it is expressed in decibels and calculated by the logarithmic formula $10\log (I_B/I_I)$. The quotient expresses the ratio of the backscattered (I_B) and incident (I_I) intensities in the linear scale, which is termed as backscatter coefficient [Urick, 1983].

While we want I_B and I_I, what we actually measure is I_S (received wave intensity by the transducer) and I_o (transmitted wave intensity by the transducer) is assumed to be known. As we can notice in Figure 2.1, the I_S/I_o ratio is a function of not just the sediment type and grazing angle ($S(\Theta i)$), but also the transmitter (Θ, Ψ) and receiver (Θ, Ψ) beam patterns, ensonified area (dA), the range between the echo sounder and the seafloor (R) and the attenuation in the water (α_w).

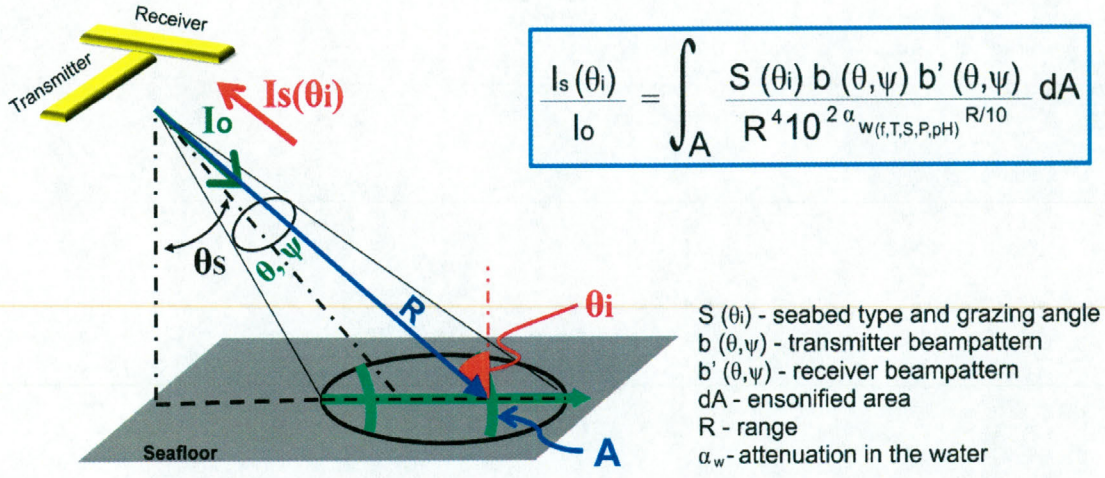

Figure 2.1 - Bottom Backscatter Strength (edited from [deMoustier, 2011]).

Thus, the backscattered energy that returns to the ship (Figure 2.2) depends not just on the seafloor physical properties themselves but also on the sonar configuration, water column propagation and measurement geometry. Once these last geometric and radiometric modulations on the backscatter intensity are properly reduced, the backscatter strength (BS) should represent only inherent properties of the seabed, becoming an useful tool for seafloor classification [Oliveira Jr., 2007].

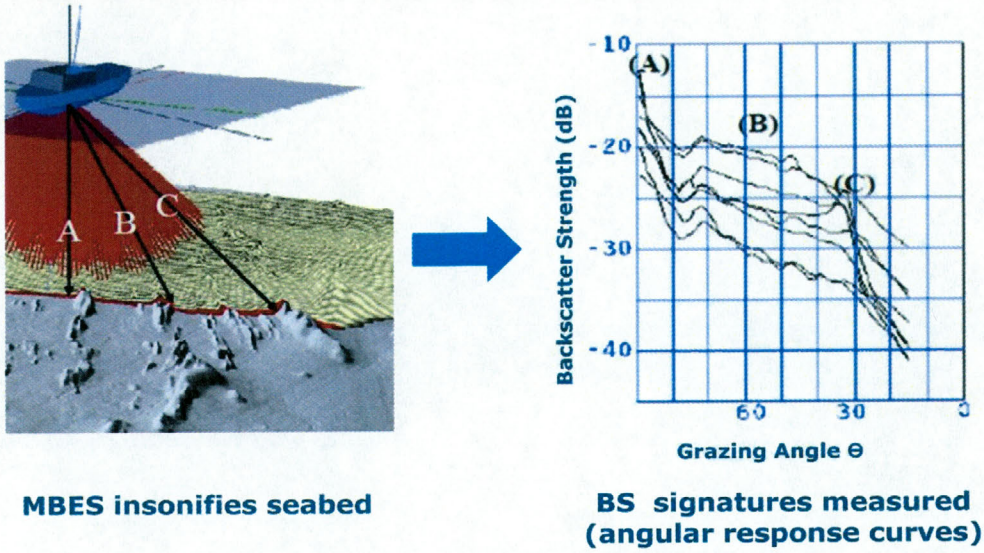

Figure 2.2 - Backscatter strength signatures measured from MBES data collected by survey ship (edited from [Hughes Clarke et al., 1997]).

Each sediment type (e.g., clay, silt, sand, gravel, cobbles, rock, shown in Figure 2.3) has its own physical properties: saturated bulk density, sound speed, spectral strength, spectral exponent, volume scattering and attenuation, which control the seabed echo strength. Thus, each sediment will present its own backscatter strength signature, also called the angular response curve (ARC), as represented in this same Figure.

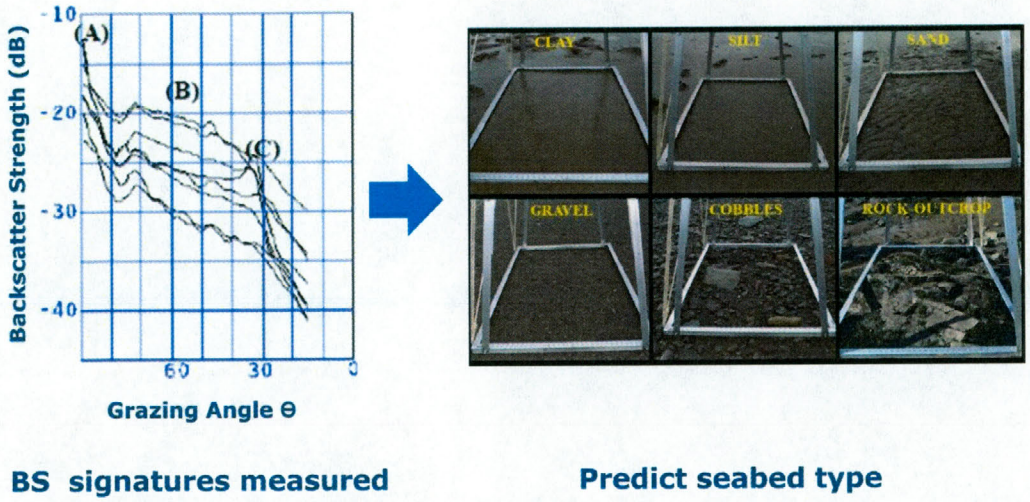

Figure 2.3 - Each different sediment type (clay, silt, sand, gravel, cobbles, rock etc) is going to present its own BS signature, also called angular response curve (edited from [Hughes Clarke et al., 1997 and Hughes Clarke, 2011c]).

Figure 2.4 represents the seabed type prediction process from measured BS signatures, after geometric and radiometric reduction. Those compensated signatures (left side) are correlated with mathematical model [Jackson et al., 1986] curves (generated for the same centre frequencies of acquisition devices), in an effort to provide seafloor characterization. Unfortunately, BS signatures measurements are imperfect for a variety of reasons including α, source level, beam patterns and seafloor slope.

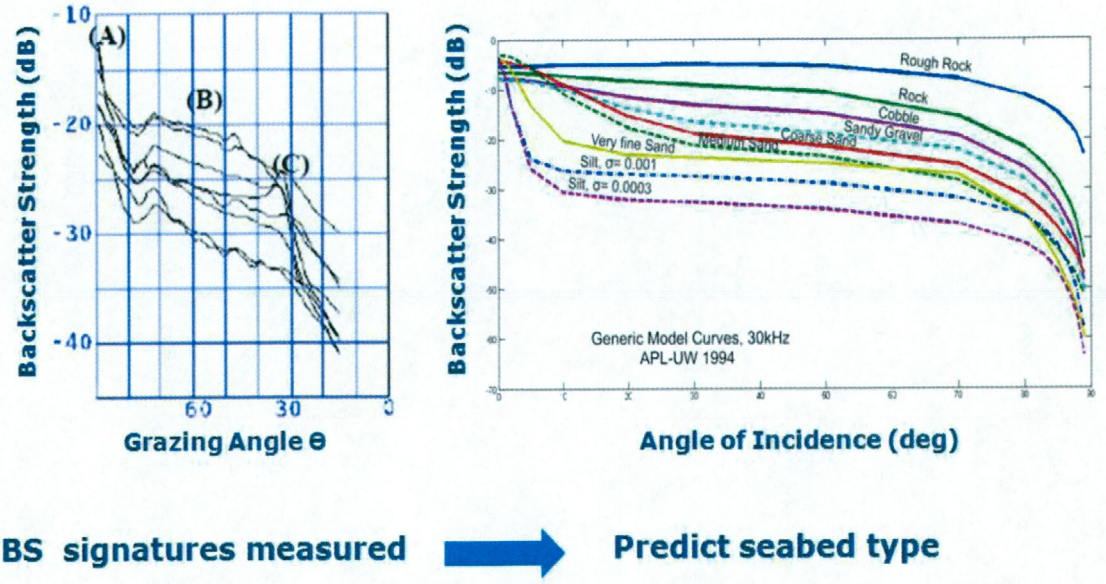

Figure 2.4 - Seabed type prediction from BS signatures measured, after geometric and radiometric reduction (edited from [Hughes Clarke et al., 1997 and APL, 1994]).

Notice also in Figure 2.4 (right), which represents model curves (angular response curves), that distinguishing rough rock from silt is easy due to its large backscatter strength difference (about 25 dB considering the middle of those two curves). On the other hand, distinguishing medium sand from coarse sand is hard due to its tiny backscatter strength difference, requiring us to be very strict in terms of environmental controls, which can generate considerable fluctuations on these angular response curves.

The proposed contribution of this research is developing a proper environmental reduction for attenuation for those multi-sector sonars, although it can also be applied to single sector sonars. It may not solve the whole issue of seabed classification from backscatter strength images, which is a big and growing problem when using these new multi-frequency devices. However, this contribution represents an effort to minimize this component.

Chapter 3: PROPAGATION OF SOUND IN THE WATER

3.1 Transmission loss, spherical spreading and attenuation itself

While travelling through water, acoustical waves suffer delay, distortion and impairment, with a gradual loss in the intensity of the original sound signal, called transmission loss (TL), and conventionally defined [Urick, 1983] as:

$$TL = 20 \log R + \alpha R \tag{3.1}$$

where R is the range and α is the attenuation coefficient.

However, considering the two-way travel of the acoustic waves in the water, transmission loss may also be expressed as:

$$2TL = 40 \log R + 2\alpha R \tag{3.2}$$

Based on equation 3.2, transmission loss consists of the sum of two parts, one due to spherical spreading of the signal (40 log R) and the other due to attenuation ($2\alpha R$). The first part, spreading loss, is related to the geometrical effect representing the regular weakening of a sound signal as it spreads outward from the source. Expressed by *decibels per total distance travelled,* spreading loss varies with range according to the logarithm of the range.

The second part, attenuation, considers the effects of absorption, scattering and leakage out of sound channels, varying linearly with range and being expressed by *decibels per unit distance.* As it comprises the conversion of acoustic energy into heat, attenuation represents the actual loss of acoustic energy to the medium in which transmission is taking place [Urick, 1983].

For many years, the constituents of sea water responsible for attenuation of sound were an intriguing mystery for scientists. It was soon clear that the attenuation of sound in the sea water was considerably higher than the one observed in pure water, and that phenomenon could not be attributed to scattering, refraction, or other anomalies assignable to propagation in the natural environment. As an example, Figure 3.1 shows the results of a laboratory measurement, where the attenuation in sea water was considered around 30 times greater than in distilled water at frequencies between 5 and 50 kHz [Urick, 1983].

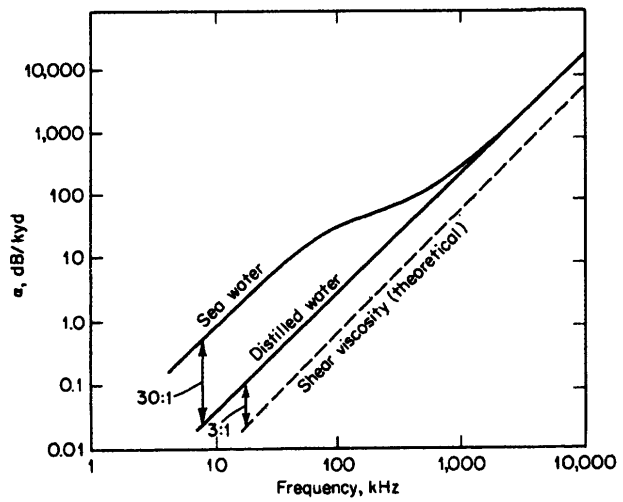

Figure 3.1 - Attenuation coefficients in sea water and in distilled water (from [Urick, 1983]).

Currently, the attenuation of sound in the sea water is considered to be the sum of three contributions: those from absorption in pure water and from chemical relaxation processes in magnesium sulfate ($MgSO_4$) and boric acid [$B(OH)_3$]. As contributions from other reactions are small, they were not included [Francois and Garrison, 1982, a, b]. Based on this, Francois and Garrison [1982b] developed a general equation for the

attenuation of sound in sea water, which applies to all oceanic conditions and frequencies from 200 Hz to 1 MHz, was written as:

Total absorption	=	**Boric Acid Contribution**	+	**Magnesium Sulfate Contribution**	+	**Pure Water Contribution**

$$\alpha = \frac{A_1 P_1 f_1 f^2}{f_1^2 + f^2} + \frac{A_2 P_2 f_2 f^2}{f_2^2 + f^2} + A_3 P_3 f^2 \qquad (3.3)$$

where f is the frequency of the sound in kHz, f_1 and f_2 are the relaxation frequencies of boric acid and magnesium sulfate (also in kHz), and P_1, P_2 and P_3 are non-dimensional pressure correction factors. Those components are calculated by:

Boric Acid *Contribution*

$A_1 = 8.86/c \times 10^{(0.78pH-5)}$ dB km^{-1} kHz^{-1}

$P_1 = 1$

$f_1 = 2.8\ (S/35)^{0.5}\ 10^{(4-1245/\theta)}$ kHz, (3.4)

where c is the sound speed (m/s), given approximately by:

$c = 1412 + 3.21T + 1.19S + 0.0167D,$

T is the temperature (°C), $\theta = 273 + T$, S is the salinity (‰), and D is the depth (m).

$MgSO_4$ Contribution

$A_2 = 21.44\ S/c\ (1+0.025T)$ dB km^{-1} kHz^{-1}

$P_2 = 1 - 1.37 \times 10^{-4}\ D + 6.2 \times 10^{-9}\ D^2$

$$f_2 = 8.17 \times 10^{(8-1990/\theta)}/(1 + 0.0018\,(S - 35)) \qquad \text{kHz,} \qquad (3.5)$$

Pure Water Contribution

For $T \leq 20°C$,

$$A_3 = 4.937 \times 10^{-4} - 2.59 \times 10^{-5}\,T + 9.11 \times 10^{-7}\,T^2 - 1.50 \times 10^{-8}\,T^3 \quad \text{dB km}^{-1}\,\text{kHz}^{-2}$$

For $T > 20°C$,

$$A_3 = 3.964 \times 10^{-4} - 1.146 \times 10^{-5}\,T + 1.45 \times 10^{-7}\,T^2 - 6.5 \times 10^{-10}\,T^3 \quad \text{dB km}^{-1}\,\text{kHz}^{-2}$$

$$P_3 = 1 - 3.83 \times 10^{-5}\,D + 4.9 \times 10^{-10}\,D^2$$

This is the most recent attenuation model in the last 30 years and in the absence of any published limitation in this model we have to take it as the best available knowledge.

3.2 Environmental controls on attenuation

Based on the Francois-Garrison equation for sound absorption in sea water presented earlier, the main factors that affect attenuation are:

- frequency, which depends on the echo sounder and variations within the sectors;
- depth, also understood as pressure;
- pH;
- temperature; and
- salinity.

As the majority of operations today do not provide temperature and salinity structures, assumptions about these water properties have to be made. This creates errors in attenuation coefficients, and is the problem addressed in this work.

Figure 3.2 shows the frequency, temperature and salinity dependence of attenuation from 10 to 500 kHz (current frequency range of multi-sector multi-frequency sonars) at 0 m depth, according to the model developed by Francois and Garrison [1982b]. We can also notice in this Figure the frequency range of new MBES: EM122 (11 to 14 kHz), EM302 (26 to 34 kHz), EM710 (70 to 100 kHz) and EM2040 (200 to 400 kHz). Inspecting these graphics, we conclude that:

- increasing frequency also increases attenuation. Thus, multi-sector multi-frequency systems have to apply unique attenuation values for each sector centre frequency;
- attenuation in salt water is much greater than in pure water and it is not a linear relationship. Thus salinity variations in coastal waters can have a particularly large impact on attenuation;
- increasing temperature decreases attenuation at all frequencies except in the immediate vicinity of relaxation frequencies f_1 and f_2 (equations 3.4 and 3.5 above), where attenuation is increased [Ainslie and McColm, 1998].

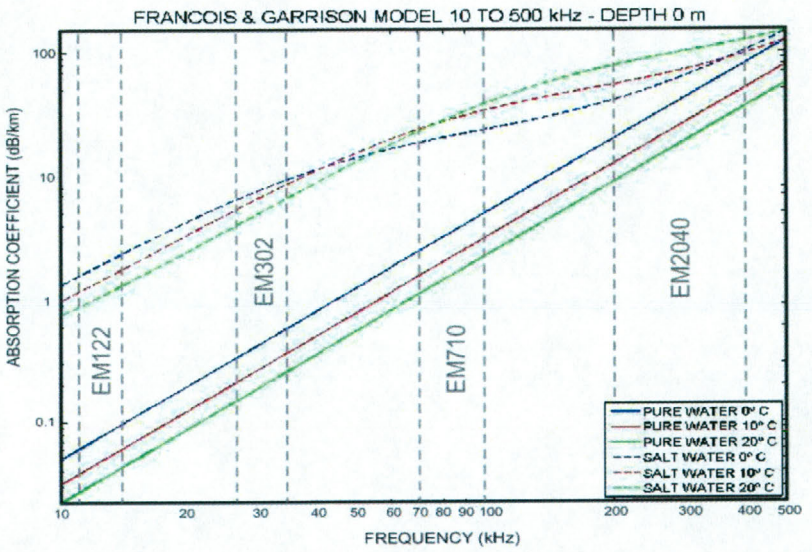

Figure 3.2 - Pure water (S= 0‰ and pH=7) and seawater (for S= 35‰ and pH=8) absorption for three temperatures (0, 10 and 20° C) for frequencies from 10 to 500 kHz, according to Francois and Garrison model [1982b]. In grey, the frequency range of the new MBES: EM122, EM302, EM710 and EM2040 (edited from [Francois and Garrison, 1982b]).

Besides that, after the thermocline (which has a significant impact in attenuation due to the temperature gradient), when temperature values get more stable, attenuation decreases while pressure (depth) increases. Finally, increasing pH slightly increases attenuation, but as the typical pH variation in the oceans is small: "The surface waters of the oceans are slightly alkaline, with an average pH of about 8.2, although this varies across the oceans by ± 0.3 units because of local, regional and seasonal variations" [Raven et al., 2005]. Consequentially, its impact on overall attenuation is also small.

3.3 Example cases

Some attenuation simulations have been done with data from two quite different areas: Hawaii (warm water) and the Arctic (cold water), both collected during the summer, as shown in Figures 3.3 and 3.4, respectively.

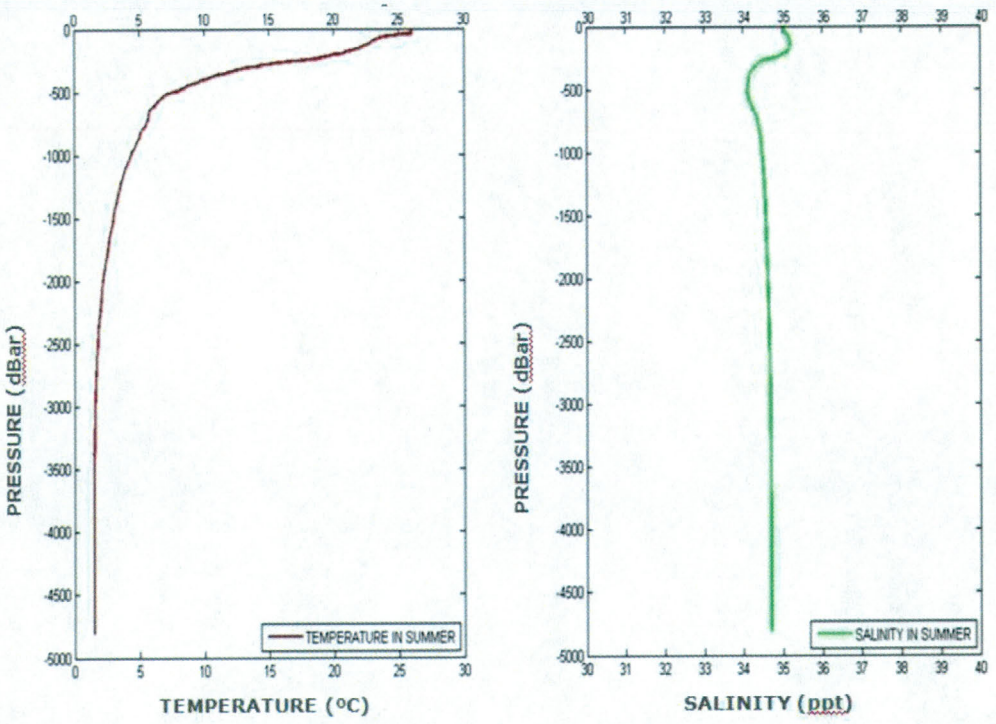

Figure 3.3 - Hawaii profile collected during the summer 2008 (from [http://www.soest.hawaii.edu/HOT_WOCE/ctd.html]).

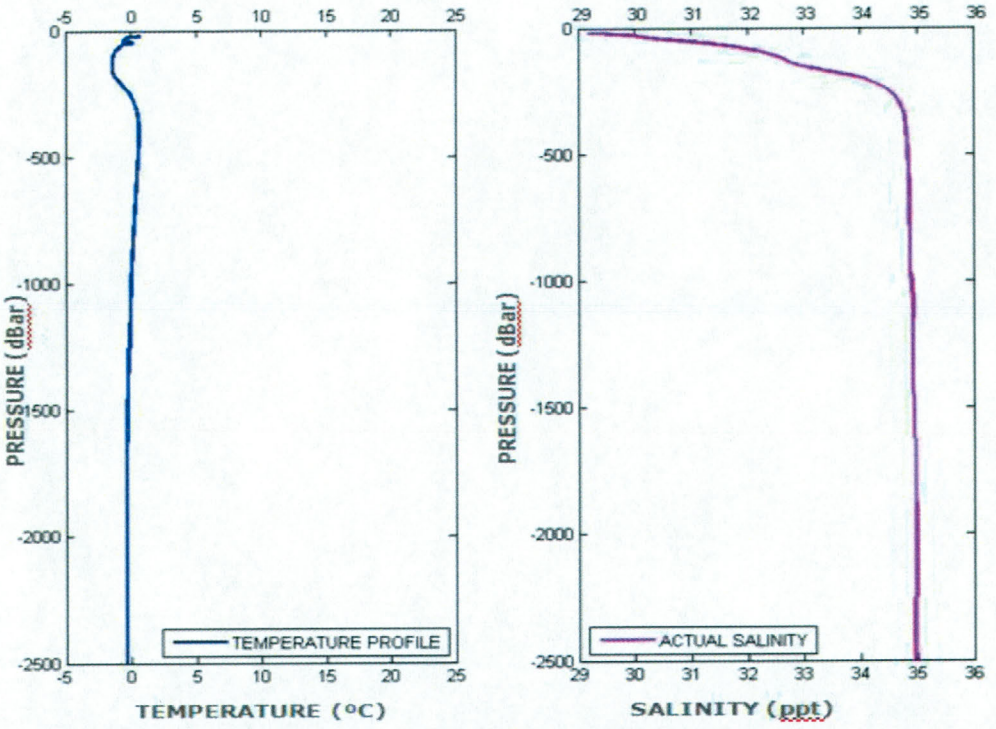

Figure 3.4 - Arctic profile collected during the summer 2011 (from [ArcticNet Program 2011]).

As we can notice in Hawaii profile (Figure 3.3), temperature in the sea surface is high, about 26° C. There is a pronounced thermocline until around 500 m depth from which the temperature gradient decreases substantially, and the profile becomes more isothermal. By contrast, the salinity profile is quite stable, varying only about 1.5 ppt (parts per thousand) from sea surface until 5,000 m deep.

On the other hand, the Arctic profile (Figure 3.4) is quite different: instead of temperature, the predominant environmental driver is salinity. Within that profile, there is a pronounced halocline, varying from 29 ppt at the sea surface to 35 ppt at the bottom. Conversely, temperature has a nearly isothermal profile through the whole water column.

Some attenuation simulations are presented and analyzed below.

- **Attenuation and its frequency and pressure dependence**

Figure 3.5 shows the simulation results for three different echo sounder frequencies using the Hawaii profile (Figure 3.3): 12kHz (red line, used by multi-sector sonars such as EM122), 70kHz (blue line, used by multi-sector sonars such as EM710) and 300kHz (green line, used by multi-sector sonars such as EM2040).

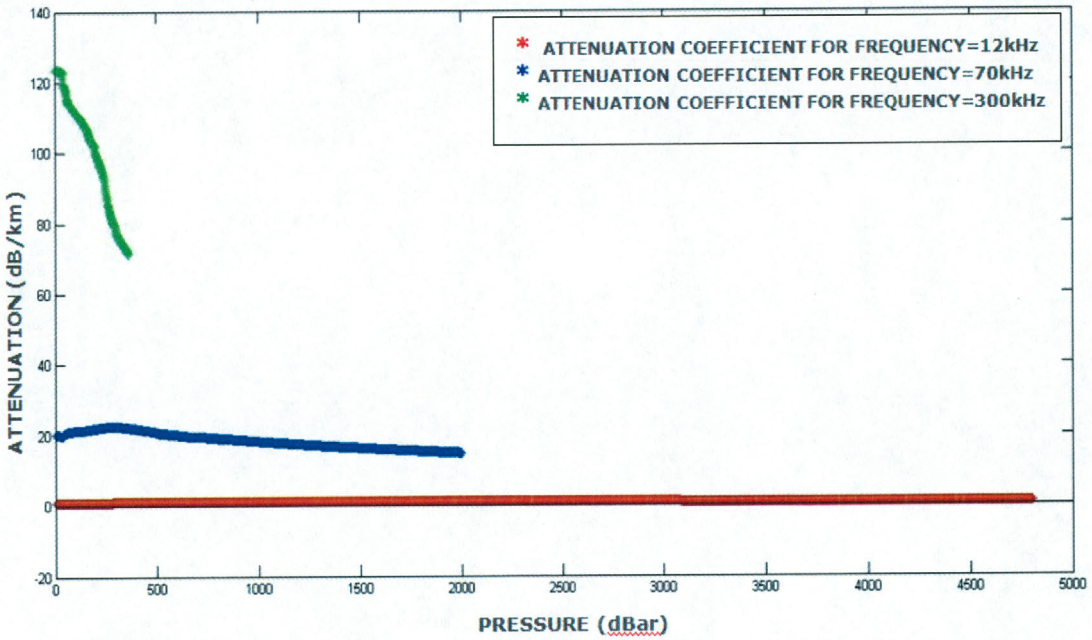

Figure 3.5 - Attenuation and its frequency and pressure dependence.

Based on Figure 3.5, we notice that increasing frequency also increases attenuation, as commented earlier. It also explains why we have that depth limitation, shown in that same Figure, for 70kHz and 300kHz compared to 12kHz.

The second environmental effect we can notice in this simulation is the pressure: after the thermocline (around 500 m deep), when temperature values get more stable, attenuation decreases while pressure increases. As shown in Figure 3.6, zoom in part of

the 12kHz curve, we can notice that attenuation slightly decreases with pressure at low frequencies: it decreases about 0.4 dB/km in almost 3,000 dBar (about 3,000 meters).

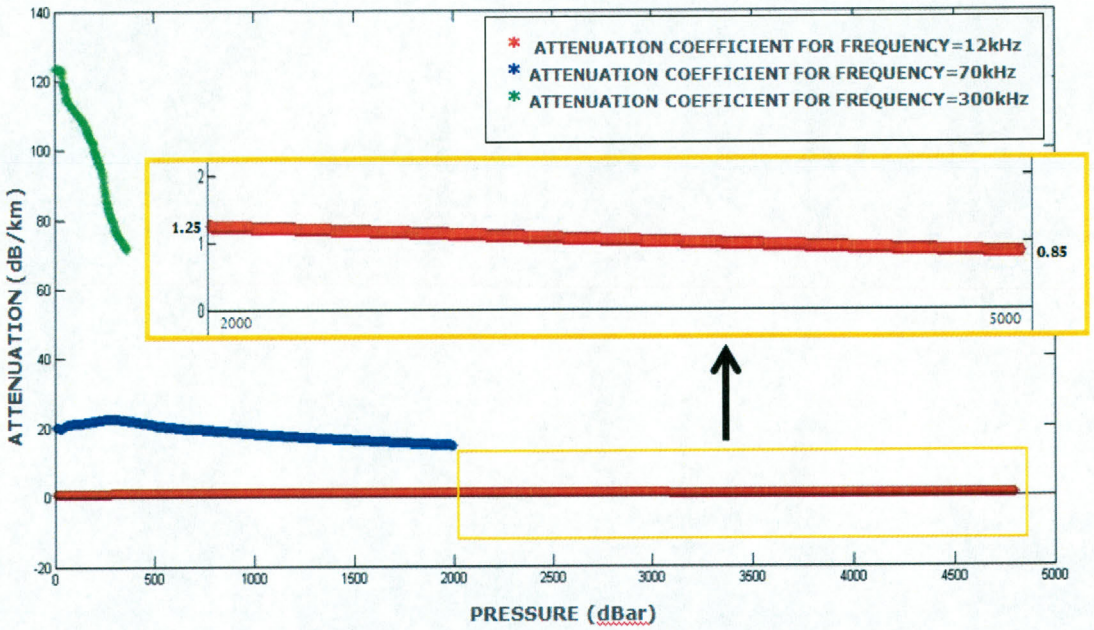

Figure 3.6 - Attenuation slightly decreases with pressure at low frequencies (12kHz, in that case).

- **Attenuation and its pH dependence**

Figures 3.7 through 3.9 show the pH simulation results done for three different pH values: 7 (red line), 7.5 (blue line) and 8 (green line), using the Hawaii profile (Figure 3.3). Each Figure presents the results for a different echo sounder frequency: 12kHz, 70kHz and 300kHz, respectively.

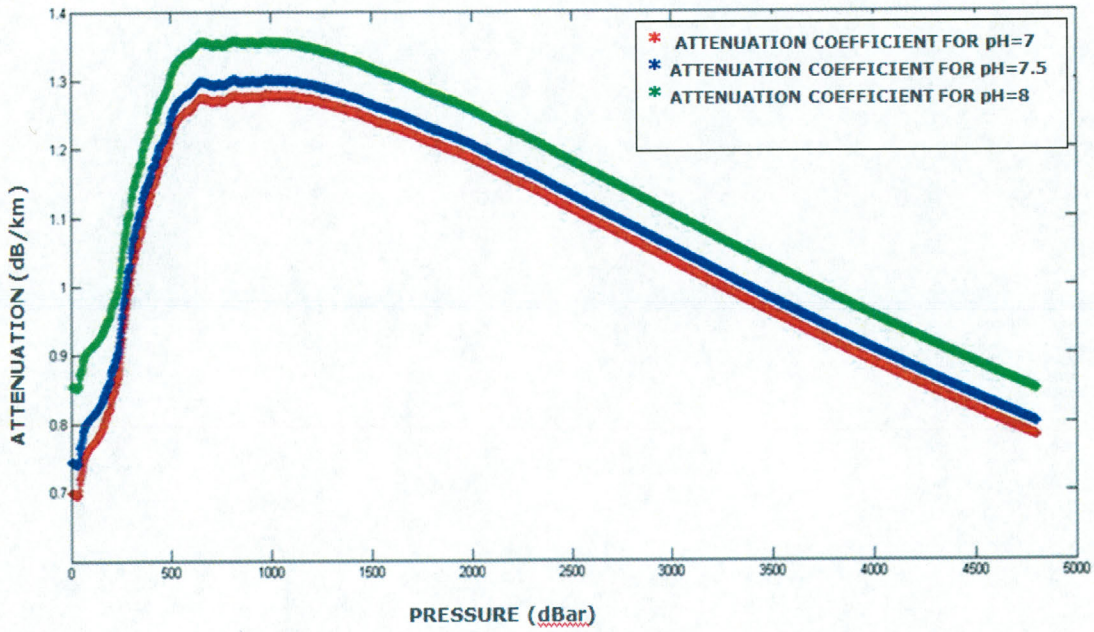

Figure 3.7 - Attenuation and its pH dependence at low frequencies (12kHz).

As we can notice in Figure 3.7, pH influence is relatively significant in attenuation for low frequencies. The average difference between the red line (pH = 7) and the green line (pH=8) is about 10% of the attenuation value.

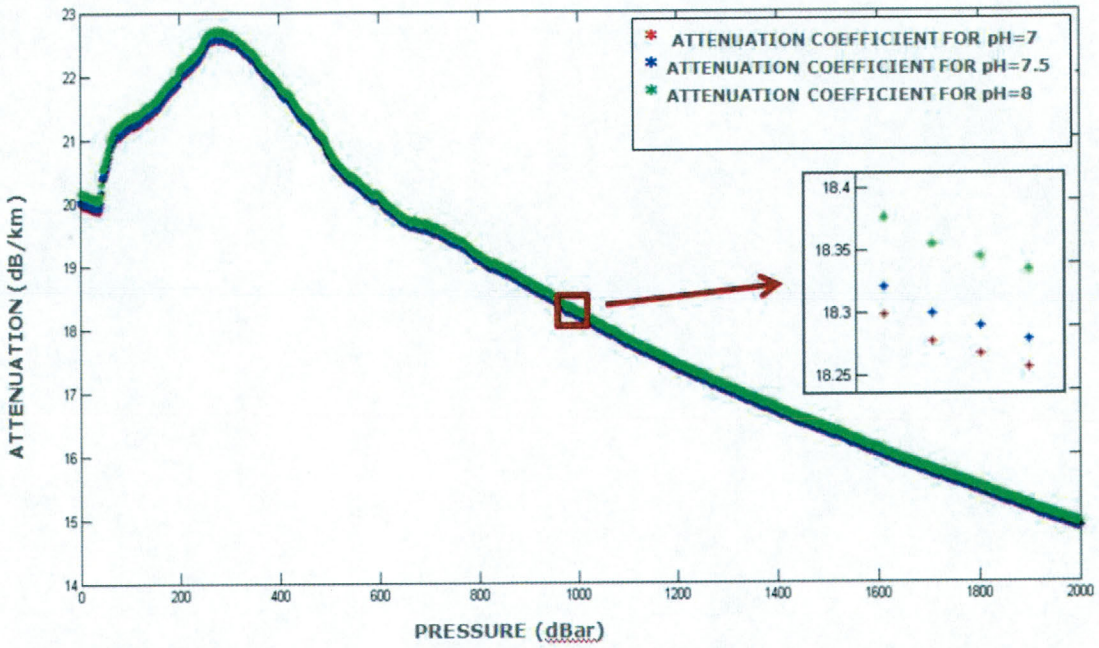

Figure 3.8 - Attenuation and its pH dependence at medium frequencies (70kHz).

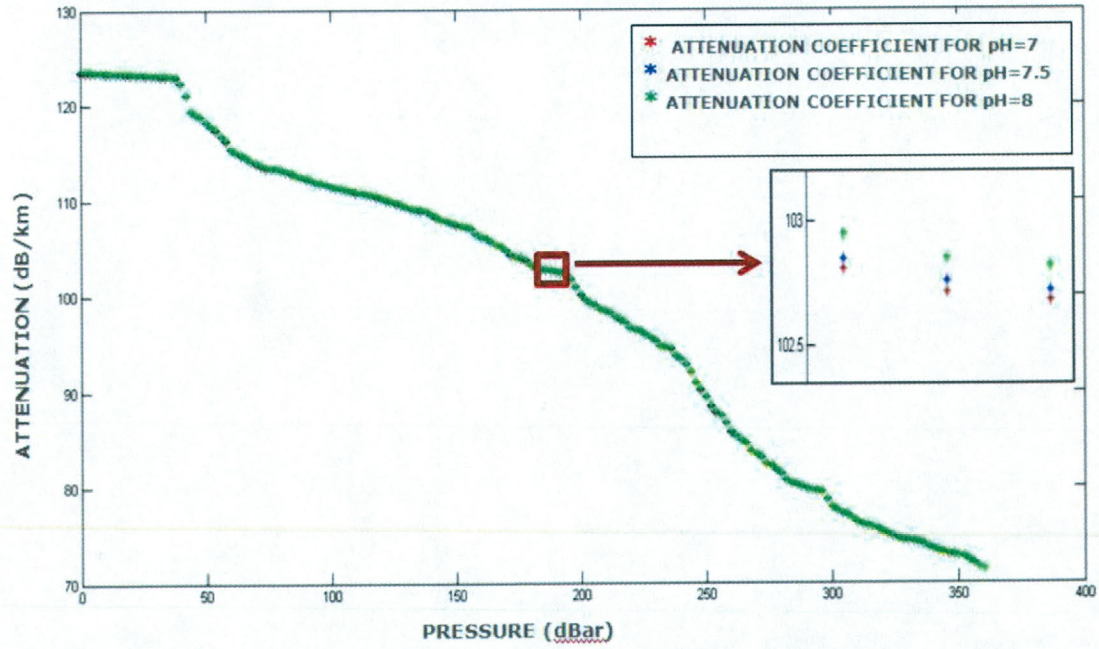

Figure 3.9 - Attenuation and its pH dependence at high frequencies (300kHz).

By contrast, as we can notice in Figures 3.8 and 3.9, pH influence is no more relatively significant for medium and high frequencies compared to the absolute attenuation values.

- **Attenuation and its temperature dependence**

In this simulation, two different Hawaii profiles have been used: a summer profile (in red) and a winter profile (in blue), as presented in Figure 3.10. Notice that most of temperature and salinity variations occur in the upper 500 meters.

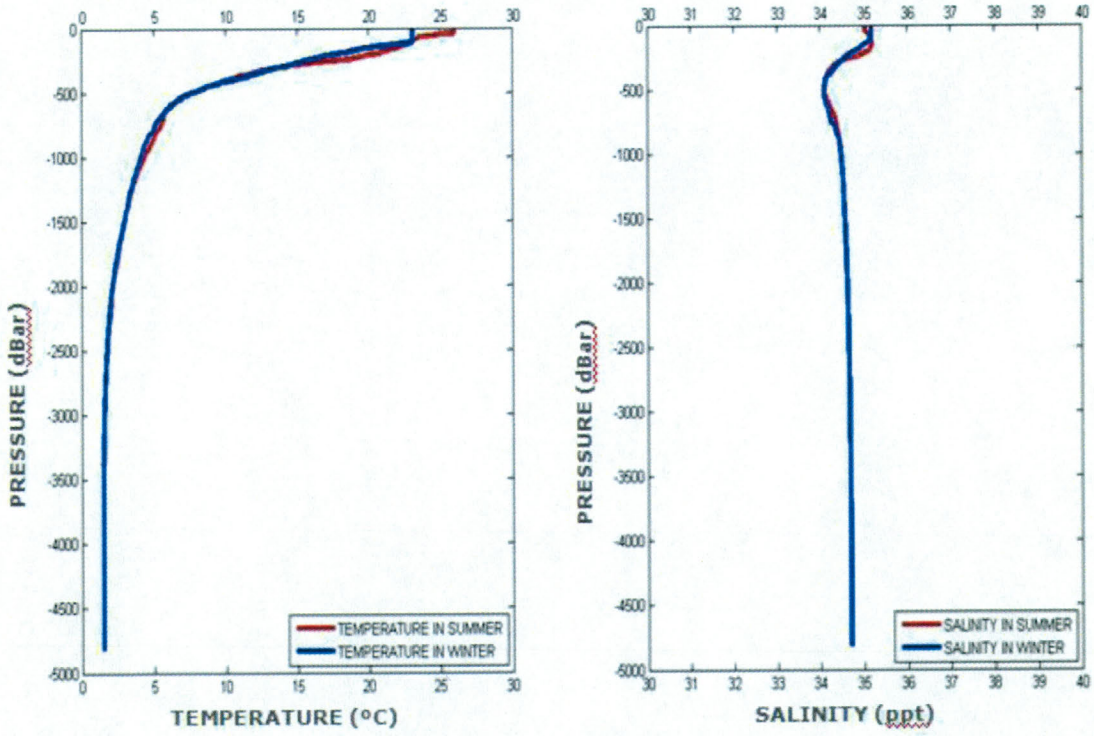

Figure 3.10 - Two different Hawaii profiles: summer profile represented in red and winter profile represented in blue.

Zoom in the first 250 meters of those profiles shown in Figure 3.10, we get the plot presented in Figure 3.11.

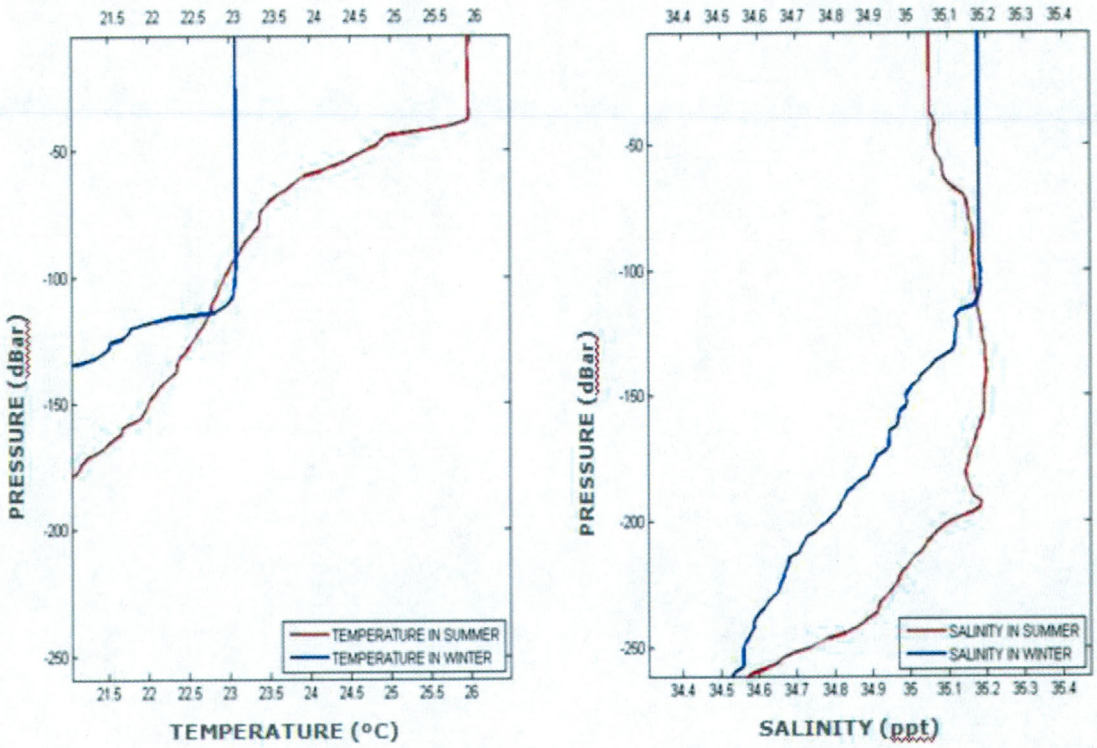

Figure 3.11 - First 250 meters of Hawaii profiles shown in Figure 3.10.

Notice in Figure 3.11 that the most significant variation occurs in temperature for the first 50 meters deep. Temperature varies up to 3°C from winter to summer (left side). On the other hand, salinity slightly changes: less than 0.2 ppt for the first 50 meters.

Considering a hydrographic survey at 50 meters in the environment presented above using a 300kHz system, we get those quite different results for attenuation during the winter and summer, presented in Figure 3.12.

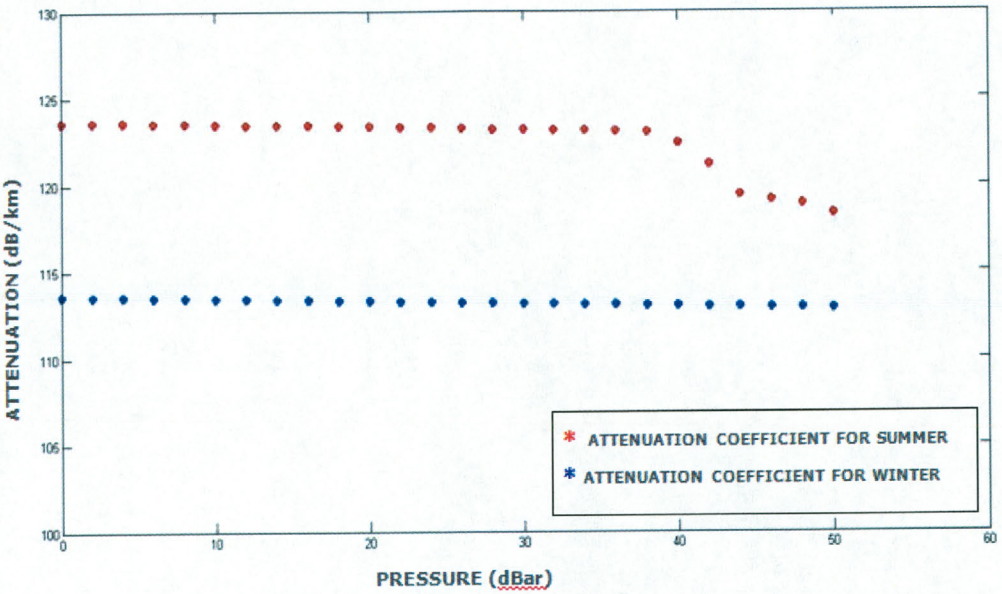

Figure 3.12 - Attenuation results considering a hydrographic survey at 50 meters in the environmental presented in Figure 3.11, using a 300kHz system during the winter and the summer.

The mean attenuation value is 113.22 dB/km during the winter and it is 122.54 dB/km during the summer, which means an attenuation difference of about 9.3 dB/km. In terms of attenuation fluctuation due to its seasonal phenomenon, it represents about 1dB for nadir beams and about 2dB for outer beams, as represented in Figure 3.13.

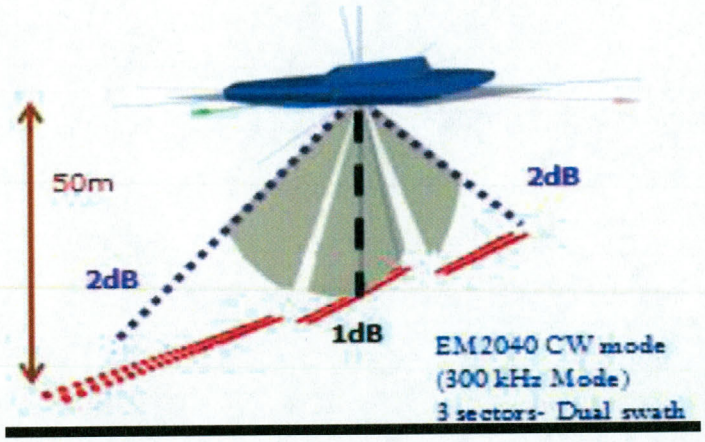

Figure 3.13 - Considering a 50m water deep, the attenuation fluctuation is about 1 dB (whole ray tracing) for nadir beams and about 2 dB for outer beams.

- **Attenuation and its salinity dependence**

Instead of using the Hawaii profile, a salinity dependence simulation has been done with the Arctic data, shown in Figures 3.4 and 3.14. In that experiment, two close salinity mean values: 33 and 35ppt (Figure 3.14, right side) were used to calculate attenuation, presented in Figure 3.15. In addition, the frequency considered for calculation was 32kHz, the same used by the EM302 installed aboard CCGS "Amundsen" (during Arctic survey); pH equal to 8 and the actual temperature profile collected by the ship using a CTD (Figure 3.14, left side).

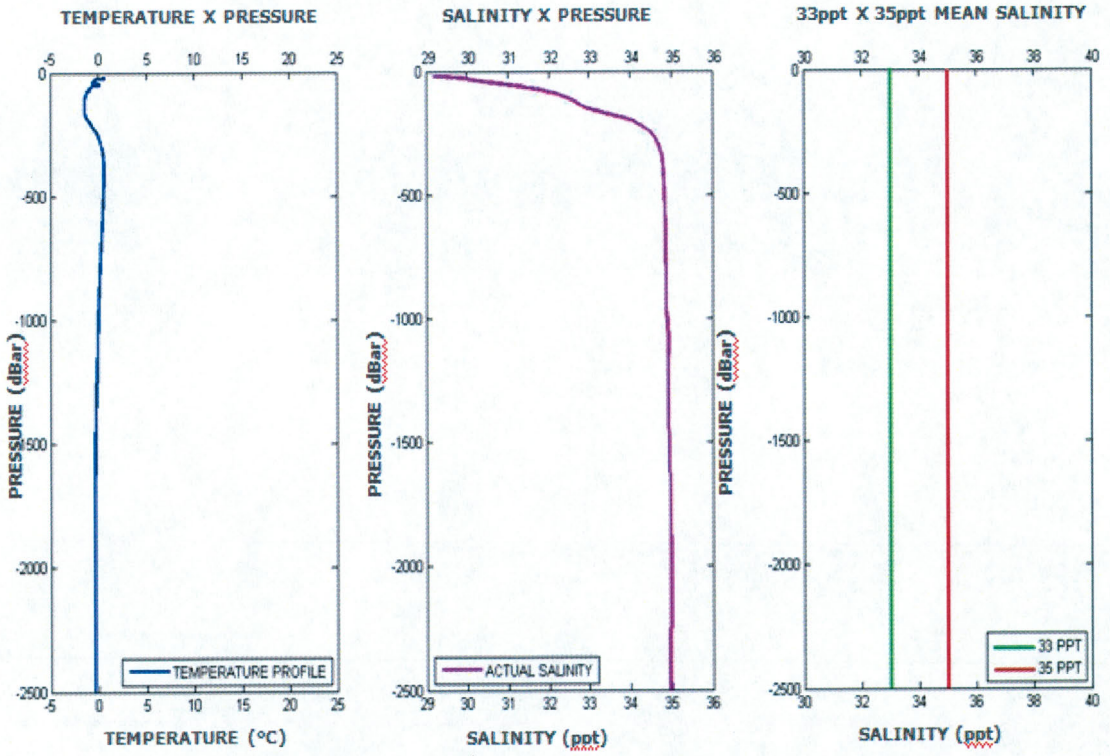

Figure 3.14 - Actual temperature and salinity Arctic profile (left and centre, respectively). In the right side, two close mean salinity values used for attenuation calculation: 33 and 35 ppt are represented.

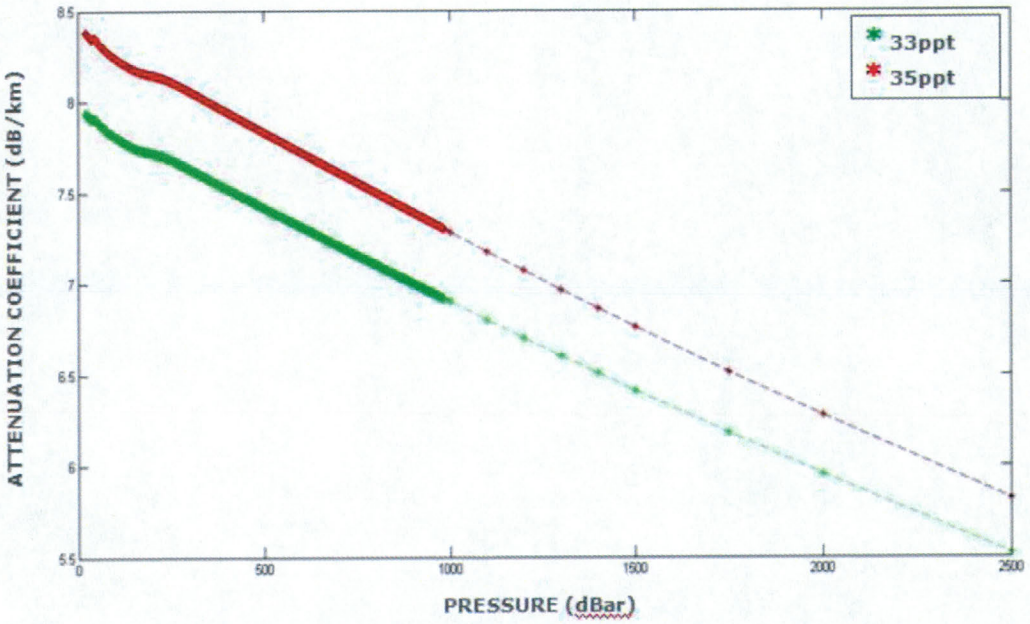

Figure 3.15 - Attenuation and its salinity dependence at 32kHz. In green, attenuation coefficient results for salinity 33 ppt and in red, attenuation coefficient results for salinity 35 ppt.

As we can notice in Figure 3.15, the difference between the attenuation for 33 and 35ppt is about 0.5 dB/km, which might seem small. Considering that the area surveyed was 2,500 meters deep, the total attenuation difference between the two salinity regimes is about 2.5 dB (whole ray tracing) for nadir beams and about 5 dB for outer beams, as shown in Figure 3.16. It compromises the seafloor classification if not properly compensated, due to the apparent backscatter strength fluctuation imposed by incorrect attenuation coefficient.

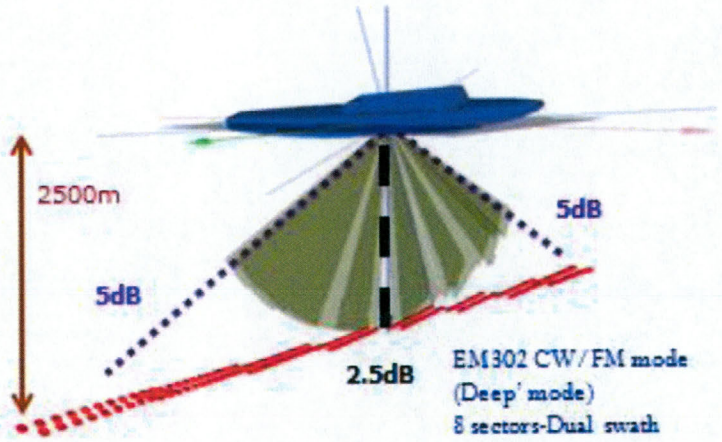

Figure 3.16 - Considering a water depth of 2,500 meters, the total attenuation difference is about 2.5 dB (whole ray tracing) for nadir beams and about 5 dB for outer beams.

Thus, as environmental controls affect attenuation and that, in turn, affects backscatter strength, we have to measure them. The previous standard hydrographic method was to measure sound speed only; so many surveys do not have the environmental information. Earlier versions of SIS (Seafloor Information System) required manual input of a single absorption value. That was empirically altered to account for sector frequency differences. Currently, SIS [Kongsberg Maritime, 2009a and 2010a] approaches are either based on providing an approximate salinity (e.g. the EM302 example illustrated earlier) and a sound speed profile to approximate the environment or an option to provide a CTD input. Both of these options are dependent on real time availability and correct extrapolation. What is being proposed herein is an automatic method that can get the environmental information that we believe better represents the survey area, from a World Ocean Atlas (WOA) or World Ocean Database (WOD), for example, and reapply it to the collected data, compensating for the attenuation difference.

3.4 Cumulative attenuation and its sensitivity analysis

3.4.1 Calculation of cumulative attenuation – Depth dependence

Cumulative attenuation is a weighted mean value of all *in situ* attenuation coefficients measured throughout the discretized layers of the water column until the depth considered. It is mathematically defined by the following equation:

$$\alpha_{Cz} = \int_{TD}^{Z} \alpha(T, S, pH, P, f) dZ \tag{3.6}$$

where TD is the transducer depth and Z is the depth considered. Equation 3.6 can be approximated by:

$$\alpha_{Cz} = \frac{\sum_{i=0}^{n} (\alpha_{in\ situ\ i} * \Delta Zi)}{\sum_{i=0}^{n} \Delta Zi} \tag{3.7}$$

where n is the layer corresponding to depth considered Z, $\alpha_{in\ situ}$ is the *in situ* attenuation coefficient (also called *in situ* absorption coefficient) and ΔZ is the thickness of each water column sampled layer.

Figure 3.17 illustrates an example of cumulative attenuation plot (right) based on synthetic *in situ* attenuation coefficients (left) sampled throughout a water column, according to the values presented in Table 3.1. Notice that layer B represents an anomalous layer, with an attenuation coefficient value (30 dB/km) quite different of the other layers A and C (20 and 18 dB/km, respectively).

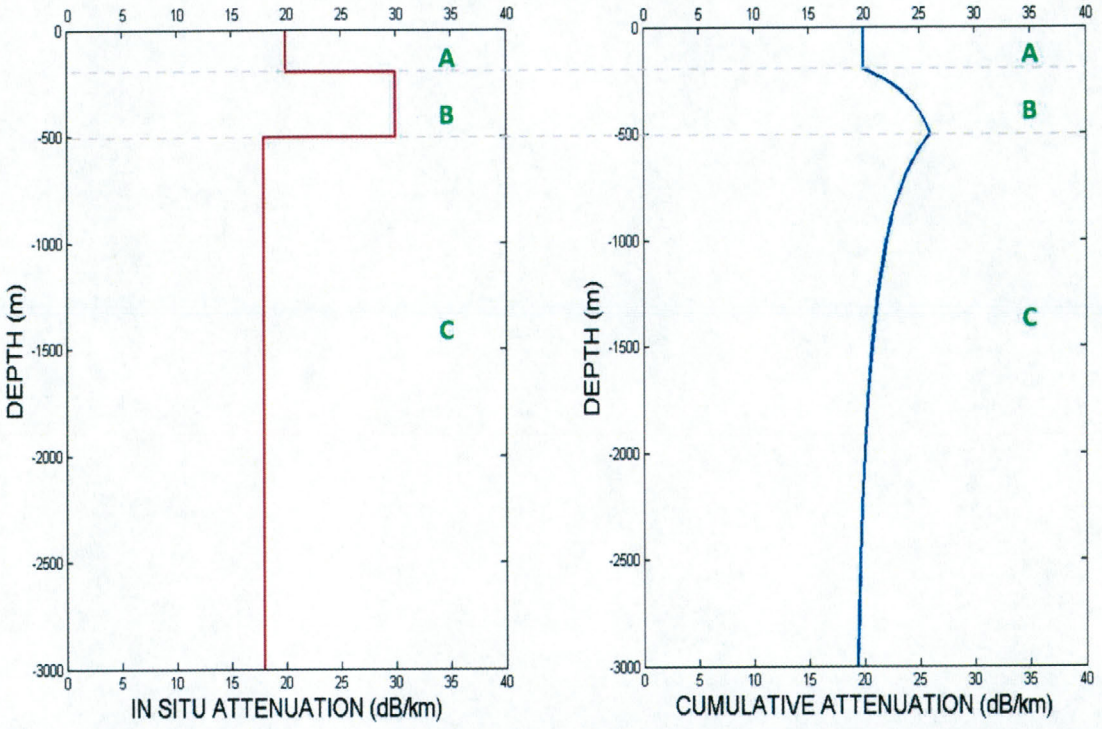

Figure 3.17 - Cumulative attenuation plot (right, in solid blue line) based on synthetic *in situ* attenuation coefficients (left, in solid red line) sampled throughout a water column. A, B and C (in green) represent the three different layers considered in this example.

Layer	Layer boundaries (m)	*In situ* attenuation coefficient ($\alpha_{in\ situ}$) (dB/km)
A	0 – 200	20
B	200 – 500	30
C	500 – 3000	18

Table 3.1 – Layers A, B and C sampled in the water column used as an example in Figure 3.17 and their synthetic *in situ* attenuation coefficient values.

As we can notice in Figure 3.17, from layer A to B there is an abrupt change in the *in situ* attenuation coefficient (left) from 20 to 30 dB/km (an increase of 50% of the value in layer A), which is minimized when considering the cumulative attenuation

(right). Observe that the cumulative attenuation curve slowly starts to rise (layer B) until the boundary between layers B and C, when the curve non-linearly decays with depth (layer C) due to the decrease in the *in situ* attenuation coefficient in this last layer (18dB/km).

Now, increasing the anomalous layer thickness from 200-500m to 200-800m, as shown in Table 3.2, and keeping the *in situ* attenuation values used in the example above, we get the results presented in Figure 3.18.

Layer	**Layer boundaries (m)**	***In situ* attenuation coefficient ($\alpha_{in\ situ}$) (dB/km)**
A'	0 – 200	20
B'	200 – 800	30
C'	800 – 3000	18

Table 3.2 – Layers A', B' and C' sampled in the water column used as an example in Figure 3.18 and their synthetic *in situ* attenuation coefficient values.

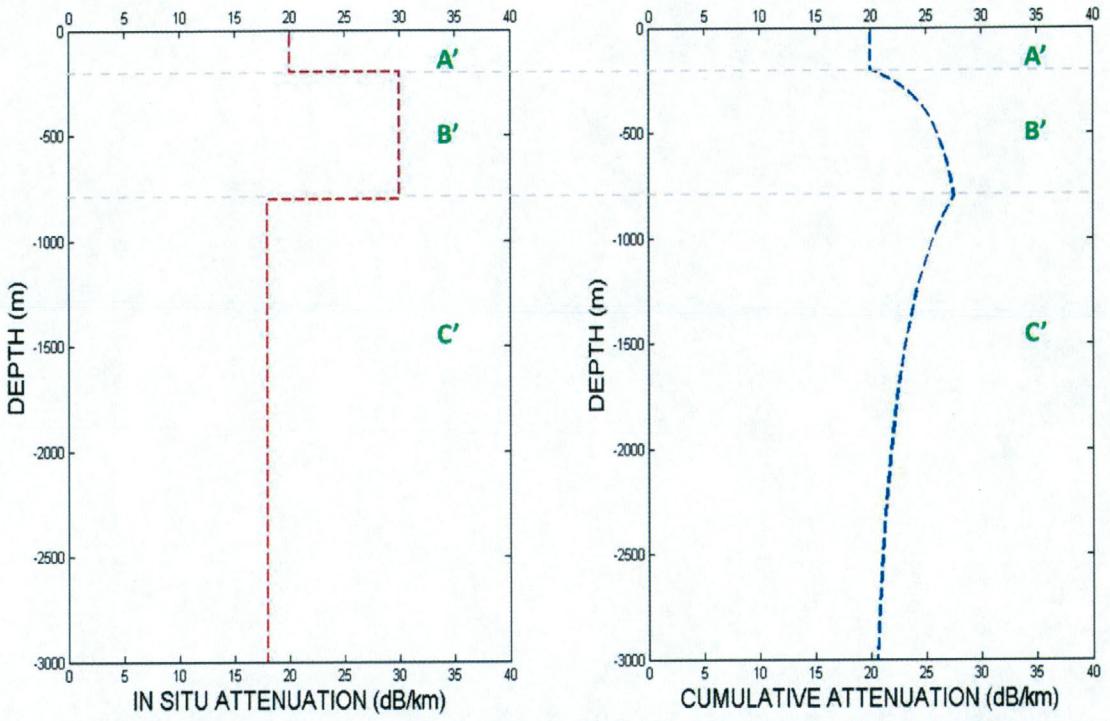

Figure 3.18 - Cumulative attenuation plot (right, in dashed blue line) based on synthetic *in situ* attenuation coefficients (left, in dashed red line) sampled throughout a water column. A', B' and C' (in green) represent the three different layers considered in this new example.

Figure 3.19 compiles the two examples (Figures 3.17 and 3.18) in the same plot. Solid lines represent data shown in Figure 3.17, and dashed lines represent data shown in Figure 3.18. Notice that the thicker the anomalous layer, the larger the $\Delta\alpha$ (cumulative attenuation difference, as shown in Figure 3.19), and the longer it takes to decay.

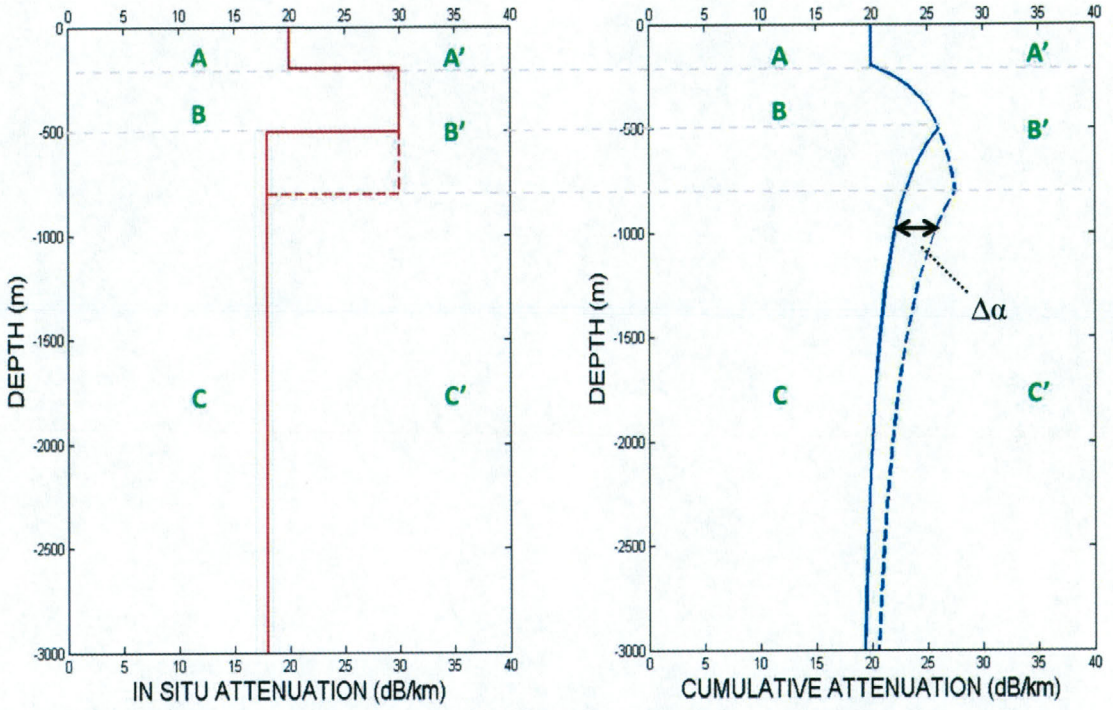

Figure 3.19 – Compilation of examples shown in Figures 3.17 and 3.18. Solid and dashed lines represent data shown in Figures 3.17 and 3.18, respectively.

3.4.2 Example cases

Two casts collected in May 2011 by an AML CTD in different areas with different depths in Upper Howe Sound, British Columbia, have been analyzed and are presented below. Figure 3.20 shows the temperature and salinity profiles for the shallower cast, collected to 170 meters, and Figure 3.21 shows these profiles for the deeper cast, collected to 280 meters.

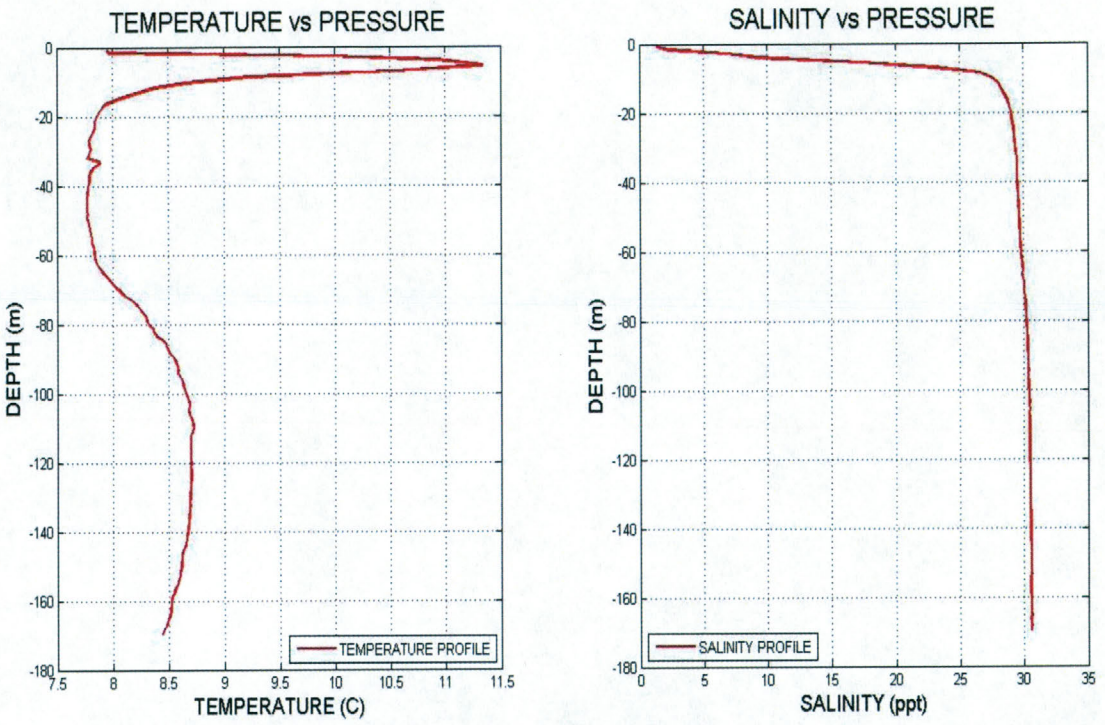

Figure 3.20 - Temperature and salinity profiles of shallower cast collected to 170 meters deep.

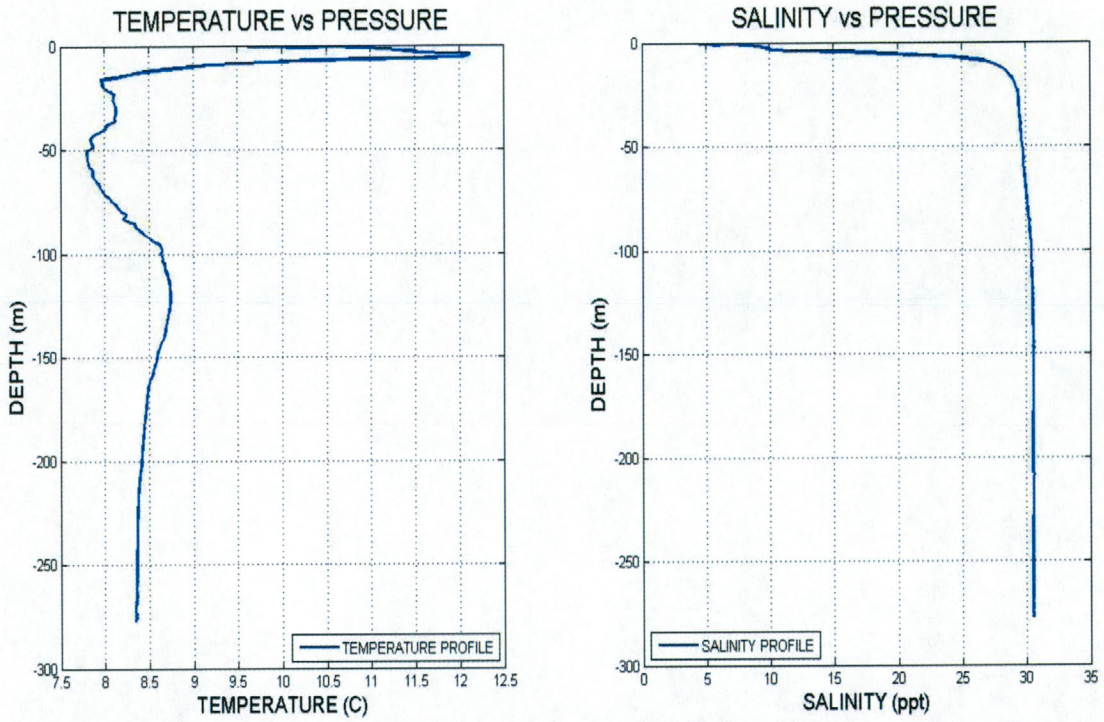

Figure 3.21 - Temperature and salinity profiles of deeper cast collected to 280 meters deep.

Comparing both casts within the same plot (Figure 3.22), we can notice that most of temperature and salinity variations occur in the upper 100 meters. An enlargement of the first 100 meters is presented in Figure 3.23.

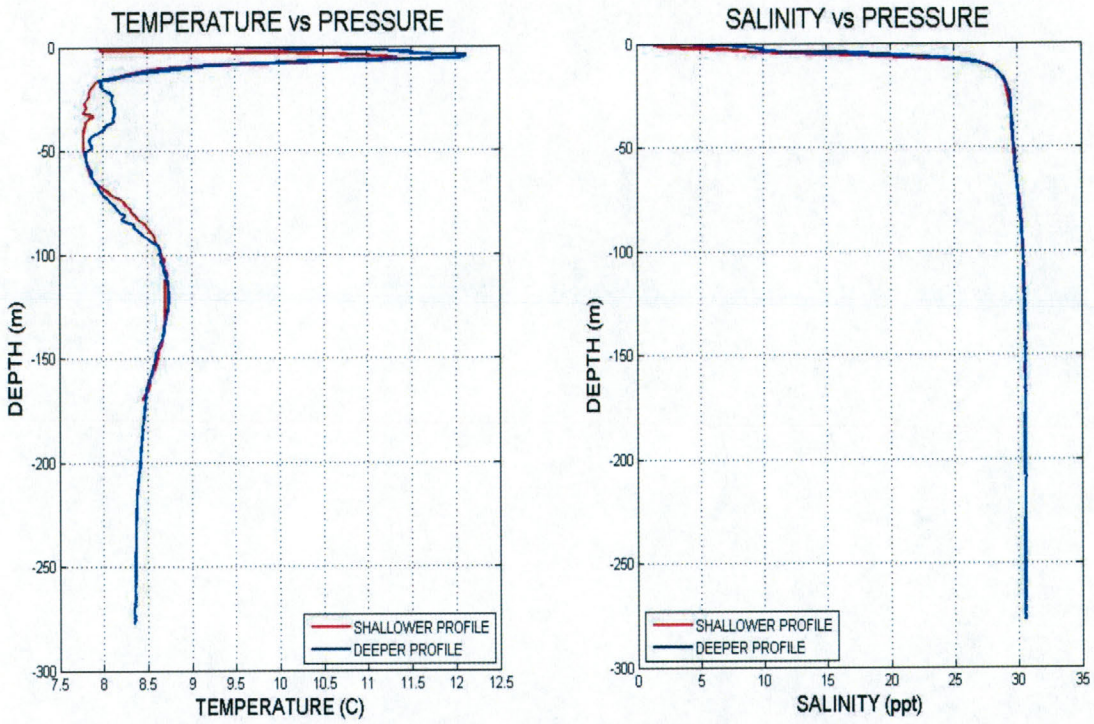

Figure 3.22 - Temperature and salinity profiles of shallower (in red) and deeper (in blue) casts represented at the same plots.

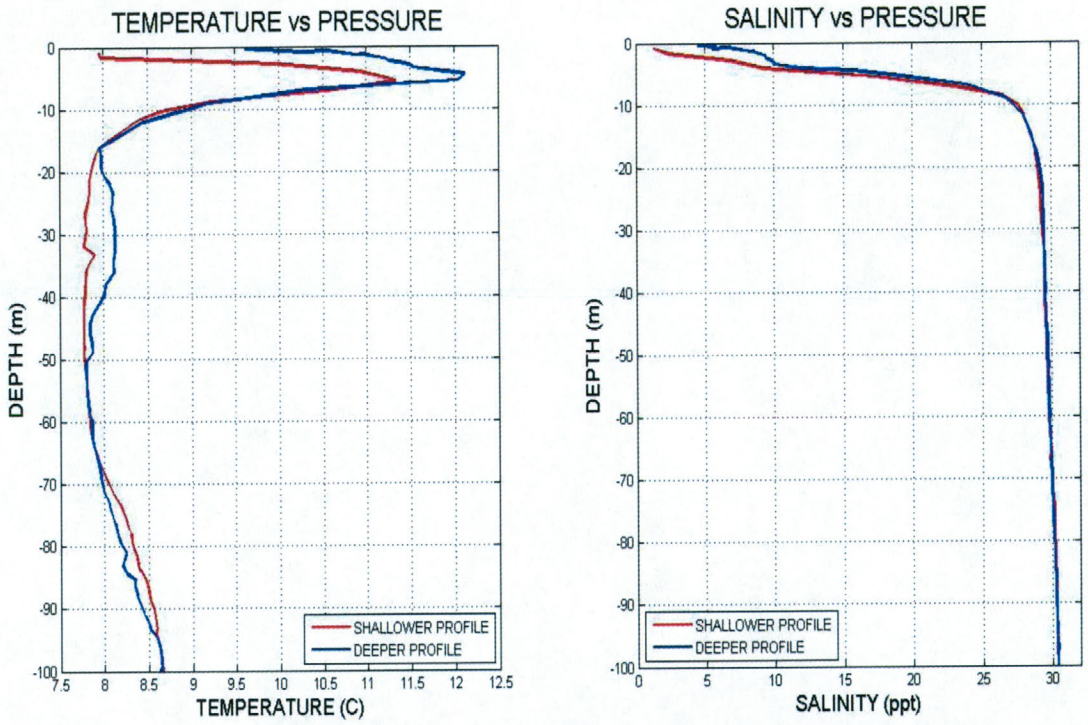

Figure 3.23 - Zoom in the first 100 meters of shallower and deeper casts, where most significant variations in temperature and salinity occur.

The following plots shown in Figures 3.24 to 3.26 have been done considering an EM2040 MBES operating at 200 kHz.

Figure 3.24 shows the absorption *in situ* and the cumulative absorption for both shallow and deep casts within the same plot. Notice that, after the first layers (about 100 meters), where most of temperature and salinity variations occur, absorption *in situ* for both casts have almost the same values (red and blue solid lines in Figures 3.24 and 3.25) and the two cumulative absorptions curves converge (red and blue dashed lines in Figures 3.24 and 3.26), demonstrating that the mixture layer and the thermocline are primarily responsible for most of the absorption coefficient variations. Furthermore, depending on the environment, the seasonal aspect also has a great impact on attenuation, especially in

fjords like Squamish, where, besides the temperature, the salinity also changes significantly from winter to spring, when ice melts and water surface salinity decreases. Besides that, there is a diurnal absorption coefficient variation due to the saline wedge effect during tide cycles, constantly changing the water attenuation, especially in estuaries.

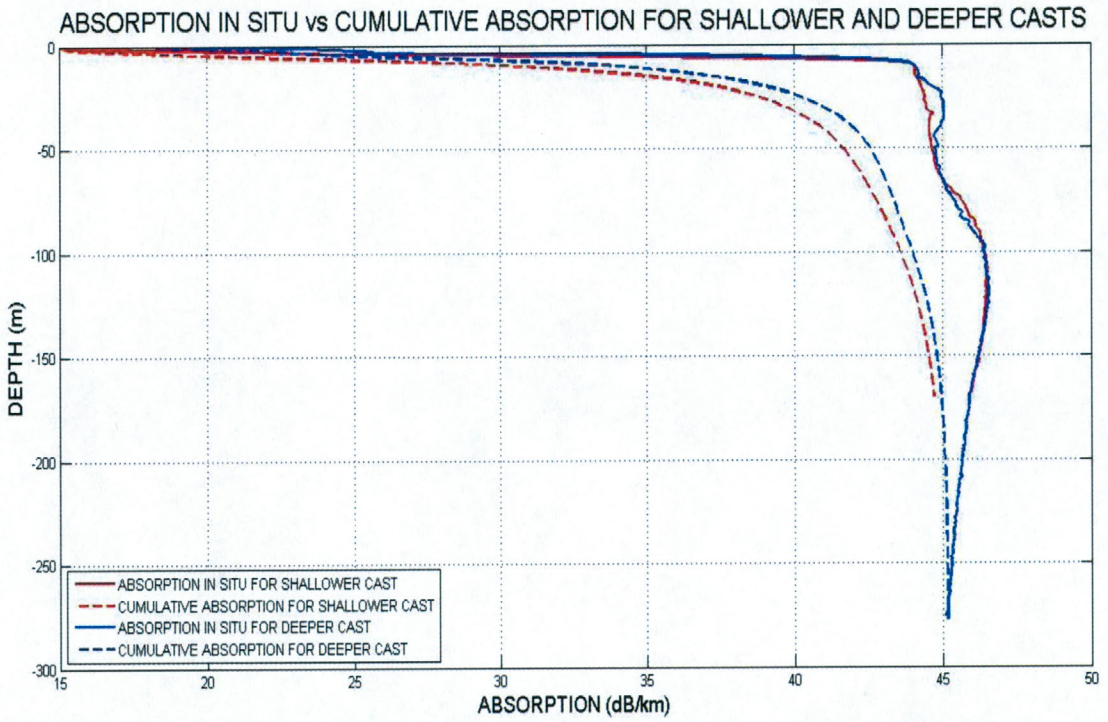

Figure 3.24 - Absorption *in situ* and cumulative absorption for both casts (shallower cast in red and deeper in blue). Notice that, after 100 meters, for both casts, absorption *in situ* has almost the same values (red and blue solid lines) and the two cumulative absorptions curves converge (red and blue dashed lines).

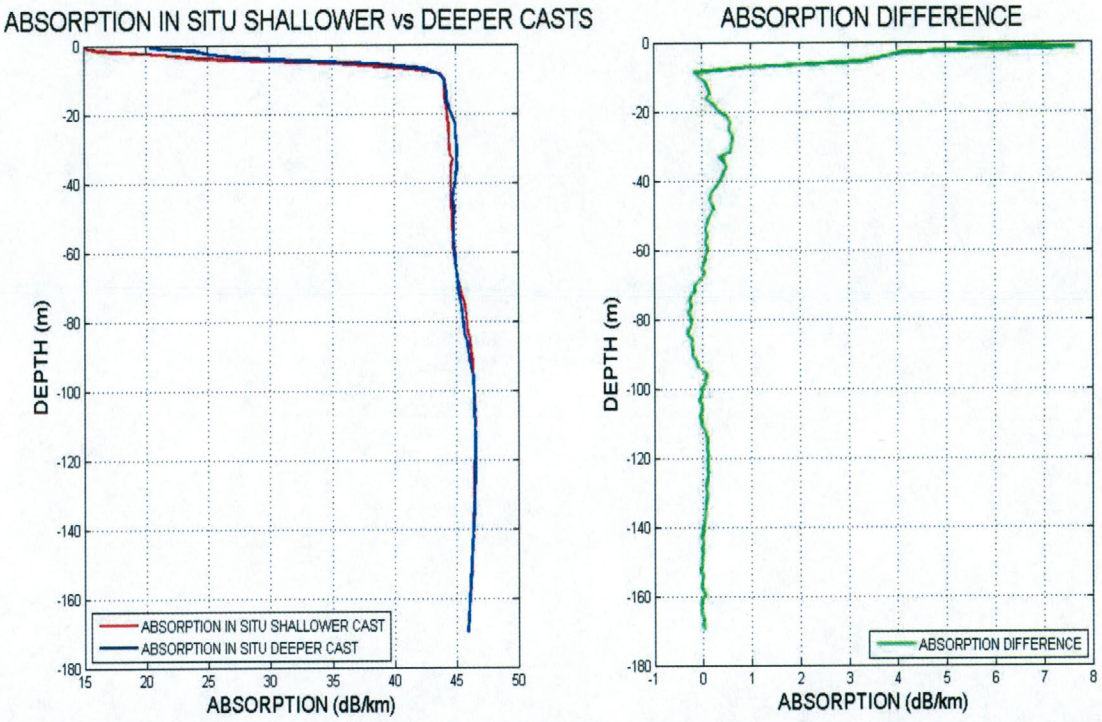

Figure 3.25 Absorption *in situ* for both casts (shallower and deeper casts in red and blue solid lines, respectively). Notice that, after 100 meters, for both casts, absorption *in situ* has almost the same values (left hand). The plot in the right hand represents the absorption *in situ* difference by a solid green line. After about 100 meters, the difference is close to zero.

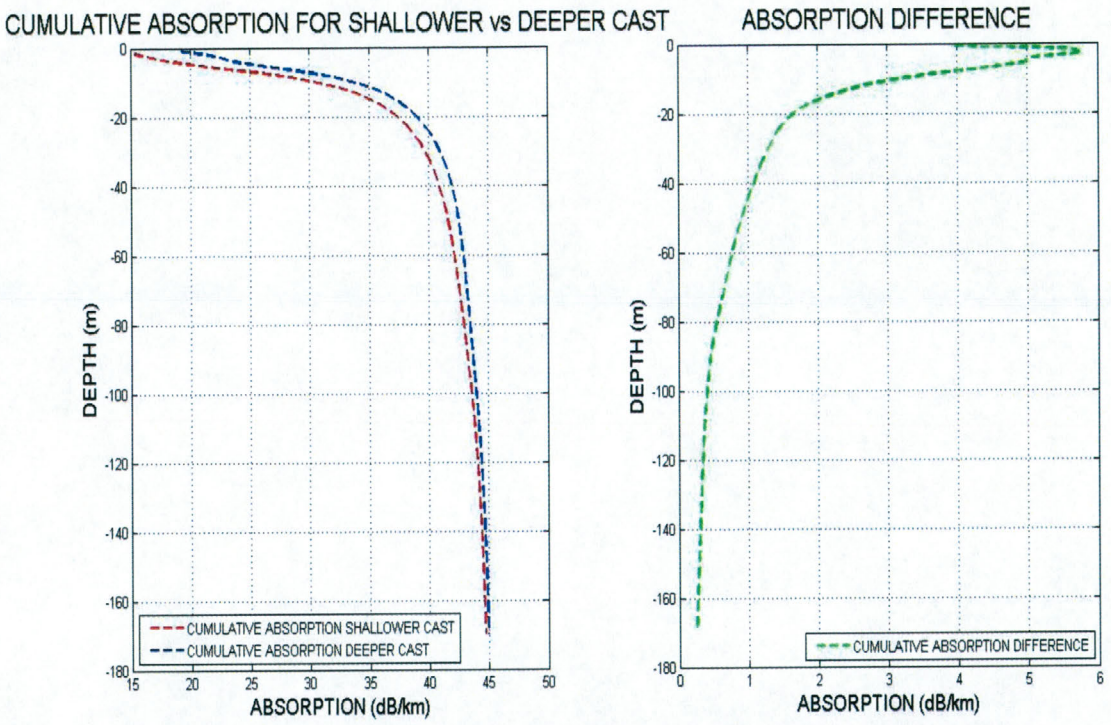

Figure 3.26 - Cumulative absorption for both casts (shallower and deeper casts in red and blue dashed lines, respectively). Notice that, after 100 meters, for both casts, the cumulative absorptions have almost the same values (left hand). The plot in the right hand represents the cumulative absorption difference by a dashed green line. After about 100 meters, the difference is close to zero.

Thus, for deep ocean work, typically the oceanographic structure of the lower 95% of the water column does not change significantly and so fluctuations in the upper 5% have minimal effect on the cumulative value at approximately 5 km depth. In contrast, in shallow shelves and coastal waters, seasonal effects extend from surface to the bottom and thus have a huge effect on cumulative absorption values.

3.4.3 Near-equivalence of refracted and straight line ray path

This section focuses on an oblique ray, while the previous analysis (section 3.4.2) was done for a vertical ray.

A sensitivity analysis has been done considering two different ray paths: the actual ray tracing (Figure 3.27, dashed red line), based on the Snell's Law and the ray refractions through the layers of the water column; and the ray path based on Pythagoras distance (Figure 3.27, dotted purple line), which is a simplification of the first method (ray tracing), calculated based on the depth and the horizontal range (also represented on this Figure), often used due to the less refined calculation, less computer memory allocation and time consuming, being faster in providing data in real time.

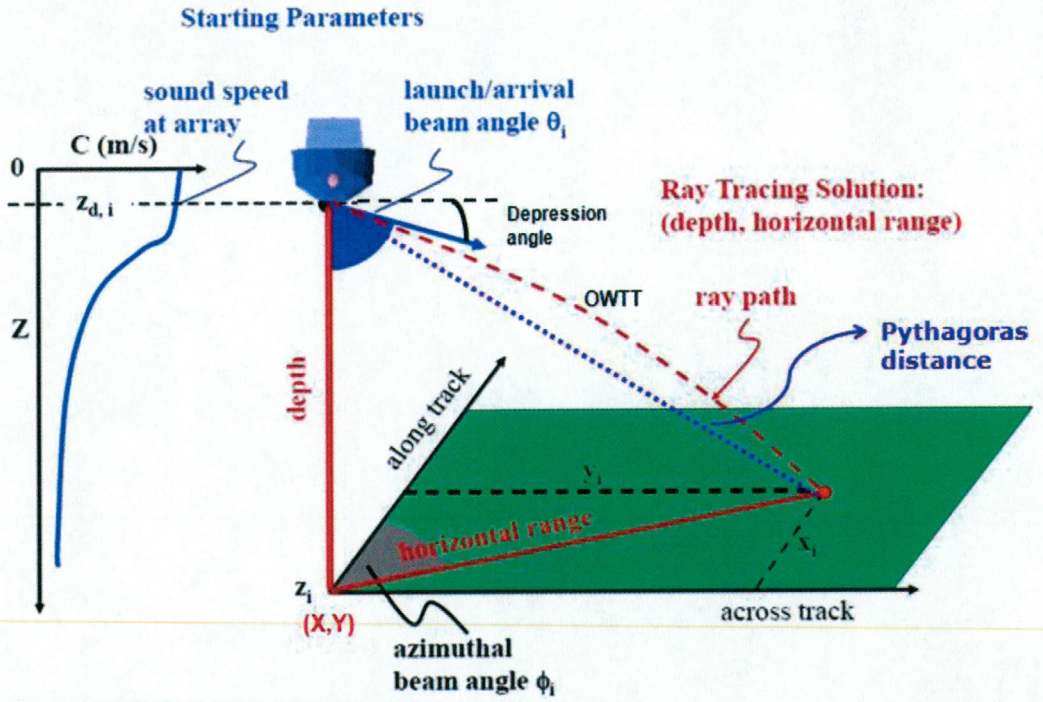

Figure 3.27 - Two different ray paths: actual ray tracing (dashed red line) and Pythagoras distance (dotted purple line) (edited from [deMoustier, 2011]).

The aim of this analysis is evaluate the impact in terms of absorption loss, which is range dependent, when considering the Pythagorian distance instead of the actual ray tracing.

Figure 3.28 illustrates a synthetic (exaggerated for demonstration) situation used for this analysis: in the left is represented a sound speed profile with two discrete values (V_1 and V_2) and, in the right, is represented two different ray paths: Pythagoras distance (represented by R_{1p} and R_{2p}) and the actual ray tracing (represented by R_1 and R_2). The water column considered is 2000 m thick and is divided equally in two different layers (different oceanographic properties), each one with 1000 m thick.

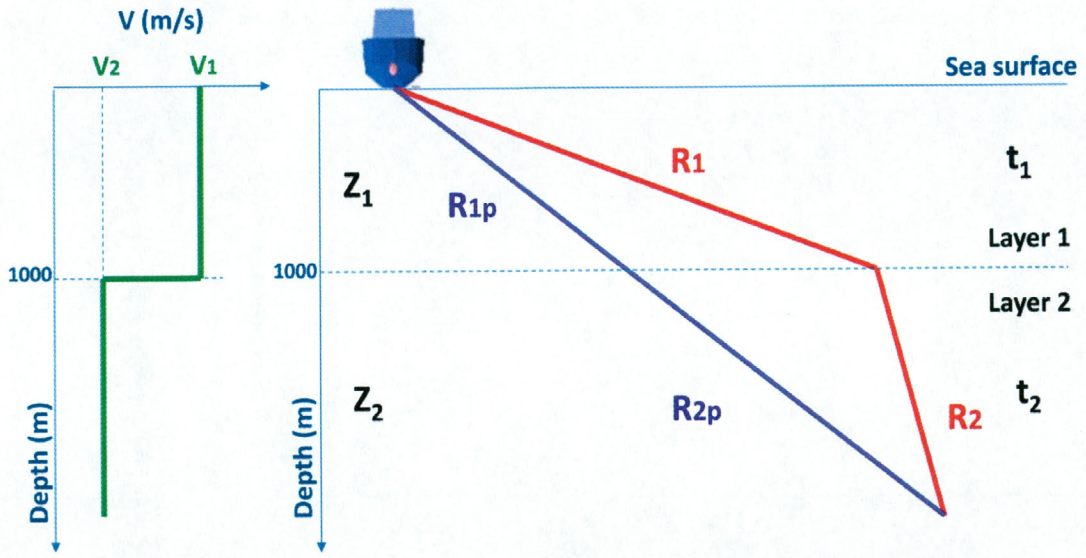

Figure 3.28 – A synthetic situation: in the left, a sound speed profile with two discrete values (V_1 and V_2) and, in the right, two different ray paths: Pythagoras distance (represented by R_{1p} and R_{2p}) and the actual ray tracing (represented by R_1 and R_2).

Three different cases were considered, each one with a different sound speed profile, as summarized in Table 3.3. As we can notice for all them, the one-way travel time (OWTT) considered was 2 seconds and the launch angle was 60°.

	OWTT (s)	Launch angle (°)	V_1 (m/s)	V_2 (m/s)
Case 1	2	60	1700	1300
Case 2	2	60	1600	1400
Case 3	2	60	1515	1510

Table 3.3 – Three different cases: same OWTT and launch angle, but different sound speed profiles.

Table 3.4 presents the results for Z_1 and Z_2 (depth penetration in each layer), t_1 and t_2 (time spent in each layer), R_1, R_{1p}, R_2 and R_{2p}.

	Z_1 (m)	Z_2 (m)	t_1 (s)	t_2 (s)	R_1 (m)	R_{1P} (m)	R_2 (m)	R_{2P} (m)
Case 1	1000	802.170	1.176	0.824	2000	1683.652	1070.588	1350.578
Case 2	1000	685.145	1.25	0.75	2000	1802.774	1050	1235.160
Case 3	1000	518.340	1.32	0.68	2000	1993.339	1026.601	1033.251

Table 3.4 - Results for Z_1 and Z_2 (depth penetration in each layer), t_1 and t_2 (time spent in each layer), R_1, R_{1p}, R_2 and R_{2p}.

Table 3.5 shows the difference in percentage between the actual ray trace (R_1, R_2) and the Pythagoras distance (R_{1p}, R_{2p}) in each layer.

	R_1 (m)	R_{1P} (m)	$\frac{R_1-R_{1P}}{R_1}$ (%)	R_2 (m)	R_{2P} (m)	$\frac{R_2-R_{2P}}{R_2}$ (%)
Case 1	2000	1683.652	15.82	1070.588	1350.578	26.15
Case 2	2000	1802.774	9.86	1050	1235.160	17.63
Case 3	2000	1993.339	0.33	1026.601	1033.251	0.65

Table 3.5 - Difference in percentage between the actual ray trace and the Pythagoras distance in each layer

Based on the results presented on Tables 3.4 and 3.5, we conclude that time spent in the layer is not exactly proportional to the thickness of the layer (Figure 3.29). But operationally the difference is small: comparing the 3 cases shown in Table 3.5, we can notice that the closer are the sound velocity profiles (less difference between sound speed in layers 1 and 2), the smaller the difference between the actual ray tracing and the Pythagoras distance.

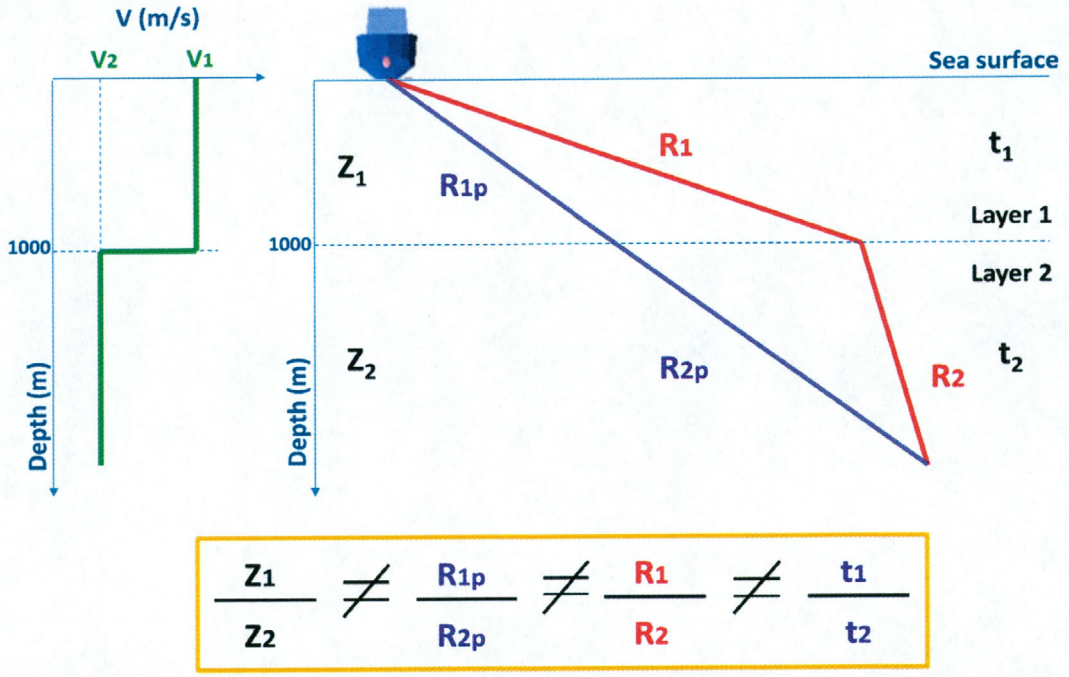

Figure 3.29 – Results show that the ratios for Z_1, Z_2, R_1, R_{1p}, R_2, R_{2p}, t_1 and t_2 are not exactly for the three cases considered earlier, but for typical sound speed variations (1490 to 1520 m/s) this is acceptable.

If we use 1700m/s and 1300m/s (first and second layers in case 1, respectively) it is clearly unacceptable to consider the final ray path as a straight line (Pythagoras distance). But for typical variations in sound speed in the water: 1490 to 1520 m/s the differences are unimportant. So, for our application (absorption loss), we can go with the

two-way travel time (TWTT) and assume fraction of time spent in each layer is proportional to layer thickness.

Chapter 4: BACKSCATTER DATA REDUCTION

4.1 Gain controls

In an effort to have the same sediment type represented by the same backscatter strength value (flatten the beam sample amplitudes) independent of the ensonification angle, SIS tries to compensate for the angular response effect (also known as grazing angle effect) using an angle dependent gain control. Besides that, as receivers of MBES have limited dynamic range, a Time-Varying Gain (TVG) is run during the ping to avoid overload or having the echo return buried in noise [Hammerstad, 2000]. For the latest MBES generation (EM2040) it is no longer necessary due to the high dynamic range of the digitizers. Nevertheless, the equivalent TVG is then applied in software afterwards.

The cumulative absorption coefficient α of the water column will be used in the gain setting in the receiver for beams from that sector. That absorption coefficient will be important in determining the correct backscattering strength of the seabed used in the seabed imaging. Thus, setting a correct value is therefore always important if the backscatter data are going to be used, especially if the results are going to be compared with backscatter data from other areas or other seasons, when absorption coefficients are different, or if data are going to be used in seafloor characterization [Kongsberg Maritime, 2010a].

Currently, Kongsberg applies a time (and implicitly angle) dependent gain that, with certain assumptions, will reduce the received intensity to an estimate of the seabed

backscatter strength. There are 5 main components to this (Figure 4.1), all of which have potential for errors:

1. Source Level (SL): a given source level is assumed for each sector transmission. If wrong, all values for the sector are shifted;
2. Spherical spreading (40logR): this is almost perfect. Actually slight ray path convergences or divergences should be included, but it is small [Urick, 1983];
3. Attenuation (α): the problem identified in this thesis;
4. Bottom Target Strength (BTS): described in detail in Hammerstad [2000]. This addresses BTS and its three issues: choice of BS_N - BS_O, choice of crossover angle (CA) and assumption of flat seafloor (Figure 4.3), briefly described below;
5. Sector specific beam patterns (also in Figure 4.2): as described more in Teng [2012].

Components 1 (source level) and 5 (sector specific beam patterns) are probably the biggest issues. Neither are explicitly described in Kongsberg documentation. Although not described, component 1 is probably a constant offset (possibly per sector) (Figure 4.1A). Informal discussions with Kongsberg (JHC, personal communications 2012) suggest that component 5 is corrected on a beam by beam basis based on elevation angle relative to the boresite of each transmit sector (Figure 4.2). This is effectively overprinted on the TVG as a function of time (Figure 4.1D). This is assumed to be result of applying the coefficients in the bscorr.txt file in the transceiver.

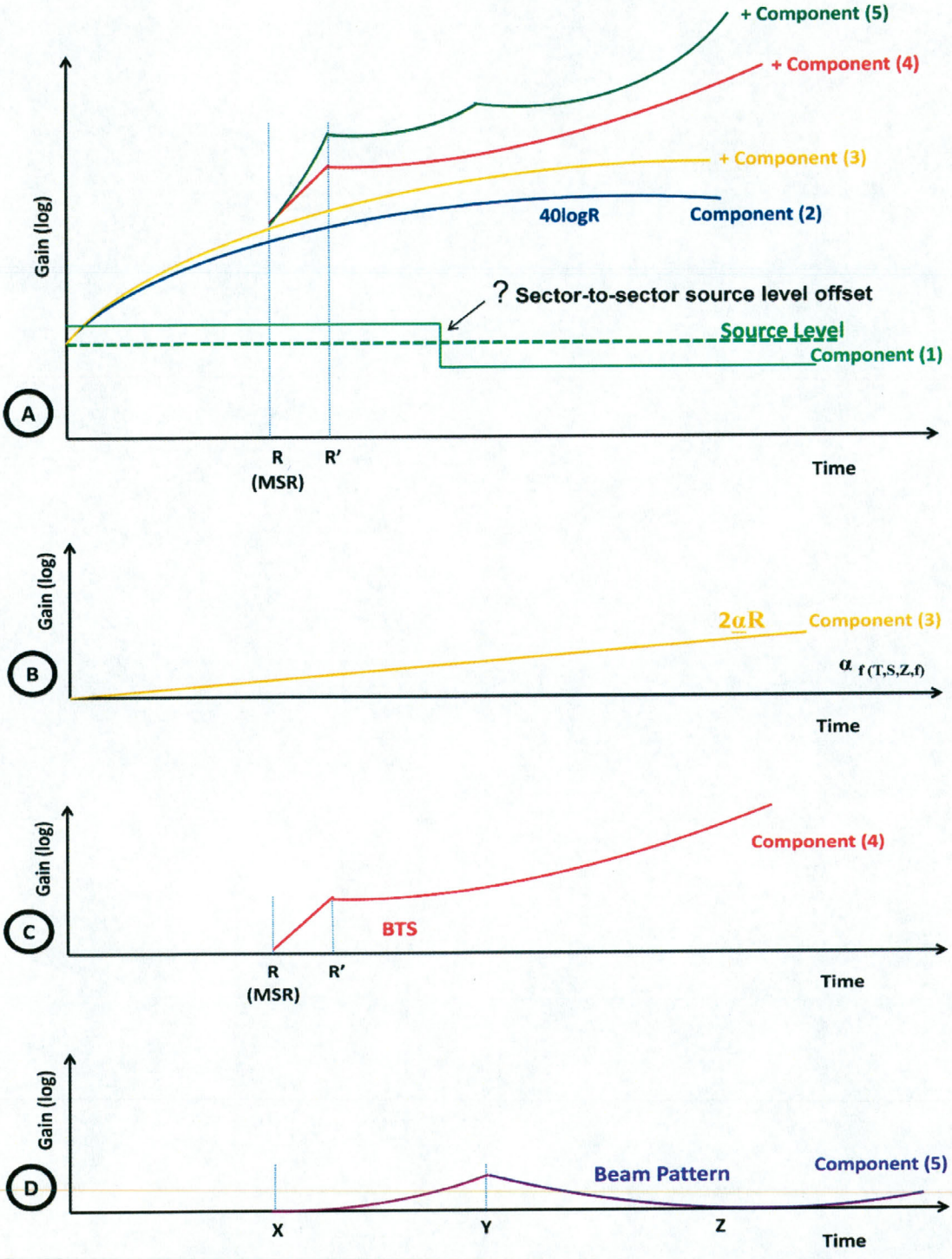

Figure 4.1 – 5 main components of gain corrections (axis Y) applied by Kongsberg in its MBES based on the time between transmission and reception (axis X).

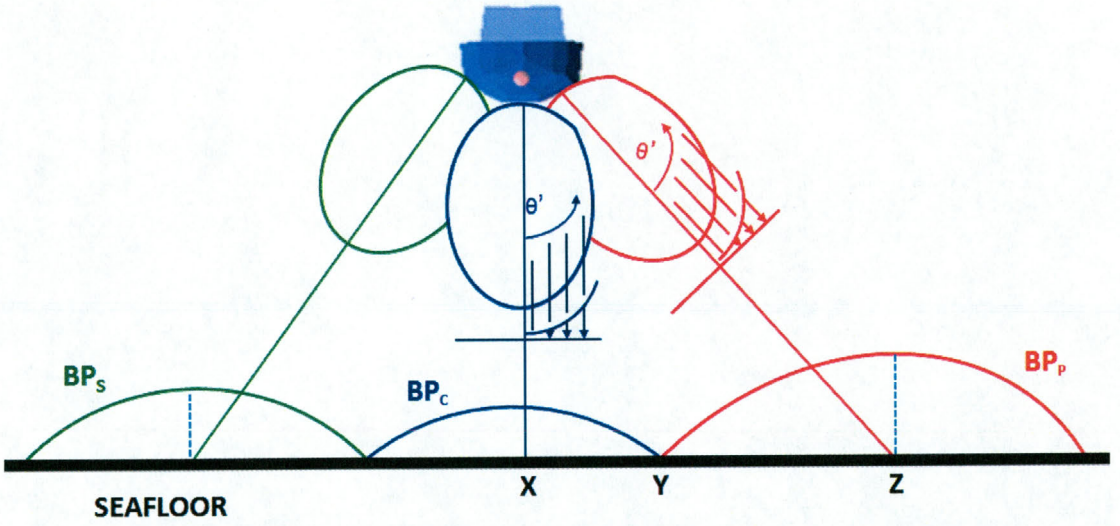

Figure 4.2 – The beam pattern issues and attempts to address them, described in detail in Teng [2012]. This image represents three beam patterns BP_S, BP_C and BP_P (starboard, center and portside, respectively) and three points X, Y and Z, which represent three different times (also represented in Figure 4.1D). As each beam has a known angle relative to the transmitter centre (θ') and the system knows the steering angle of each received beam for each frequency, SIS is assumed to add a certain amount of correction for each beam for each sector centre frequency, represented by the blue and red arrows.

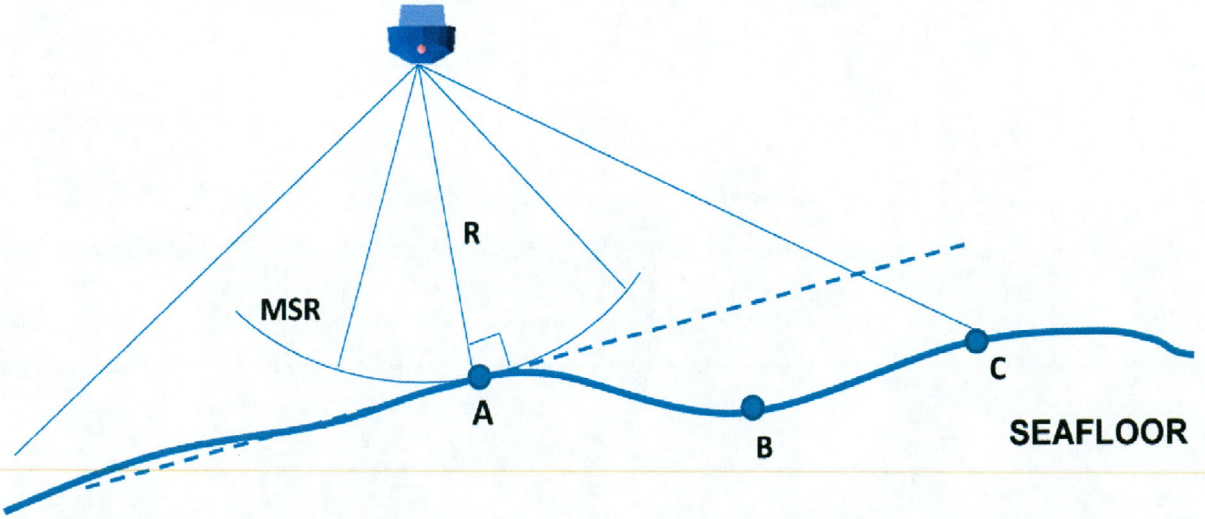

Figure 4.3 – The flat seafloor assumption of Hammerstad [2000] based on the Minimum Slant Range (MSR), corresponding to point "A" on the seafloor.

Hammerstad [2000] described the assumptions inherent in component 4 of the TVG (Figure 4.1C), notably the model of the shape of the seabed angular response (AR). Trying to understand how backscattering coefficients varies with incidence angle, he concluded that a good approximation for most conditions would be to assume that a uniform flat bottom (Figure 4.3) is characterized by mean backscattering coefficient BSo and that angular variation is given by Lambert's law, i.e.:

$$BS = BSo + 20\log(\cos\varphi) \tag{4.1}$$

Hammerstad [2000] also explained that for smaller incidence angles (larger grazing angles) a reasonable fit to the data can be achieved by assuming that the backscattering coefficient changes linearly with the incidence angle from BS_N at 0° to BSo at an angle which the backscattering coefficient curve starts to become flatter (Figure 4.4). That angle is the crossover angle (CA). For each of the main frequencies used by Kongsberg devices, a default CA is used reflecting typical sediment ARC at that frequency [Teng, 2012]. If the incident angle is larger than CA, the ARC is assumed to become Lambertian ($BS(\Theta) = BSo\cos^2(\Theta)$).

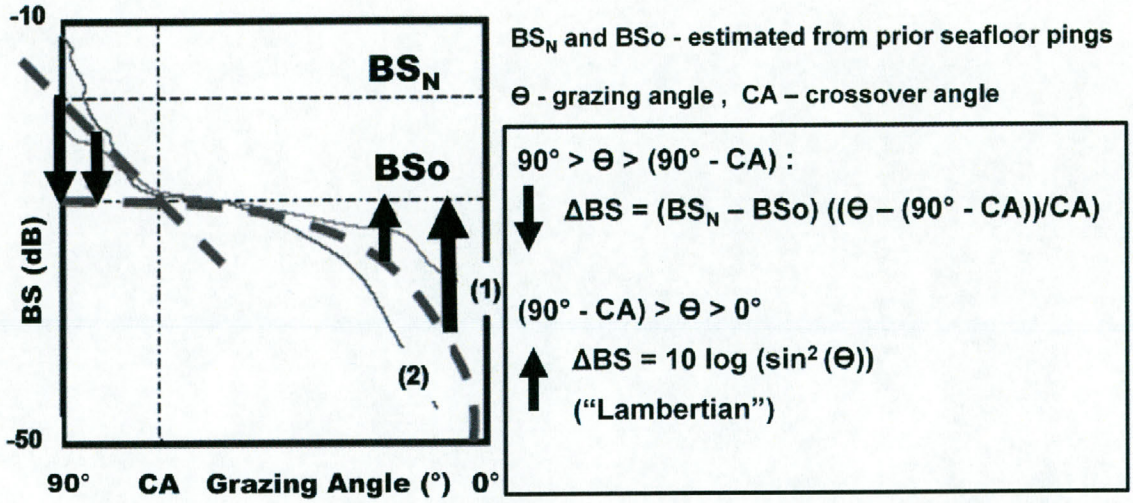

Figure 4.4 – SIS compensates the angular response effect: by estimating BS_N and BSo values from previous pings, Kongsberg model draws the dashed lines and considers they are the appropriate model for normalizing next pings to the crossover level. The model assumes a linear behavior for nadir region (90° > Θ > (90° – CA)) and a "Lambertian" behavior for the oblique incidence region ((90° – CA) > Θ > 0°). However, next pings can present different shapes, such as the ones represented by curves (1) and (2). Therefore, corrections applied will under-compensate or over-compensate backscatter curves (edited from [Oliveira Jr., 2007 and Hughes Clarke, 2011c]).

The range R' at the CA and the range R to normal incidence (Figure 4.5) can be expressed as:

$$R' = R \sec (CA) \tag{4.2}$$

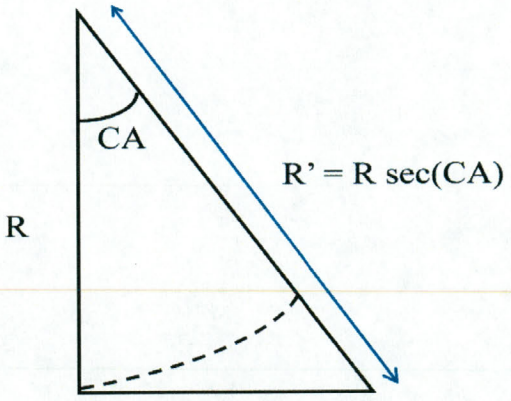

Figure 4.5 – The relationship of the range to the normal incident crossover angle (CA).

All these assumptions limit the absolute fidelity of the backscatter strength estimate. For typical low relief (sedimented) seafloors the flat seafloor assumption is reasonable and using a single attenuation coefficient per sector is also reasonable, as discussed later in section 5.1. But it is all still limited by appropriated choice of attenuation coefficient. This thesis addresses how to, in post processing, adjust absorption coefficients α (Component 3, Figure 4.1B).

4.2 Options to apply absorption coefficient in SIS

The Kongsberg documentation states the following: "A correct value for the absorption coefficient is important with respect to the validity of the bottom backscatter measurements" [Kongsberg Maritime, 2010a].

Old MBES, such as the EM1000 system, compensated the transmission loss during data acquisition assuming a fixed value for the absorption coefficient inserted in the operator unit before the survey. As the water column properties are constantly changing both in time and geographically, it was a crude simplification of environmental controls on attenuation, creating systematic underestimation or overestimation of the true backscatter, with an impact to backscatter mosaics and seabed classification [Oliveira Jr, 2007].

Currently, this process is automatically implemented in the newer EM sonar series softwares. On broadband sonar systems such as EM710, absorption coefficient matrixes can be automatically calculated by SIS using Francois and Garrison Equation (equation 3.3 presented in Chapter 3, considering the pH of the oceans in the order of 7.6 to 8.2)

from sound speed profiles and salinity and CTD (Conductivity-Temperature-Depth) profiles. Altogether, there are three alternatives (also called *Source* in SIS, Figure 4.6) to apply attenuation in SIS: based on salinity input, based on full CTD profile or manually selected [Kongsberg Maritime, 2010a].

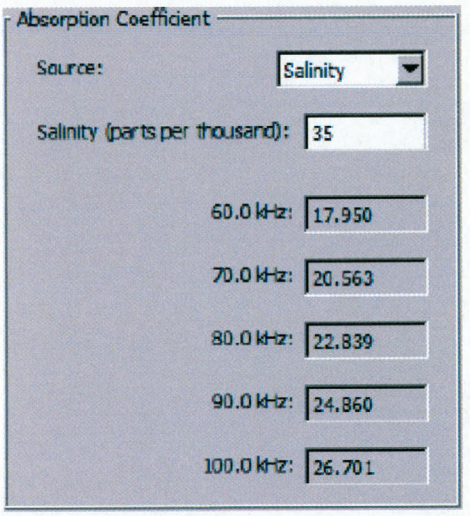

Figure 4.6 - Absorption coefficient window in SIS for an EM710 device. In that case, the Source selected was Salinity and the value inserted was 35 ppt, which is also the default value. If necessary, the user can correct that value. When the Source is set to Salinity or CTD, the frequency field is disabled (greyed), but it shows the current value of absorption coefficient in dB/km used for each one of those 5 frequencies (from [Kongsberg Maritime, 2010a]).

If the source is based on salinity input, the average absorption coefficient is calculated using an estimate of the temperature derived by inverting the current sound speed profile Vp (T = f' (S, Z, Vp)), the depth and the specified average salinity. With T, S and Z, SIS uses those values to calculate the absorption coefficient *in situ* (α= f (T, S, pH, Z, frequency)). That *in situ* attenuation is then converted to cumulative attenuation from transducer depth. The cumulative absorption coefficient is calculated by SIS for each relevant frequency (60, 70, 80, 90 and 100 kHz, as shown in Figure above) for the

current depth and it is updated and displayed with changing depths. In the absence of full CTD information that setting is recommended when the salinity in the water is relatively constant.

When the source is a CTD profile, the absorption coefficient is calculated directly from a temperature and salinity profile, which directly includes the parameters necessary to calculate the absorption profile for the full range of required frequencies used by the echo sounders: 12, 32, 60, 70, 80, 90, 95, 100, 200, 250, 300, 350 and 400 kHz (Figures 4.7 and 4.8). Note that although not stated in the manuals, a slope of attenuation as a function of frequency must be used to get sector specific α (e.g. to get different attenuation coefficients required for different sector centre frequencies from 26 to 34kHz used by the MBES EM302). Using the CTD profile option increases the accuracy of the bottom reflectivity data, once SIS calculates the cumulative absorption coefficient through the water column for all depths encountered. In that case, depending upon the depth, the attenuation coefficient values displayed are continuously updated [Kongsberg Maritime, 2010a].

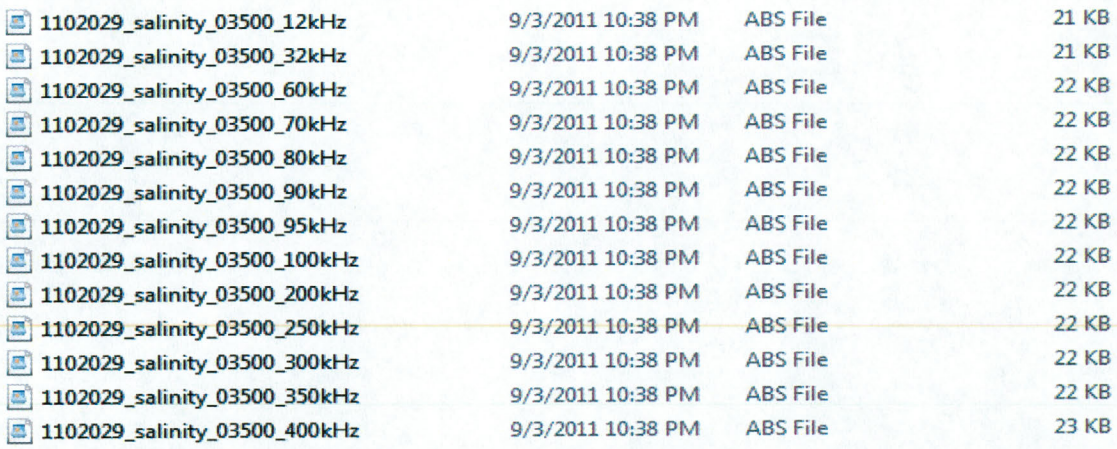

Figure 4.7 - Absorption coefficient profiles made by SIS while operating the EM302 onboard CCGS Amundsen. Notice that SIS creates one absorption profile

for each one of the full range of required frequencies used by the echo sounders: 12, 32, 60, 70, 80, 90, 95, 100, 200, 250, 300, 350 and 400 kHz.

```
( Absorption 1.0 0 201109032210 71.069167 -136.550667 -1 0 0
unknown_instrument P 1953396066 )

19.000 8.343 8.343
20.000 8.340 8.341
21.000 8.345 8.341
22.000 8.322 8.341
23.000 8.307 8.340
```



```
983.000 7.292 7.818
1000.000 7.273 7.808
1100.000 7.167 7.755
1200.000 7.063 7.702
1300.000 6.959 7.649
1400.000 6.857 7.596
1500.000 6.757 7.543
1750.000 6.511 7.413
2000.000 6.273 7.286
2500.000 5.818 7.038
12000.000 1.547 4.381
```

Figure 4.8 - Absorption coefficient profile "1102029_salinity_03500_32kHz.abs" made by SIS for 32kHz while operating the EM302 onboard CCGS Amundsen in the Arctic 2011. Notice that the file contains three columns: depth, which is already extended until 12,000 m, absorption coefficient *in situ* and cumulative absorption coefficient, respectively.

It is important to emphasize that potentially both Vp or CTD profiles may have to be extended and that their quality will only be as good as extensions. Therefore, the absorption coefficients calculated will similarly be only as good as the fidelity of Vp or CTD provided and extensions done.

The third and last option to apply an absorption coefficient in SIS is to insert its value manually for the relevant frequencies of the multibeam echo sounder, i.e. 60, 70, 80, 90 and 100 kHz for EM710. In that case, those values inserted must correspond to the

cumulative absorption coefficient for the whole water column for each one of those frequencies.

Printing out some parameters from the "raw range and angle 78" datagram (that same datagram format is also used for new MBES EM302, EM122, ME70) for the EM710 (1° x 2°) mounted on CSL Heron (UNB survey launch) from data collected during a hydrographic survey in Squamish Fjord (Howe Sound, British Columbia) in 2011, we can notice that SIS calculates one mean absorption coefficient (expressed in 0.01 dB/km) for each sector, based on its centre frequency, as shown in Figure 4.9. That same datagram also provides information such as the transmission sector number and the centre frequency of transmission sector, as presented below.

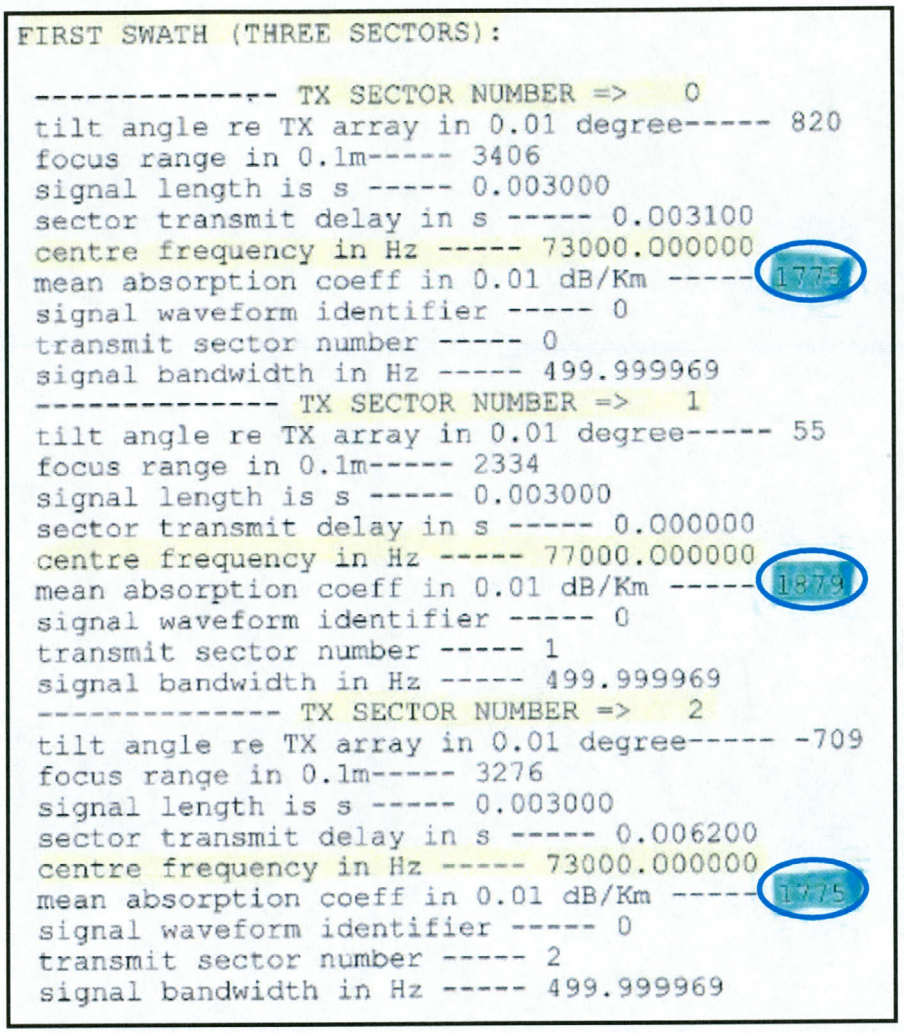

Figure 4.9 - Some printed parameters from the "raw range and angle 78" datagram for the first swath (three sectors, in that operating mode) of the EM710 mounted on CSL Heron. In blue is highlighted the mean absorption coefficient (expressed in 0.01dB/km) calculated by SIS for each one of the three sectors of first swath.

Note this approach, as implemented by Kongsberg, assumes that all beams within a sector fall within a depth range that has the same cumulative α.

4.3 The problem of SIS SVP/CTD extrapolations

Occasionally, SVP/CTD profiles are not deep enough to guarantee coverage of the range of depths encountered during a hydrographic survey and the profiles have to be extended beyond the maximum sampling depth. When using SIS, all input sound velocity profiles are automatically extended to a standard depth of 12,000 m through a default profile or through a user-provided profile that is expected to be representative of the conditions in the survey area. The user profiles are extended using the gradient between the last valid values until the depth of at least 500 meters is reach, at which level the system profile is used [Beaudoin, 2010].

The user is often forced to manually alter the extending profile offline. This way, the user is responsible for ensuring that this method of extending the profile is reasonably correct or acceptable.

When using a CTD profile in SIS, no explanation is given in the SIS manuals when (or even whether) extrapolation is done on a CTD. In this case, there are no default T, S profiles available for extrapolation.

Considering that a change of 1°C gives 4.8 m/s change in sound speed, changing salinity by 1 ppt offsets the resulting sound speed by 1.3 m/s and that every meter of change in depth has an effect of 0.016 m/s [Beaudoin, 2010], collecting profiles in the deepest parts of work area (or utilizing archived deep measurements) in an effort to minimize the amount of profile extension and errors inserted (which also affects the absorption coefficient and ultimately the bottom backscatter strength) is a well recommended practice.

Given the problem of doing the correct extrapolation, it is potentially very easy to have a false attenuation coefficient. Hughes Clarke et al. [2011] noted this for the case of the Squamish surveys. This thesis is, in part, developed to compensate for those operational mistakes.

Chapter 5: PROPOSED METHODOLOGY TO REAPPLY ATTENUATION

This proposed methodology represents an alternative to the method currently used to calculate the mean absorption coefficient within the several sectors of new MBES, in an effort to reduce backscatter strength fluctuations among different sectors presented in some data collected during hydrographic surveys with those new devices, such as the one presented in Figure 5.1.

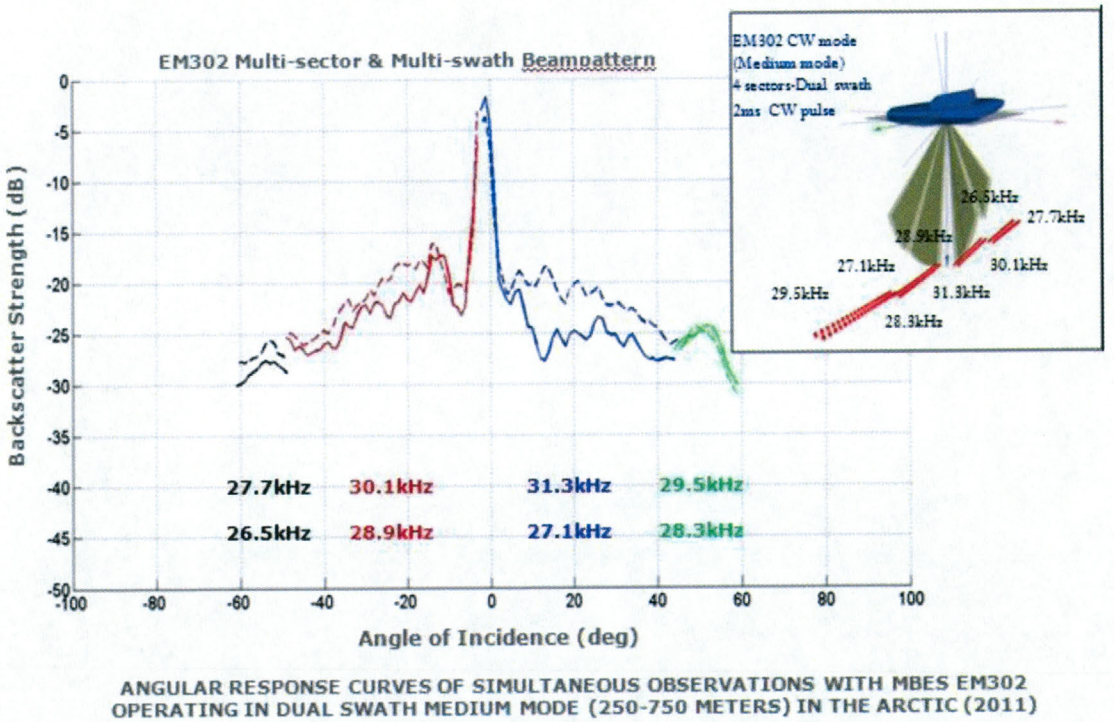

Figure 5.1 - Backscatter strength fluctuations observed between data collected by the first and second swaths of MBES EM302 surveying in the Arctic during the summer 2011.

Figure 5.1 represents the angular response curves collected by MBES EM302 during the summer of 2011 in the Arctic from simultaneous observations across the swath

on a seabed that was believed to have no change in geology. Notice that the backscatter strength fluctuation within the different sectors is remarkable.

When data in the left side of that Figure is projected to the right side of axis X to correlate with model curves to predict seabed type, we get the Figure 5.2 as result.

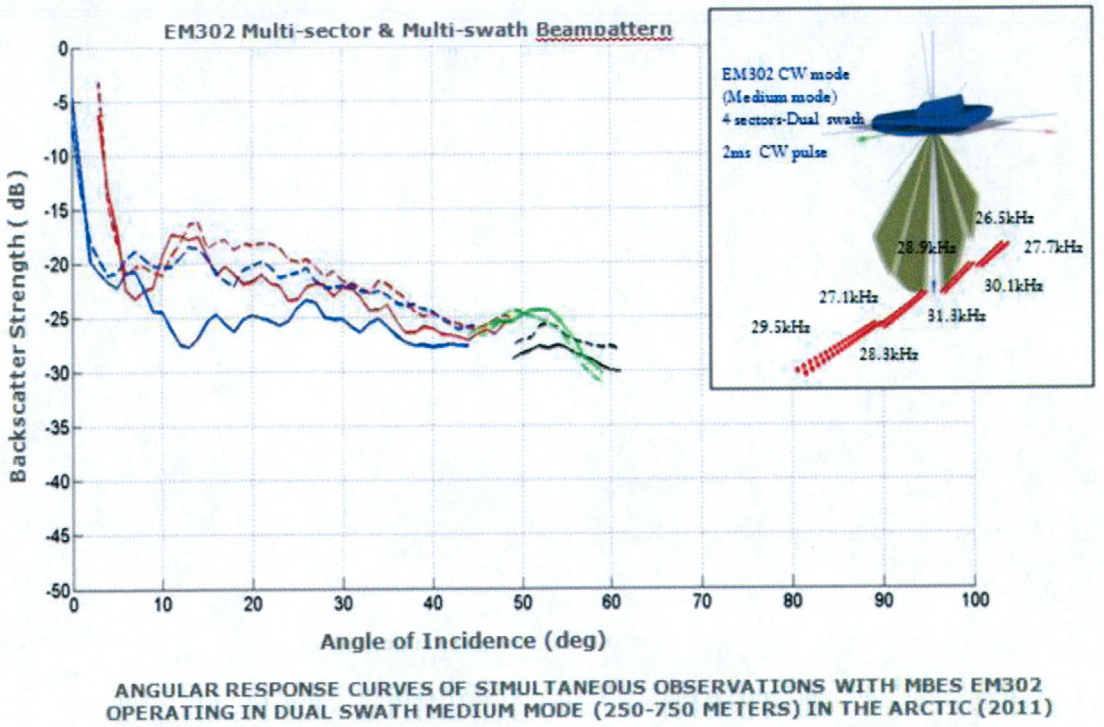

Figure 5.2 - All backscatter strength data projected to the same side of the axis X (in that case, right side).

Now, instead of all 8 sectors presented above, we are going to consider only 2 sectors, each one belonging to a different swath: 27.1kHz and 31.3kHz, as shown in Figure 5.3. Notice that in some parts the backscatter strength difference is about 8 dB between sectors. Part of the issue is imperfect reduction of sector-specific source level and beam patterns [Teng, 2012], but an additional component is attenuation.

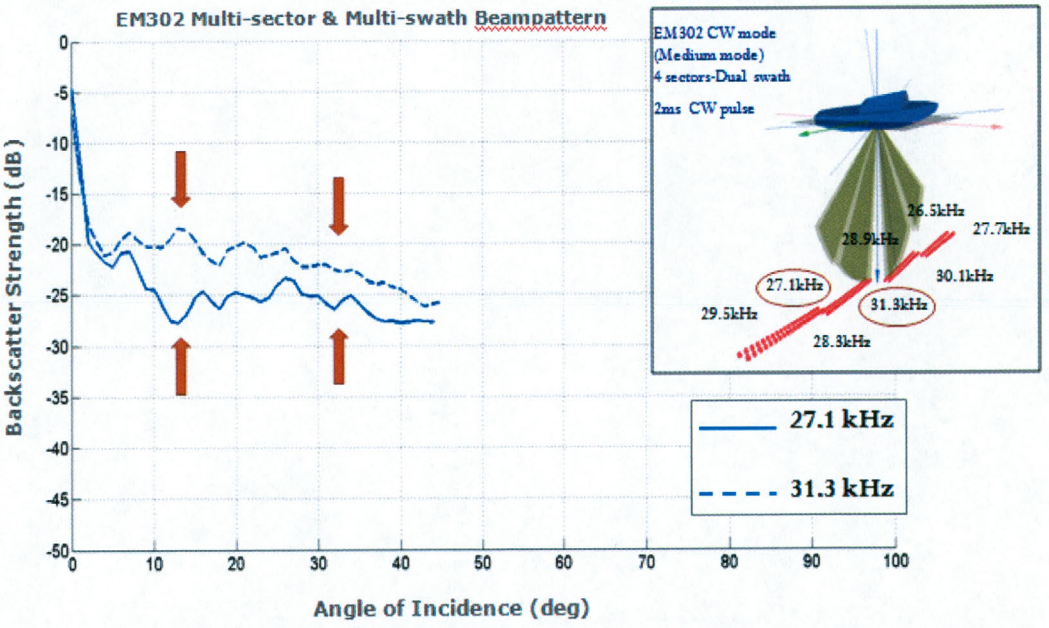

Figure 5.3 - Backscatter strength fluctuations between two different sectors: 27.1kHz and 31.3kHz, each one belonging to a different swath. Notice that in some parts the backscatter strength difference is about 8 dB.

It is important to mention that attenuation errors tend to be correlated (as explained below) in multi-sector multi-frequency multi-swath systems when the operator chooses the "Absorption Coefficient Source" as "Salinity" or "CTD Profile" (Figure 5.4 below). Considering the two frequencies shown in Figure 5.3 (27.1kHz from first swath and 31.3kHz from second swath), if they have wrong attenuation, they both will have wrong backscatter strength signatures, but the "amount of wrongness" will be almost the same (although not exactly the same). In this case, if we move the EM302 system considered in this example from salt water to fresh water, both backscatter strength signatures will move up. Thus, if those curves (signatures) are significantly offset (as

shown in Figure 5.3) it is evidence that most of the problem faced here is due to source level.

In the particular case of EM302, SIS only allows the operator to insert one attenuation coefficient value for 31.5kHz (Figure 5.4, left), although that system switches from 26 to 34kHz depending on the mode it is operating. Presumably a fixed linear scaling is applied to adjust for attenuation at frequencies above and below 31.5kHz. In this case, the attenuation errors will always move together (up and down). In an EM710, in contrast, SIS allows the operator to insert different attenuation coefficient values for 5 discrete frequencies: 60, 70, 80, 90 and 100kHz (Figure 5.4, right). This reflects the fact that the trend in attenuation from 70 to 100kHz can change shape significantly as salinity varies (Figure 3.2). In this case, when choosing "Manual" as "Absorption Coefficient Source" we can have the backscatter strength signatures shifting up and down independently in each sector (according to the wrong values inserted by the operator for each discrete frequency).

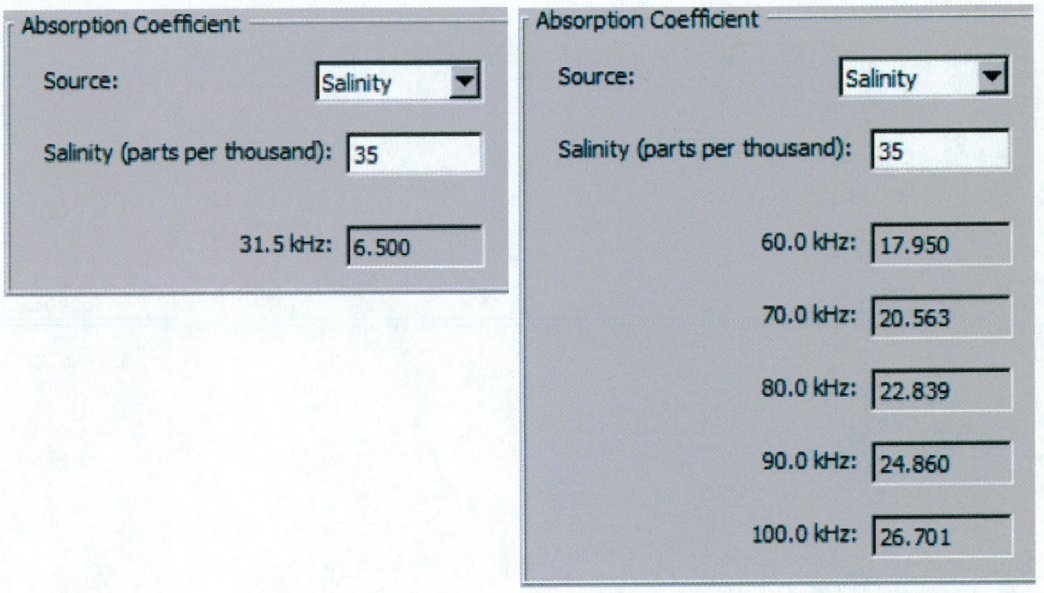

Figure 5.4 – Absorption coefficient windows in SIS for an EM302 (left) and an EM710 (right) (from [Kongsberg Maritime, 2006a and 2010a]).

Thus, this research is an effort to determine a proper attenuation reduction method that minimizes those backscatter strength fluctuations before the seafloor characterization, bearing in mind that only part of this difference is due to attenuation (much is due to source level and beam patterns). Otherwise, it will continue to be hard to distinguish medium sand from coarse sand, as shown earlier in Figure 2.4.

5.1 Current and proposed methodology

As currently implemented in SIS, the mean absorption coefficient is calculated for an average depth for each sector centre frequency, which is reasonable most of time due to the fact that the cumulative absorption curve normally varies only slowly with depth, as shown in Figure 5.5. Left side image represents a ship and three different sonar sectors (different sector centre frequencies) of a MBES, each one with a different mean

absorption coefficient (α_{mean}). Right side plot represents the cumulative absorption curve and the small cumulative absorption difference, represented by red circles, between the boundaries of Sector 1 (S1).

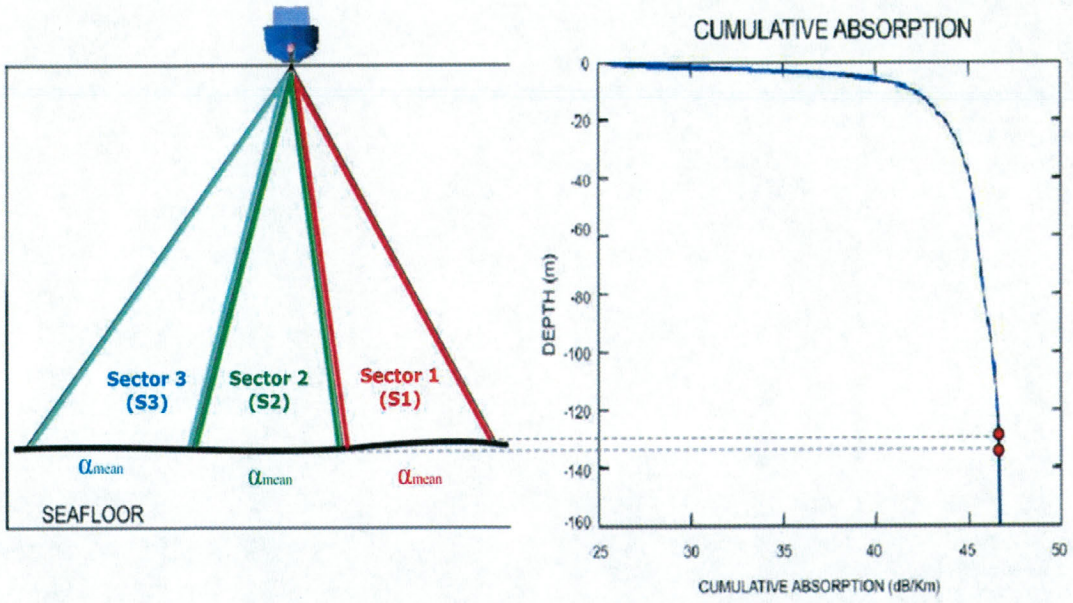

Figure 5.5 – Multi-sector MBES operating in a regular seafloor geometry. Notice that the cumulative absorption in the boundaries of Sector 1 slightly varies, as represented by red circles in the plot in the right side.

On the other hand, under special geometries such as that shown in Figure 5.6, where some sectors are going up hill and others are going down hill, that assumption is not quite right. Notice also in Figure 5.6 that inside the same sector (same centre frequency) the cumulative absorption varies with depth, as represented by red circles in the plot in the right side. Therefore, in some circumstances, if not properly compensated, that cumulative absorption difference can generate backscatter strength fluctuations that may affect backscatter mosaics used for seabed characterization.

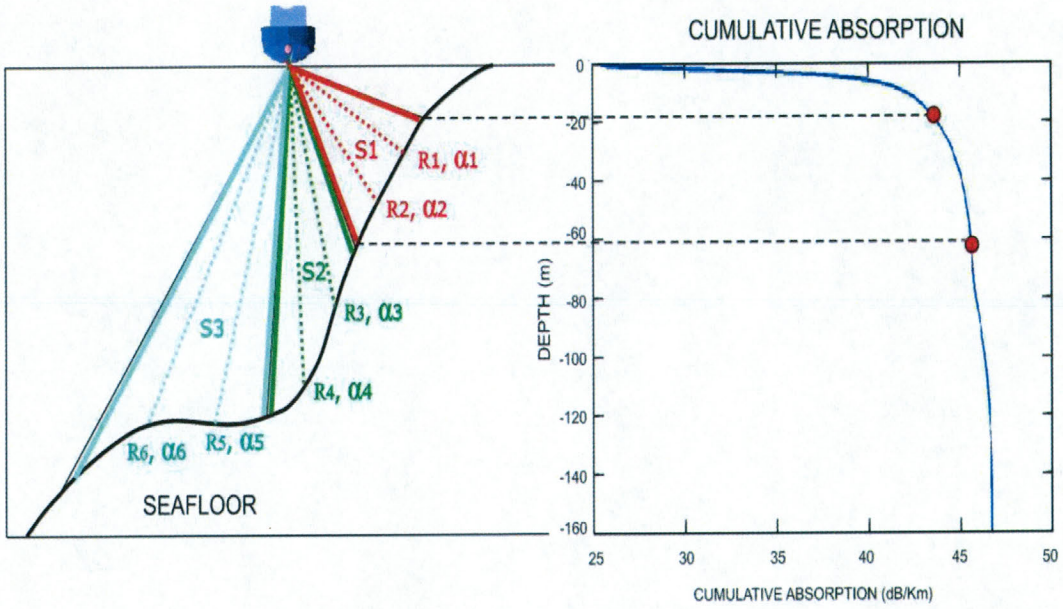

Figure 5.6 – Multi-sector MBES operating in special seafloor geometry. Notice that inside the same sector (same centre frequency) the cumulative absorption varies with depth, as represented by red circles in the plot in the right side.

Based on that limitation and on the several attenuation controls discussed earlier, the proposed methodology comprises the following steps:

1. Ray trace each beam individually inside each different sector (different centre frequency) throughout the several layers of the water column, resulting in one different range for each beam: R_1, R_2 … R_6, as shown in Figure 5.6.
2. Apply Francois and Garrison Equation [1982] to calculate the absorption coefficient *in situ* for each layer of water column.
3. Calculate the cumulative absorption coefficient (α) for each beam (as discussed in Section 3.4), resulting in an individual α for each one (not just by sector as it is currently done): $\alpha 1$, $\alpha 2$ … $\alpha 6$, also shown in Figure 5.6.

4. If the cumulative absorption coefficient for each beam is different from the mean absorption coefficient provided by SIS [Kongsberg Maritime, 2009a and 2010a] for each sector, the difference is used to calculate the gain correction in dB (based on the range), which should be applied to the original backscatter strength image (created based on mean absorption coefficient provided by SIS), to generate the corrected backscatter strength image.

Besides that, as commented earlier in Chapter 2, the majority of operations nowadays do not provide temperature and salinity structures. In these cases, assumptions about these water properties have to be done creating errors in attenuation coefficients. Thus, the proposed model, which represents a post processing tool, also allows the MBES operator to utilize an environmental information from a CTD, which is believed to better represents the survey area, to properly compensate backscatter strength data reduced imperfectly for attenuation. The CTD can come from WOD, WOA or any other source and if the extrapolation (of sound velocity or T, S) done by SIS was inappropriate, this allows a proper extrapolation.

Figures 5.7 and 5.8 represent the flowcharts with the current (SIS approaches) and the proposed model, respectively, summarizing their main steps.

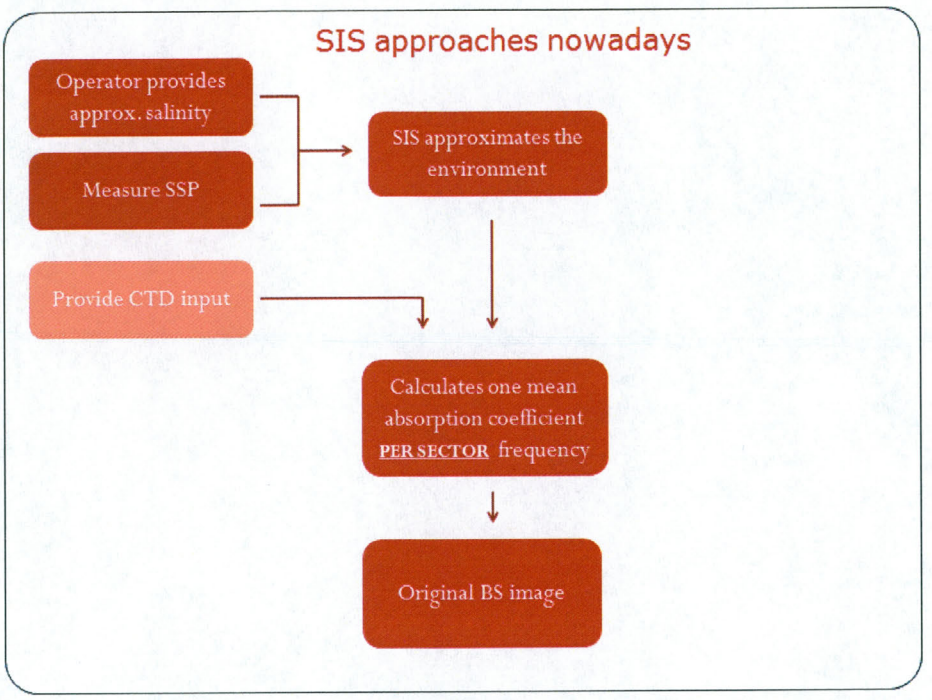

Figure 5.7 – Current model representing SIS approach.

As previously discussed, SIS approaches nowadays (Figure 5.7) are based on providing approximate salinity and measuring sound speed profile to approximate the environment or providing a CTD input. Any one of these options depends on real time availability and correct extrapolation. Once SIS gets the environment, it calculates one mean absorption coefficient per sector frequency, which is going to be applied to the original backscatter strength image.

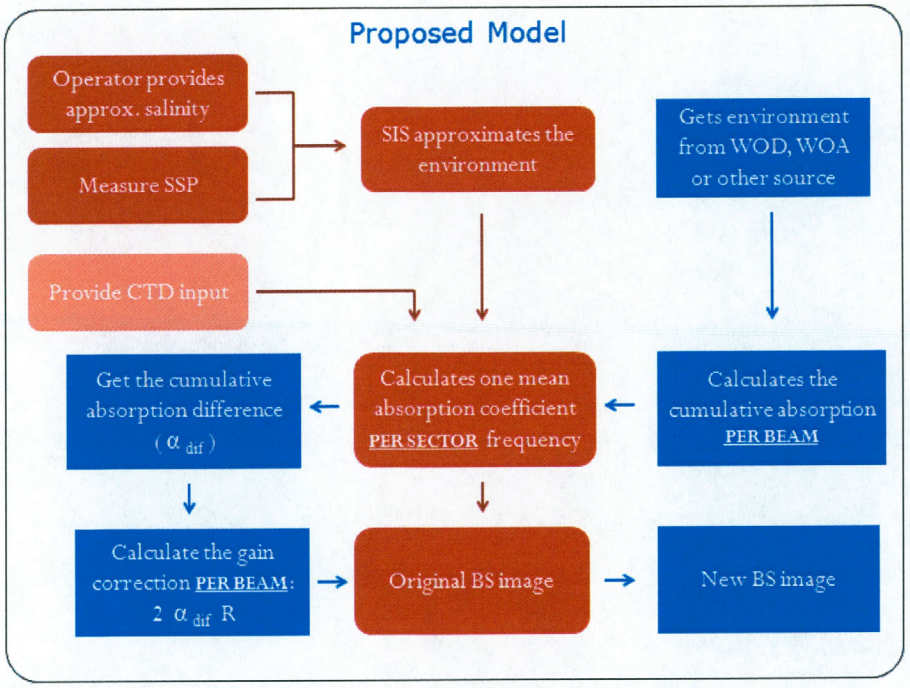

Figure 5.8 – Proposed model.

In the first place, the proposed model (Figure 5.8) gets the environment from WOD (that has a large collection of CTD casts around the world available internationally without restriction) or from the WOA (that is a prediction based on the WOD that provides oceanographic data anywhere in the world using interpolations by distance and time) or any other source. Then, it calculates the cumulative absorption for each beam, compares with the mean absorption coefficient calculated by SIS, getting the cumulative attenuation difference. Finally, it calculates the gain correction (2αR), applies it to the original backscatter strength image, getting the new one.

5.2 Case study: Upper Howe Sound

Two historical surveys done in Upper Howe Sound (British Columbia), shown in Figure 5.9, that had inappropriate attenuation compensation are used to demonstrate the proposed methodology. The first one was collected during the spring 2006 by an EM3002 on CCGS Otter Bay and the other was collected during the winter 2011 by an EM710 (1° x 2°), mounted on a 10 meter launch (CSL Heron). Both surveys used incorrect attenuation values: the EM3002 data were collected using the Kongsberg default value, which seems not to be the most appropriate for Upper Howe Sound; and the EM710 data used attenuation coefficients calculated based on an incorrectly entered average salinity value of 35 ppt, quite different to the right one for the same period, that is usually lower than 32 ppt in that area.

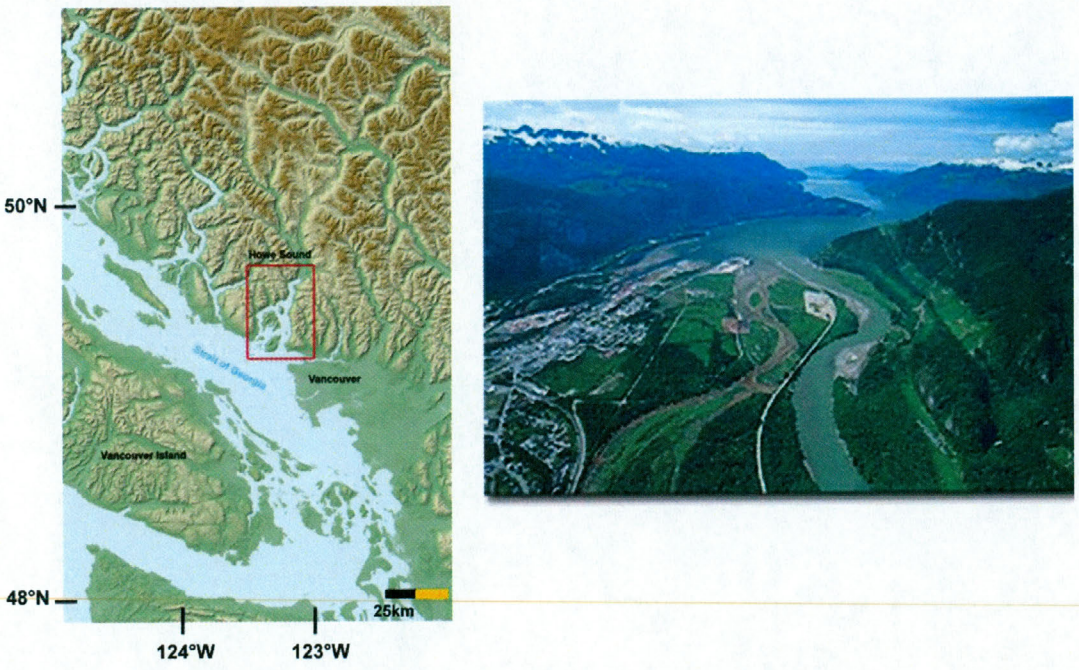

Figure 5.9 – Howe Sound in British Columbia (from [http://www.britishcolumbia.com] (left) and [http://en.wikipedia.org/wiki/Howe_Sound] (right)).

5.2.1 EM3002

As the 300 kHz system has just one sector, it is simpler. No CTD was acquired at the time of survey, only sound speed; and SIS version at time only allowed input of a single attenuation value.

Figure 5.10 represents the Howe Sound map (left) and the zoom in done in the survey line collected from 8 to 140 m deep and the three closest CTD available in the WOD for this time of the year in this area (right), indicated by red circle.

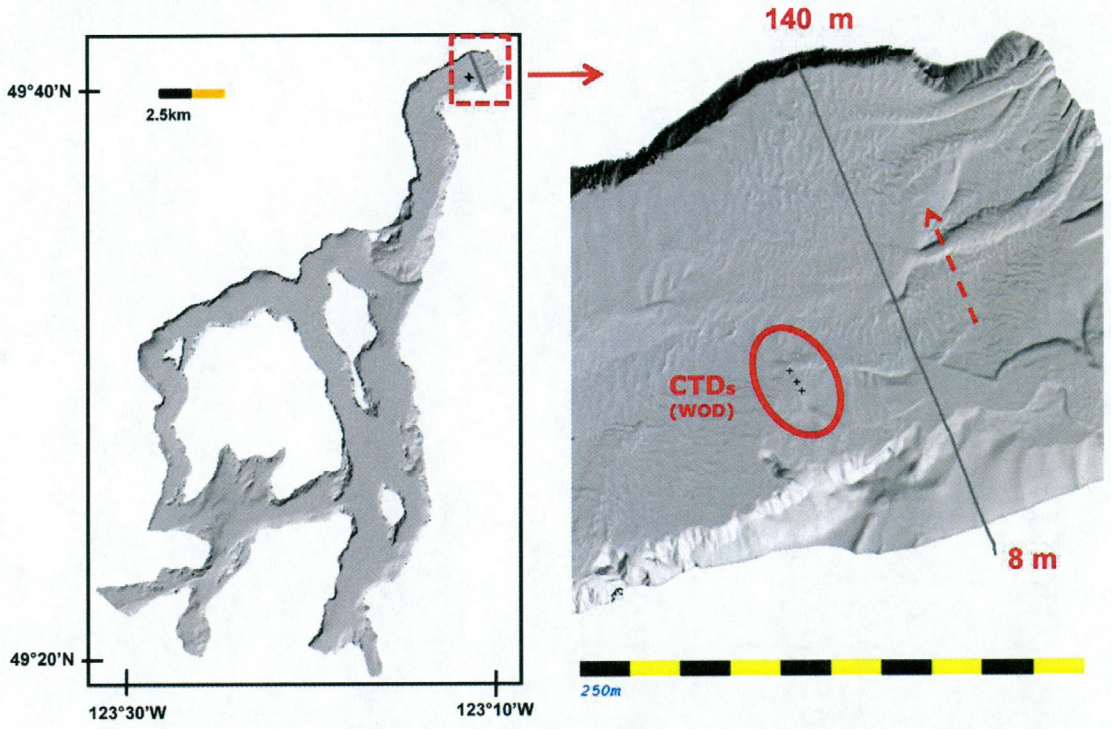

Figure 5.10 – Howe Sound map (left), survey line collected from 8 to 140 m deep and the three closest CTD available in the WOD (right).

If we are going back to correct all data, we have to be very careful when selecting the new profile to apply. Figure 5.11 shows an EM3002 original backscatter data (left hand), collected from 8 to 140 m, and corrected based on the proposed methodology by

two quite different profiles (Figure 5.12) selected for the same period and location from different data sources: WOA and WOD, centre and left hand images, respectively. It is important to highlight that WOD is observations in that month (but some other years) and that WOA is a spatial interpolation of all data in that month. Notice that in both these gain correction images (GCI) we can visualize the depth and incidence angle dependence, as the gain is slant range dependent. Gain corrections to be applied to the original backscatter strength image are smaller in shallower waters and for nadir beams and are greater in deeper waters and for outer beams. Furthermore, in both cases, gain corrections are negative, which means that the original backscatter strength image was over compensated by TVG.

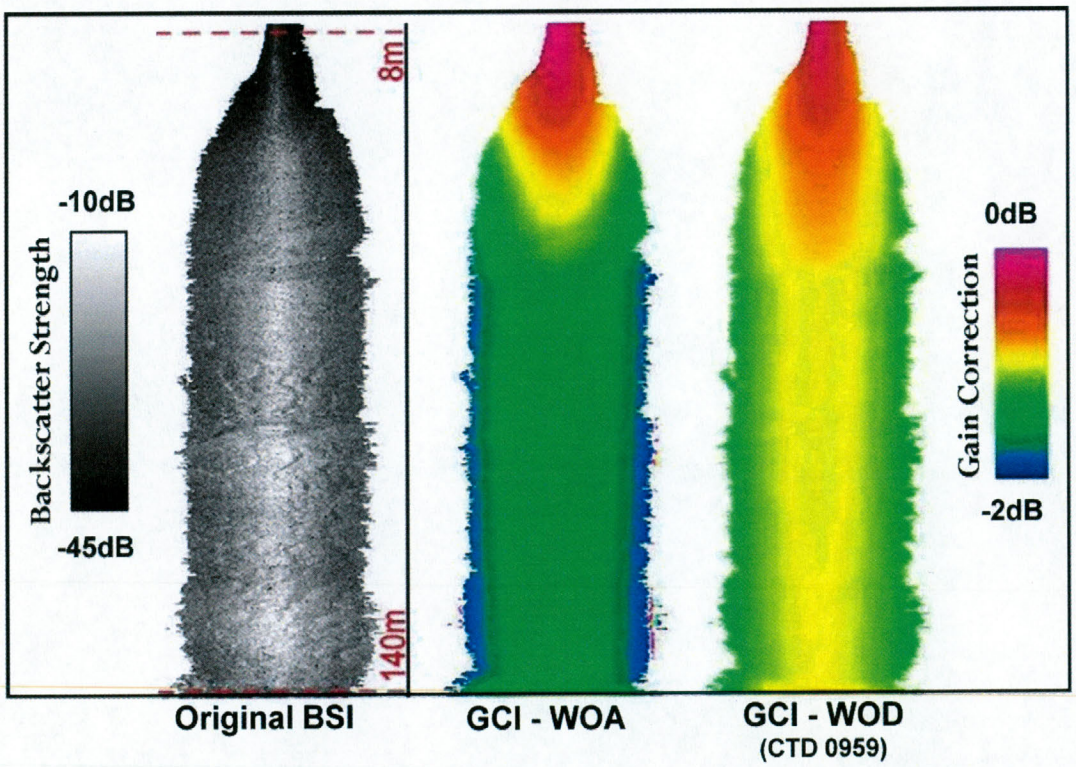

Figure 5.11 – EM3002 original BS image (left) and the gain correction in dB to be applied to the original BS image based on WOA (centre) and WOD (right) oceanographic data selected for the same period and location.

Figure 5.12 shows *in situ* and cumulative absorption plots for 4 oceanographic profiles: one from WOA (in black) and the other three from WOD (in blue, green and magenta). The solid lines represent *in situ* absorption coefficients and dashed lines represent the cumulative absorptions. Notice that the three WOD profiles, actually collected in Upper Howe Sound [Conkright et al., 2002], are very close to each other, while the WOA profile, generated by interpolations by distance and time [Stephens et al., 2002], has quite different values, generating quite different gain corrections (Figure 5.11, centre) when compared to the image represented in the right on Figure 5.11, which was calculated based on WOD CTD profile number 0959 (Figure 5.12, in blue). This clearly illustrates the danger of using interpolated oceanographic climatologies in coastal waters where distinct water masses exist and can change dramatically between discrete coastal embayments. Besides that, it is very important to emphasize that trying to correct this after the fact is only worthwhile if the profile we are correcting with is better than the original observation.

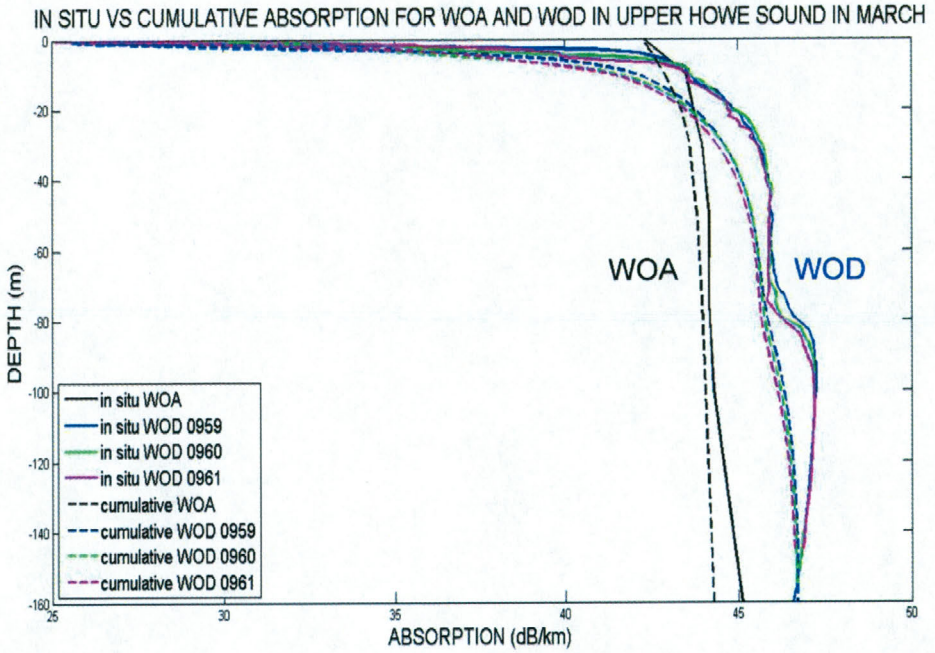

Figure 5.12 – *In situ* and cumulative absorption plots for 4 oceanographic profiles: one from WOA (in black) and the other three from WOD (in blue, green and magenta). The solid lines represent *in situ* absorption coefficients and dashed lines represent the cumulative absorptions.

Figures 5.13 and 5.14 show us the cumulative absorption difference between the original value manually input into SIS and the value calculated using the proposed methodology, based on WOD CTD profile 0959, for the nadir beams and outer beams at 45° launch angle, respectively. Notice that in both Figures the variations in cumulative absorptions are greater in the first layers (represented in green), where most oceanographic variation occurs, getting more stable with depth due to both more stable water mass and the integration approach used to calculate the "cumulative" value. Gain corrections that should be applied to the original backscatter strength image are represented in cyan and we can clearly notice that gain increases with range, represented in magenta, highlighting its range dependence relationship.

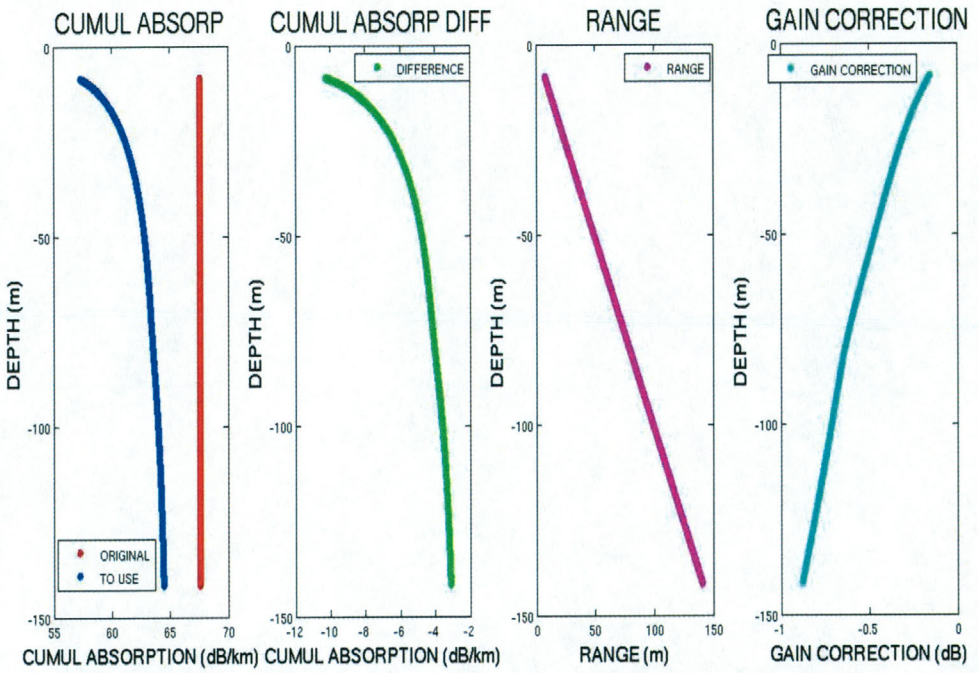

Figure 5.13 - EM3002 corrections for nadir beams considering the WOD CTD profile number 0959. Red represents the mean absorption coefficient calculated by SIS and applied to the original BS image shown in Figure 5.11 (left); blue represents the cumulative absorption calculated by new methodology and green represents the difference between them. Magenta represents the nadir beam range and cyan shows the gain correction that should be applied to those beams.

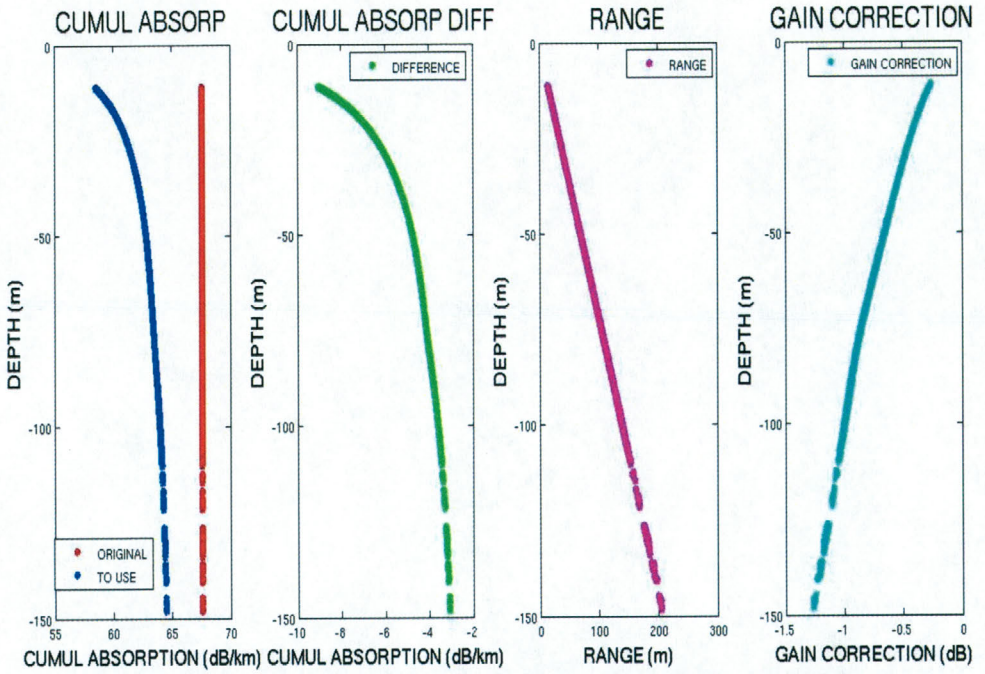

Figure 5.14 - EM3002 corrections for outer beams at 45° launch angle considering the WOD CTD profile number 0959. Red represents the mean absorption coefficient calculated by SIS and applied to the original BS image shown in Figure 5.11 (left); blue represents the cumulative absorption calculated by new methodology and green represents the difference between them. Magenta represents the outer beam range and cyan shows the gain correction that should be applied to those beams.

Figure 5.15 shows the original and the final backscatter strength images after applying the proposed methodology. Images A and C represent the original backscatter strength in grayscale and in color, respectively; and images B and D represent the final backscatter strength also in grayscale and in color, respectively. As we can notice, in both grayscale and color images, it is very difficult to distinguish the difference between them, as the 1-2dB gain correction is barely noticeable over the 35dB of dynamic range from black to white (or from blue to purple, in color images). It is subtle and will only affect precise sediment classification, not the gross appearance of the images.

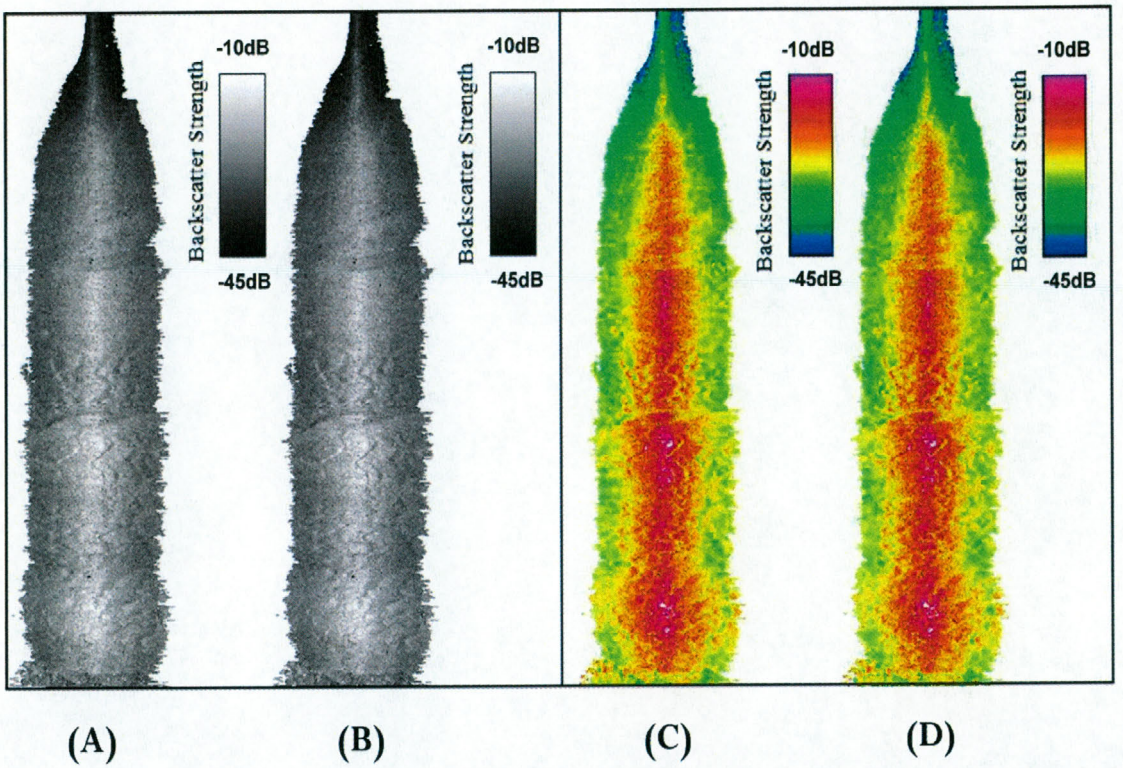

Figure 5.15 - Images A and C represent the original BS image in grayscale and in color, respectively; and images B and D represent the final BS image also in grayscale and in color, respectively.

On the other hand, when we plot the angular response curves we can clearly notice the difference between the original and the corrected backscatter strength images (Figure 5.16). Notice once again that the gain corrections applied to the original backscatter strength image are negative and that they are smaller for nadir beams and greater for outer beams.

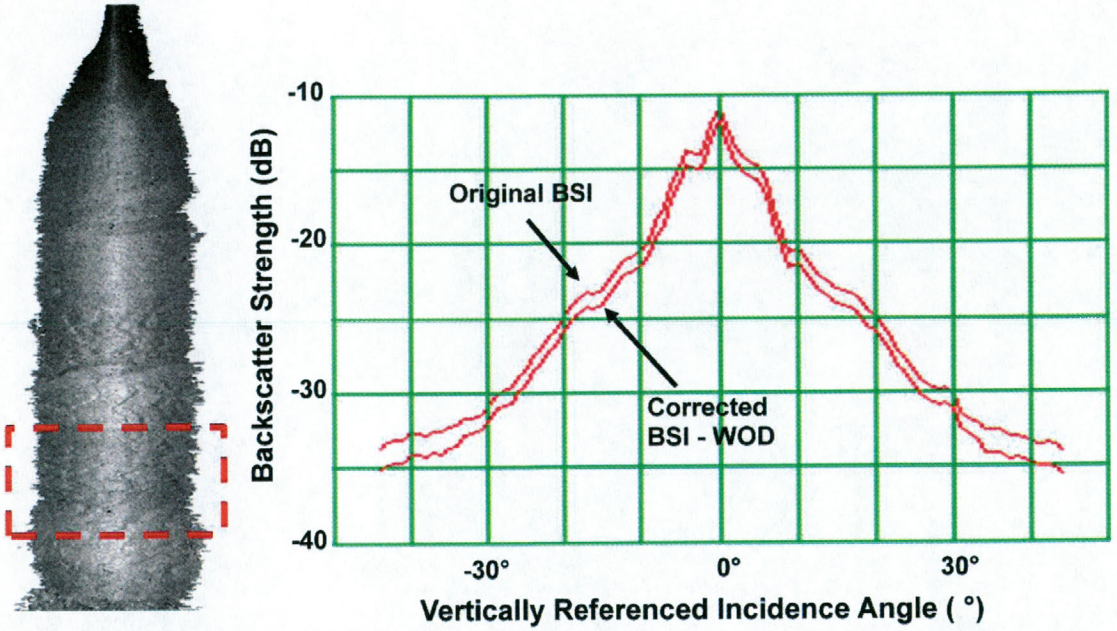

Figure 5.16 - Angular response curves of the original and the corrected BS images represented in Figure 5.15, for the region bounded by the red rectangle (left).

5.2.2 EM710

Unlike the EM3002, the EM710 system is more complex. Instead of a single sector we have several sectors, up to six, that switch through several centre frequencies depending on the operating mode, as shown in Table 5.1 (EM710 dual swath mode).

Dual swath mode

Mode	Depth	Typical total coverage		TX pulse (ms) and frequency (kHz)		
		Deg	Meter	Port	Center	Starboard
Very Shallow	2 -100	140		0.2 ms 73 kHz 81 kHz	0.2 ms 89 kHz 97 kHz	0.2 ms 73 kHz 81 kHz
Shallow	100 – 200	140		0.5 ms 73 kHz 77 kHz	0.5 ms 81 kHz 85 kHz	0.5 ms 73 kHz 77 kHz
Medium	200 – 300	140		2 ms 73 kHz 75 kHz	2 ms 77 kHz 79 kHz	2 ms 73 kHz 75 kHz
Deep	300 500	140 136	1650 2500	20 ms FM 73 kHz 75 kHz	2 ms 77 kHz 79 kHz	20 ms FM 73 kHz 75 kHz

Very Deep and Extra Deep modes does not support dual swath.

Table 5.1 – EM710 dual swath mode overview (from [Kongsberg, 2010b]).

For the example used here, while a CTD was used for 0-30m, no extrapolation was available. The sound speed was extrapolated (erroneously using default Northeast Atlantic values) and the attenuation coefficient calculated by inversion, erroneously assuming 35 ppt.

Figure 5.17 represents the Howe Sound map and the survey line collected from 36 to 280 meters deep (left) and the zoom in (at right) in that same map representing the end of the survey line at 280 meters and the only CTD available in the WOD for this area in this month, indicated by the red circle.

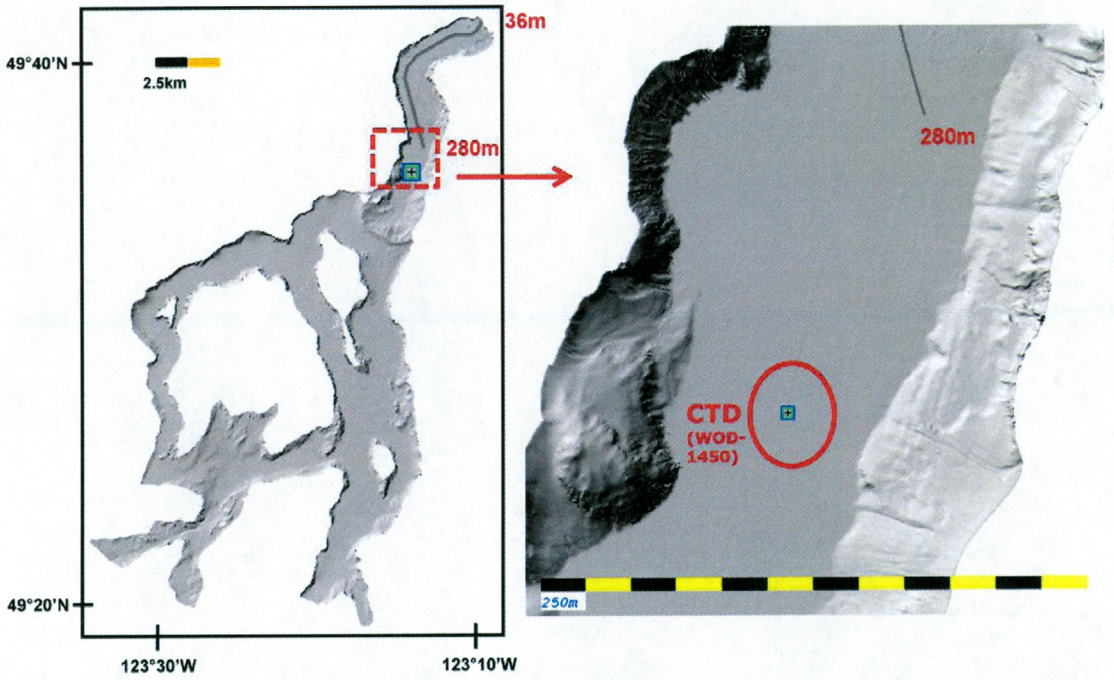

Figure 5.17 – Howe Sound map and the survey line collected from 36 to 280m deep (left) and the zoom in (at right) in that same map representing the end of the survey line at 280m and the only CTD available in the WOD for this area in this period.

Figure 5.18 shows an EM710 original backscatter strength data (left), collected from 36 to 280 m, and the corrections required by using the WOD CTD profile number 1450 that we believe better represents the Upper Howe Sound surveyed area at that time (January 2011). Notice the GCI in the centre and the zoom in (at right) in that figure at the boundary where the EM710 switches from shallow mode (100 to 200 m, Table 5.1) to medium mode (200 to 300 m, also in Table 5.1). Now, besides the depth and grazing angle dependence, we can even notice the distinct gain corrections applied to the differing frequencies in the inner and outer sectors, and to the first and second swaths of the dual ping system (horizontal light and dark stripes along the image at right, consecutively) and to the change in mode at 200 m (shallow to medium). Furthermore,

once again, the gain corrections are negative, which means that the original backscatter strength image was over compensated by TVG.

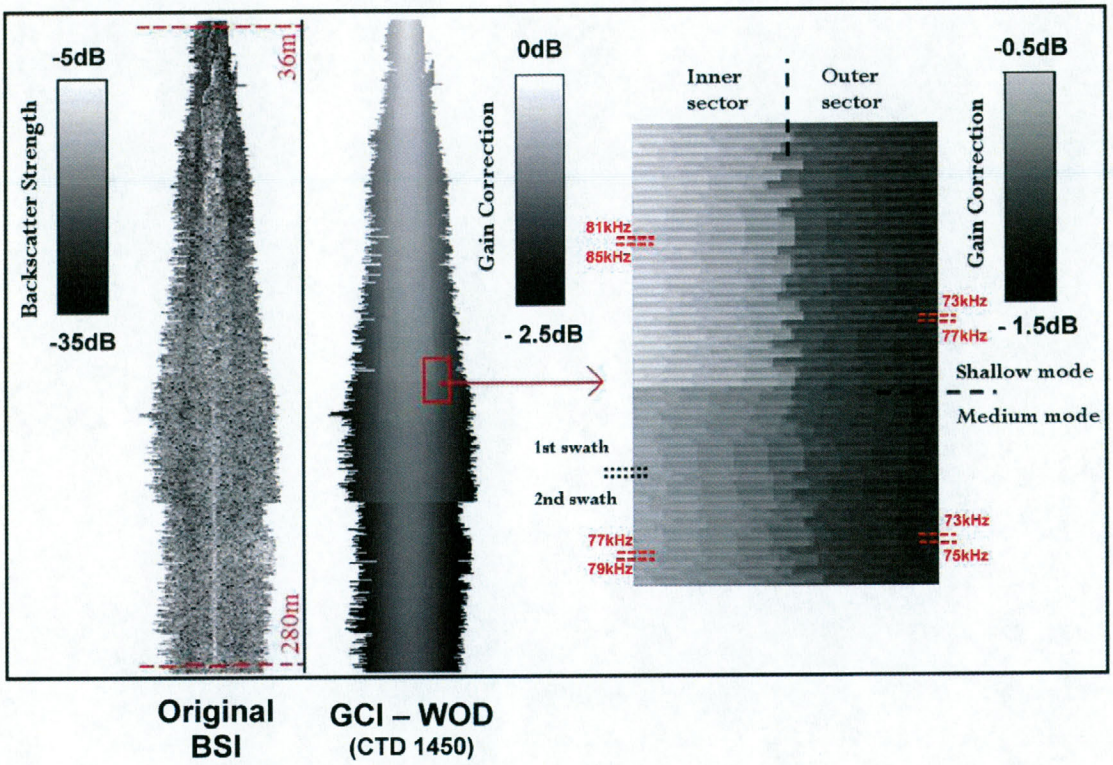

Figure 5.18 - EM710 original BS image (left), the gain correction image in dB (centre) and the zoom in of the boundary where EM710 switches from shallow to medium mode (right).

Figures 5.19 and 5.21 show us the cumulative absorption differences between the original values calculated by SIS and the values calculated using the proposed methodology for each different centre sector frequency detected. The nadir beams are shown in Figure 5.19 and for the outer beams at a 60° launch angle are shown in Figure 5.21. Notice that the cumulative absorptions applied by SIS for all centre frequencies are more than 2 dB/km greater than the cumulative values calculated using the new CTD profile, which means that the original backscatter image was over compensated by TVG,

as commented earlier. In addition, observe that, as the sector centre frequency switches according to the operating mode (summarized in Table 5.1 and also signalized in the right side of Figures 5.19 and 5.21), which also depends on the depth, each plot only contains information for specific depth ranges. The dashed lines on these plots highlight the depth boundaries of three EM710 MBES modes: very shallow, shallow and medium.

Figures 5.20 and 5.22 represent the nadir beams at 77, 81 and 89 kHz sector centre frequencies and outer beams (60° launch angle) at 73 kHz sector centre frequency, respectively, the cumulative absorption difference (in green) between the values calculated by SIS (in red) and the values calculated using the proposed methodology (in blue), the range (in magenta) and the gain correction (in cyan) that should be applied to the original backscatter strength image. Analyzing these plots, once again, we visualize the range dependency.

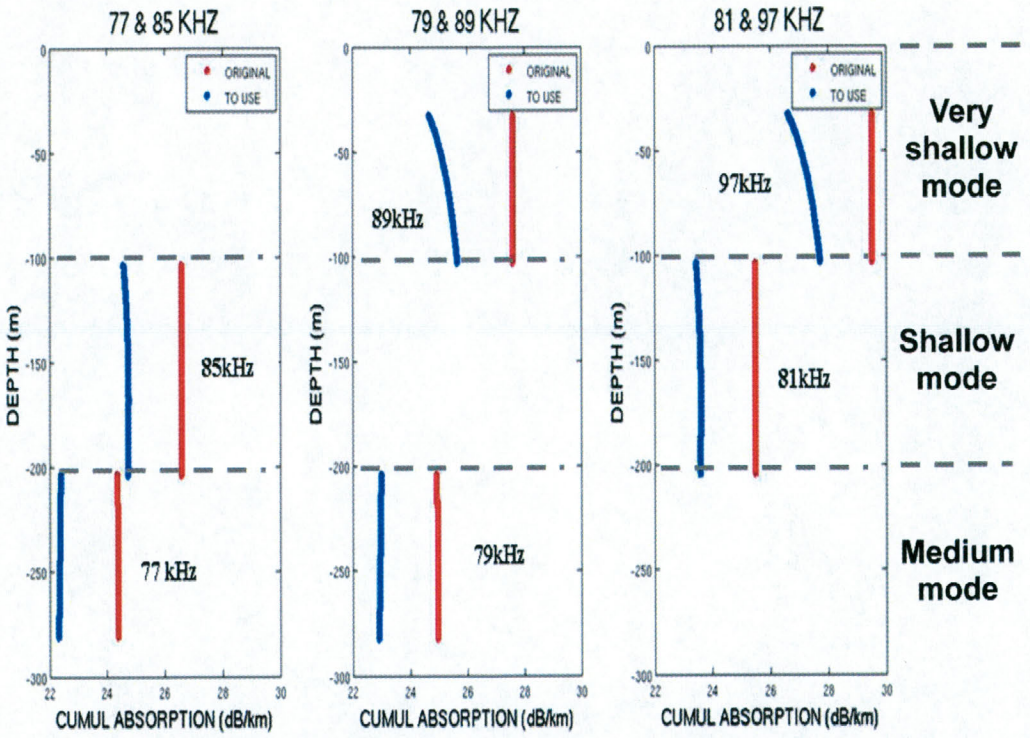

Figure 5.19 - Cumulative absorption calculated by SIS (in red) and the one calculated using the proposed methodology (in blue) for detected centre frequencies: 77 and 85kHz (left); 79 and 89kHz (centre); 81 and 97kHz (right), considering only nadir beams. The dashed lines highlight the depth boundaries of three EM710 MBES modes: very shallow, shallow and medium.

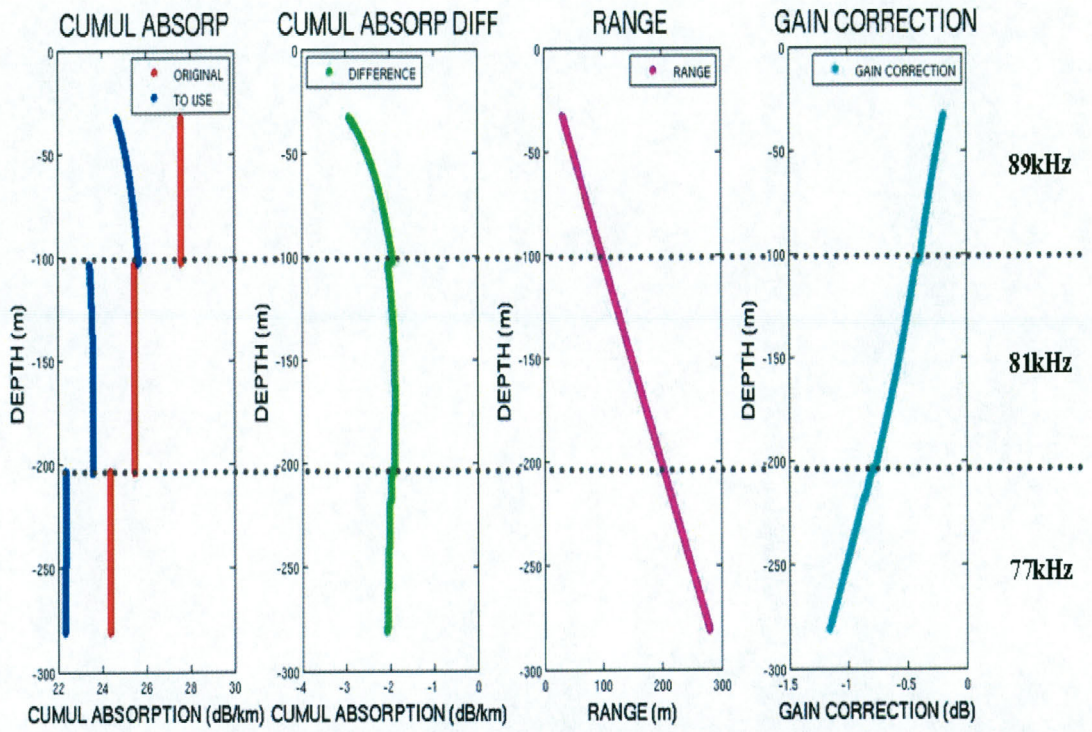

Figure 5.20 - EM710 corrections for nadir beams for detected centre frequencies 77, 81 and 89 kHz. Red represents the original mean absorption coefficient calculated by SIS and applied to the original BS image shown in Figure 5.18 (left); blue represents the cumulative absorption calculated by new methodology and green represents the difference between them. Magenta represents the nadir beams range and cyan shows the gain correction that should be applied to them, also representing its range dependence.

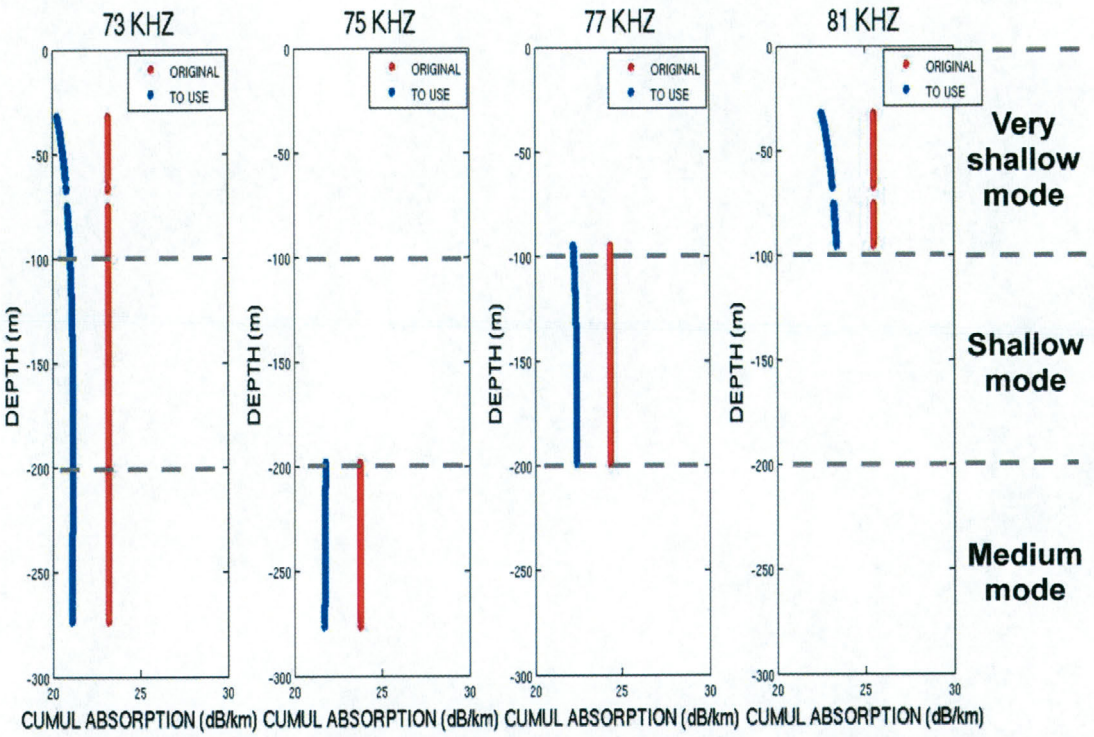

Figure 5.21 - Cumulative absorption calculated by SIS (in red) and the one calculated using the proposed methodology (in blue) for detected outer beam frequencies: 73, 75 and 77 and 81 kHz considering only outer beams at 60° launch angle. The dashed lines highlight the depth boundaries of three EM710 MBES modes: very shallow, shallow and medium.

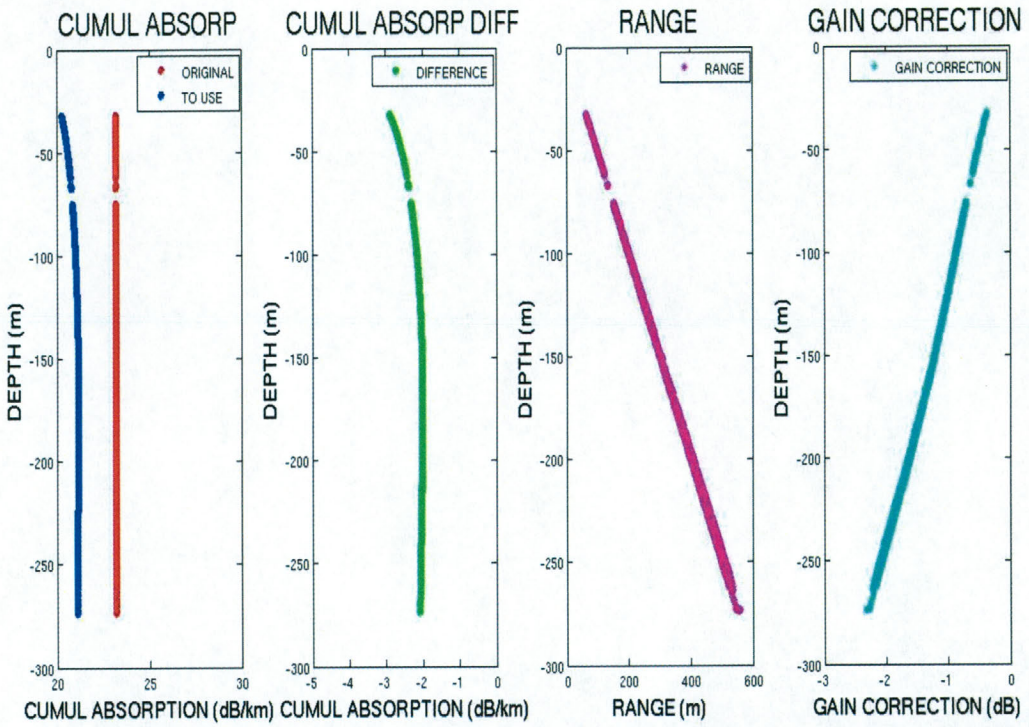

Figure 5.22 - EM710 corrections for outer beams (launch angle 60°) and detected centre frequency 73 kHz. Red represents the mean absorption coefficient calculated by SIS and applied to the original BS image shown in Figure 5.18 (left); blue represents the cumulative absorption calculated by new methodology and green represents the difference between them. Magenta represents the outer beams range and cyan shows the gain correction that should be applied to them, also representing its range dependence.

In the same way it was presented earlier for EM3002, Figure 5.23 shows the original and the final backscatter strength images after applying the proposed methodology. Images A and C represent the original backscatter strength in grayscale and in color, respectively; and images B and D represent the final backscatter strength also in grayscale and in color, respectively. Once again, as we can notice in both grayscale and color images, it is very difficult to distinguish the difference between them, as the 1-2.5dB gain correction is barely noticeable over the 30dB of dynamic range from black

to white (or from blue to purple, in color images). It is subtle and will only affect precise sediment classification, not the gross appearance of the images.

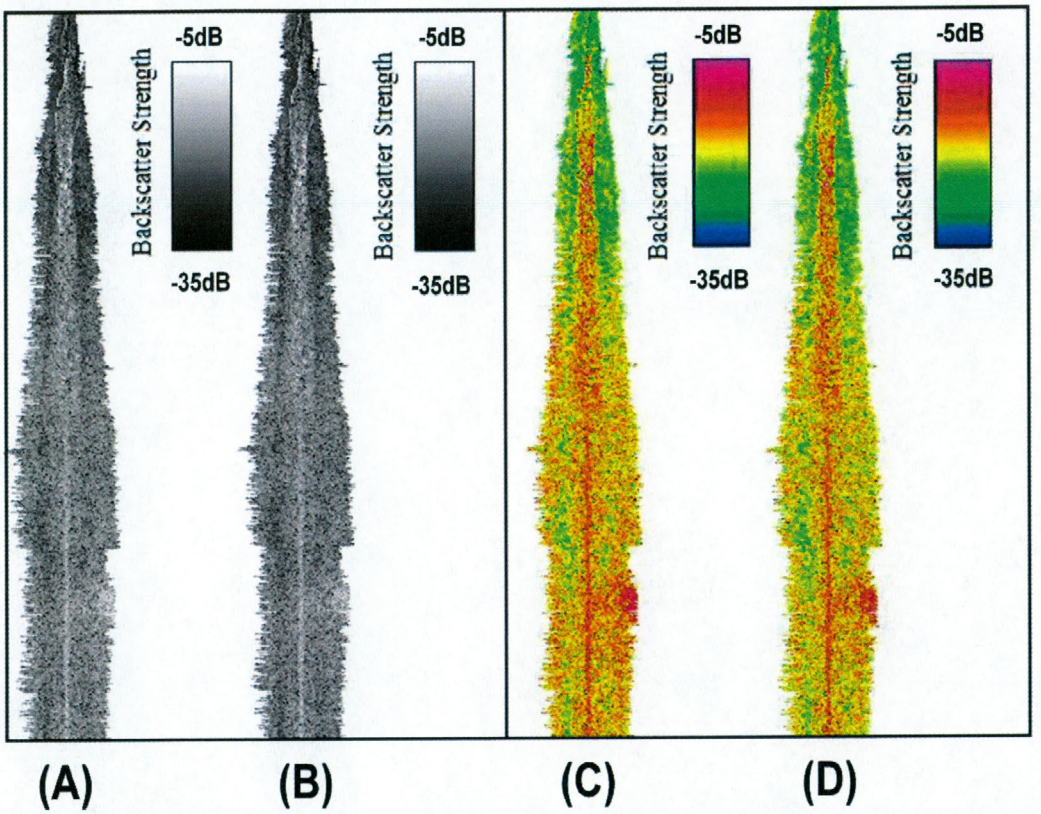

Figure 5.23 - Images A and C represent the original BS image in grayscale and in color, respectively; and images B and D represent the final BS image also in grayscale and in color, respectively.

On the other hand, when we plot the angular response curves we can clearly notice the difference between the original and the corrected backscatter strength images (Figure 5.24). Notice once again that the gain corrections applied to the original backscatter strength image are negative and that they are smaller for nadir beams and greater for outer beams.

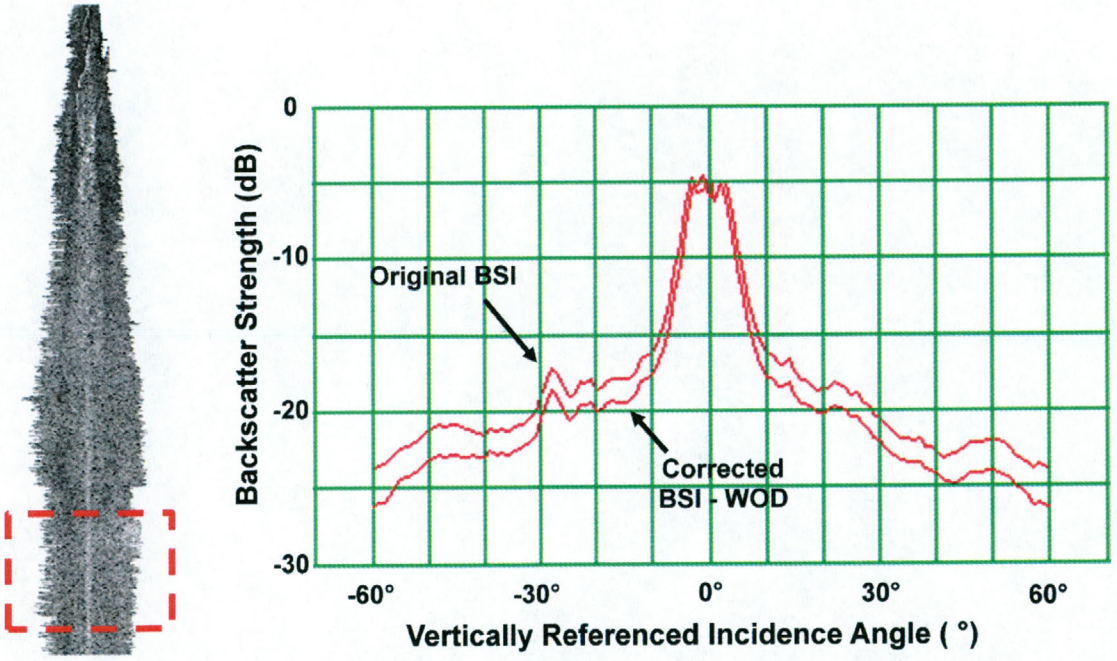

Figure 5.24 - Angular response curves of the original and the corrected BS images represented in Figure 5.23, for the region bounded by the red rectangle (left).

Finally, this research represents an effort toward better calibrated backscatter strength measurements. As a practical example of the importance of a precise attenuation coefficient, let's consider we are surveying an area which seabed type is medium sand, using a 70kHz system. If we do not apply the gain corrections discussed earlier: about -1dB for nadir beams and about -2.5dB for outer beams, instead of the dashed green curve represented in Figure 5.25, the measured backscatter strength signature is going to be between the two solid green curves represented in Figure 5.26. In this case, there will be a family of curves that it can be on, as shown in Figure 5.27, and we may commit a mistake classifying that seabed type (medium sand) as coarse sand or very fine sand.

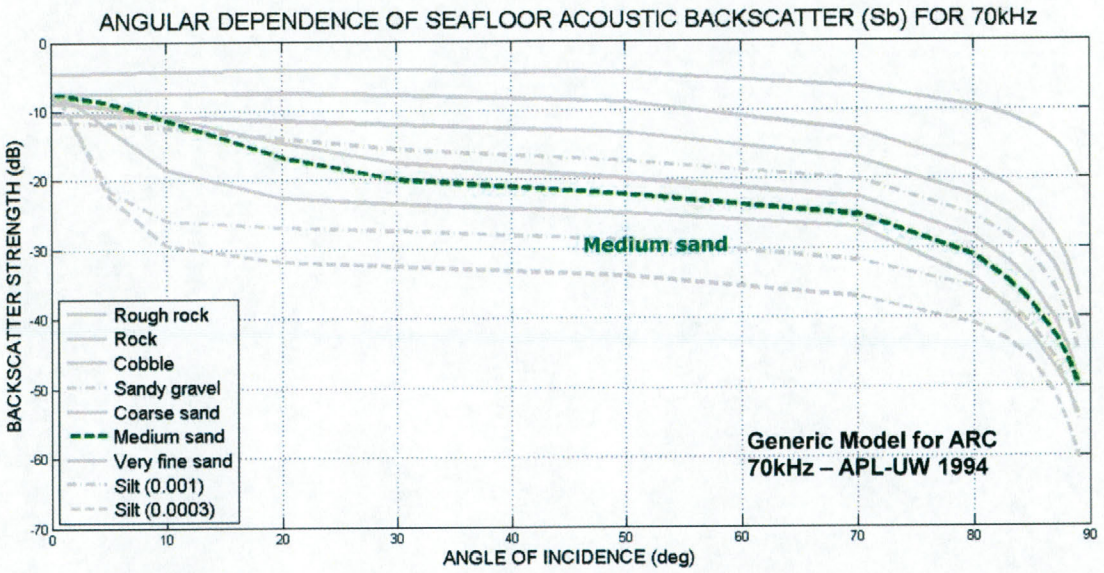

Figure 5.25 – Backscattering model for 70kHz developed by Applied Physics Laboratory (APL) at University of Washington, based on a compilation of calibrated BS observations, highlighting the medium sand ARC (modified from [APL, 1994]).

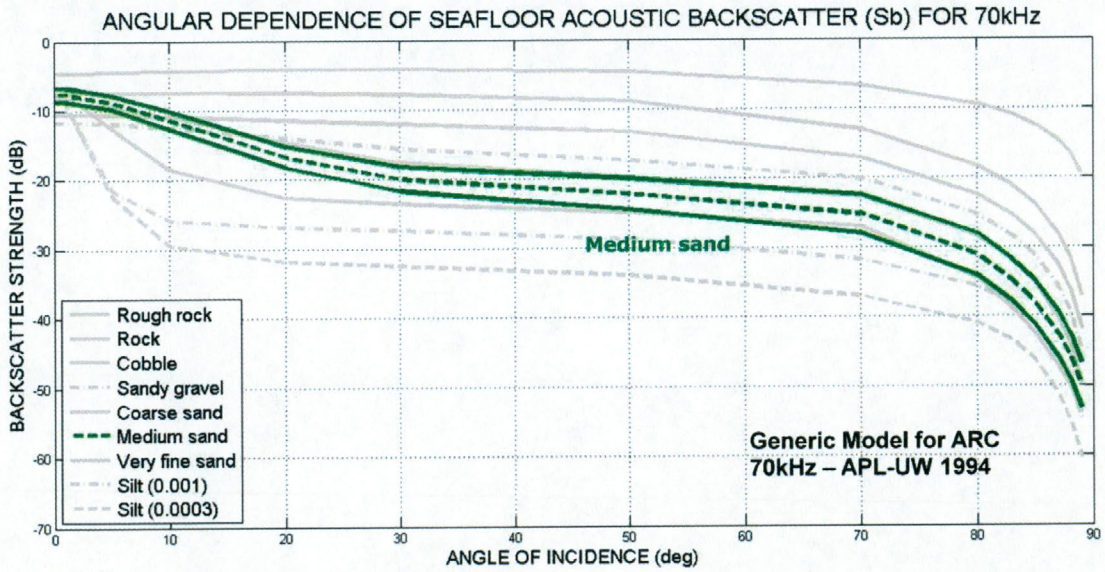

Figure 5.26 – Limits of medium sand ARC (represented by the solid green curves) if not applied the proper gain corrections: about 1dB for nadir beams and 2.5dB for outer beams.

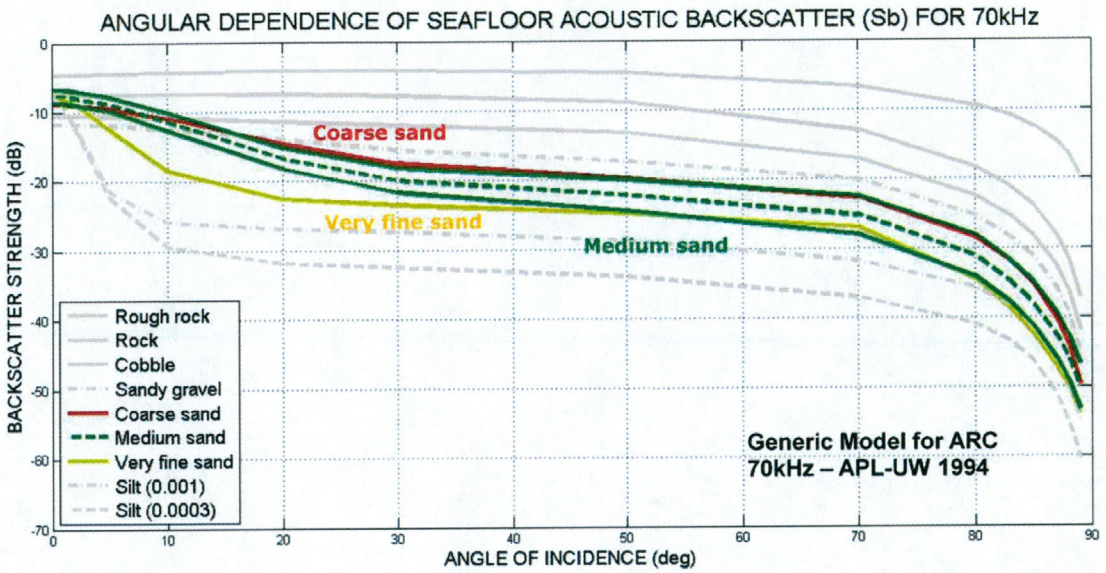

Figure 5.27 – A family of curves that the seabed type can be on if not applied the proper gain corrections.

Chapter 6: THE NEW OMG ATTENUATION CORRECTION ALGORITHM

To implement the proposed methodology to reaply attenuation in multi-sector multi-frequency multi-swath multibeam echo sounders as a post processing tool, a new software module has been developed as part of this research: ***r_atten.c/h***, and some modifications to the original OMG software were also necessary to accommodate this new model.

The original OMG software has two packages: ***getBeamPattern*** and ***makess*** (and functions contained in ***Echo_calib.c*** and ***Echo_calib.h***), which can be divided in 2 parts [Teng, 2012]:

1. **getBeamPattern**: beam pattern calculation software, which is used to determine the backscatter strength fluctuation for the single sector Sidescan or multibeam. The pattern is derived with respect to the vertically referenced incidence angle (VRIA).
2. **makess:** backscatter registration software to combine the individual beam trace data into a horizontal range image. It also can be combined with a beam pattern correction file (from ***getBeamPattern***) to adjust the backscatter strength as a function of VRIA.

Before Teng [2012], these two packages were just suited for single sector and single swath systems, such as MBES EM3002. During his research, the OMG software

has been changed to handle beam pattern issues in multi-sector multi-frequency multi-swath multibeam echo sounders.

6.1 Algorithms developed

The new software module developed during this research (***r_atten.c/h)*** allows the MBES operator to utilize an environmental information from a CTD to properly compensate backscatter strength data reduced imperfectly for attenuation. It comprises the following steps:

1. Based on the CTD provided by the operator and on the sonar sector centre frequency considered, it calculates the *in situ* absorption coefficient, based on Francois and Garrison equation (presented earlier in Chapter 3), for each sampled layer of the whole water column provided by the CTD.
2. Next, it calculates the cumulative absorption coefficient, discussed in Chapter 3, also for each sampled layer of the water column provided. Note it is specific for the vessel draft because any water mass variability above that has no effect.
3. Based on the depth considered for each beam, the algorithm calculates the cumulative absorption coefficient for that certain depth interpolating the cumulative absorption coefficient values of the layers immediately above and below. The output value is the new cumulative attenuation that we should use for each beam. * Note that for the first two swaths in a file, typically 6-8 sector centre frequencies will be identified and thus 6-8 indexed cumulative

curves will be generated. Thereafter, unless the sonar switches mode, these curves will just be reused.

4. Once known, the new cumulative attenuation that we should use for each beam is subtracted from the mean absorption coefficient provided by SIS for each sector centre frequency for the average depth of the beams in that sector for that ping. This information is contained in "raw range and angle 78" datagram for the new multibeam echo sounder models [Kongsberg Maritime, 2009b], shown in Table 6.1. In this manner the cumulative attenuation difference for each beam ($\Delta\alpha_{cum}$) can be calculated.

Data Description	Format	Valid range	Note
Number of bytes in datagram	4U	—	—
Start identifier = STX (Always 02h)	1U	—	—
Type of datagram = N (4eh, 78d)	1U	—	—
EM model number (Example: EM 710 = 710)	2U	—	—
Date = year*10000 + month*100 + day (Example: Sep 26, 2005 = 20050926)	4U	—	—
Time since midnight in milliseconds (Example: 08:12:51.234 = 29570234)	4U	0 to 86399999	—
Ping counter (sequential counter)	2U	0 to 65535	—
System serial number	2U	100 –	—
Sound speed at transducer in 0.1 m/s	2U	14000 to 16000	—
Number of transmit sectors = Ntx	2U	1 –	—
Number of receiver beams in datagram = Nrx	2U	1 –	—
Number of valid detections	2U	1 –	—
Sampling frequency in Hz	4F	—	—
Dscale	4U	—	5
Repeat cycle 1 - Ntx entries of:	24*Ntx	—	—
Tilt angle re TX array in 0.01°	2S	-2900 to 2900	6
Focus range in 0.1 m (0 = No focusing applied)	2U	0 to 65534	—
Signal length in s	4F	—	—
Sector transmit delay re first TX pulse, in s	4F	—	—
Centre frequency in Hz	4F	—	—
Mean absorption coeff. in 0.01 dB/km	2U	—	—
Signal waveform identifier	1U	0 to 99	1
Transmit sector number / TX array index	1U	—	7
Signal bandwidth in Hz	4F	—	—
End of Repeat cycle 1			

Table 6.1 – The "raw range and angle 78" datagram for the new multibeam models. The red rectangle highlights the mean absorption coefficient provided by SIS for each sector centre frequency [Kongsberg Maritime, 2009b].

5. Then, the gain correction (in dB) is calculated by multiplying the cumulative attenuation difference (in dB/km) by twice the range (in km): $2 * \Delta\alpha_{cum} * R$, considering the round trip.
6. That gain correction value is going to be used in the two OMG packages: ***getBeamPattern*** and ***makess***. In ***getBeamPattern,*** it is going to be used to compensate the angular response curves of the original backscatter strength data reduced imperfectly for attenuation, creating a new "beampatt". In ***makess***, more specifically in ***Echo_calib.c*** and ***Echo_calib.h,*** it is going to be used to compensate the original backscatter strength images, creating the new ones applying these new gain corrections.

Besides the standard processing sequence, two other functions have been implemented in this package (also in ***Echo_calib.c*** and ***Echo_calib.h***) for explanatory and testing purposes: "show_atten_shift" and "show_recalc_atten". The first one provides us gain correction images like the ones presented earlier in Figures 5.11 (centre and right) and 5.18 (centre and right), showing us the different gain corrections that should be applied to the original backscatter strength images (Figures 5.11 and 5.18, in the left hand for both) based on the CTD provided by the MBES operator. These gain correction images allow us to clearly visualize the depth and incidence angle dependence: in a regular seafloor (close to flat), these gain corrections should be smaller in shallow waters and nadir beams; and greater in deeper waters and outer beams, as it is range dependent. Besides that, as attenuation is frequency dependent, the gain corrections applied to the different sectors and swaths in the new MBES (multi-sector multi-frequency multi-swath)

should be also different (Figure 5.18, right). The second function ("show_recalc_atten") provides us an image with the new cumulative attenuation values calculated by the proposed model for each beam, as shown in Figures 6.1 (for an EM3002, using CTD0959 from WOD) and 6.2 (for an EM710, using CTD1450 from WOD).

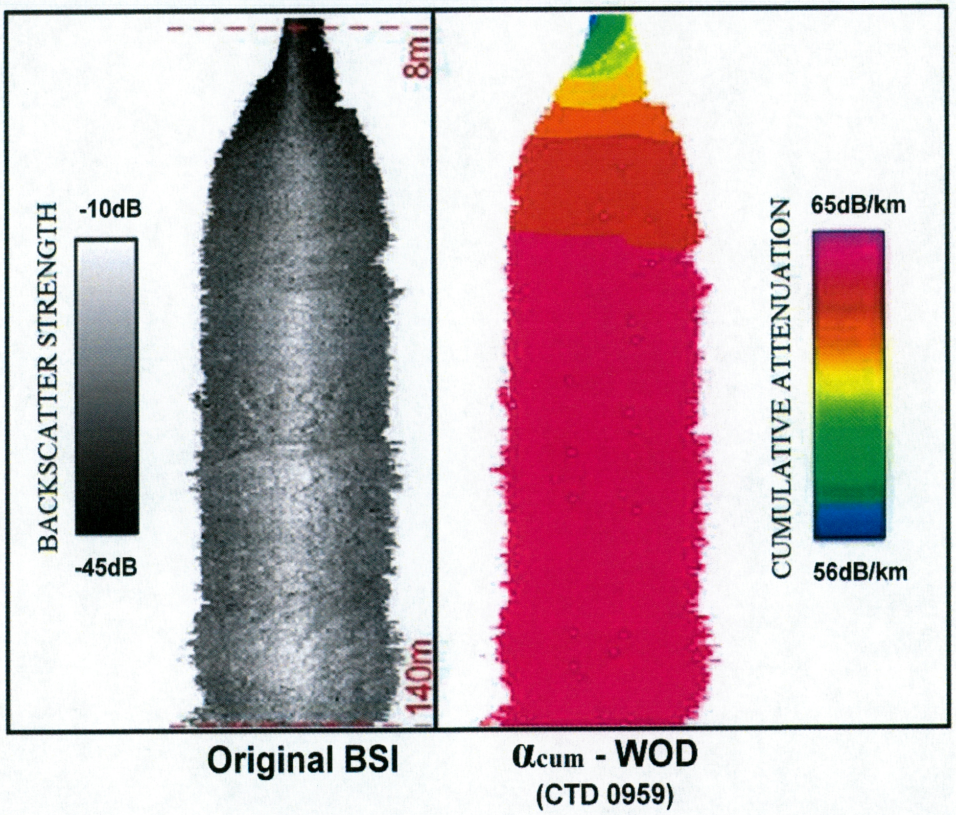

Figure 6.1 – EM3002 original BS image (left) and the cumulative attenuation image, calculated by the proposed model and based on CTD 0959 from WOD (right).

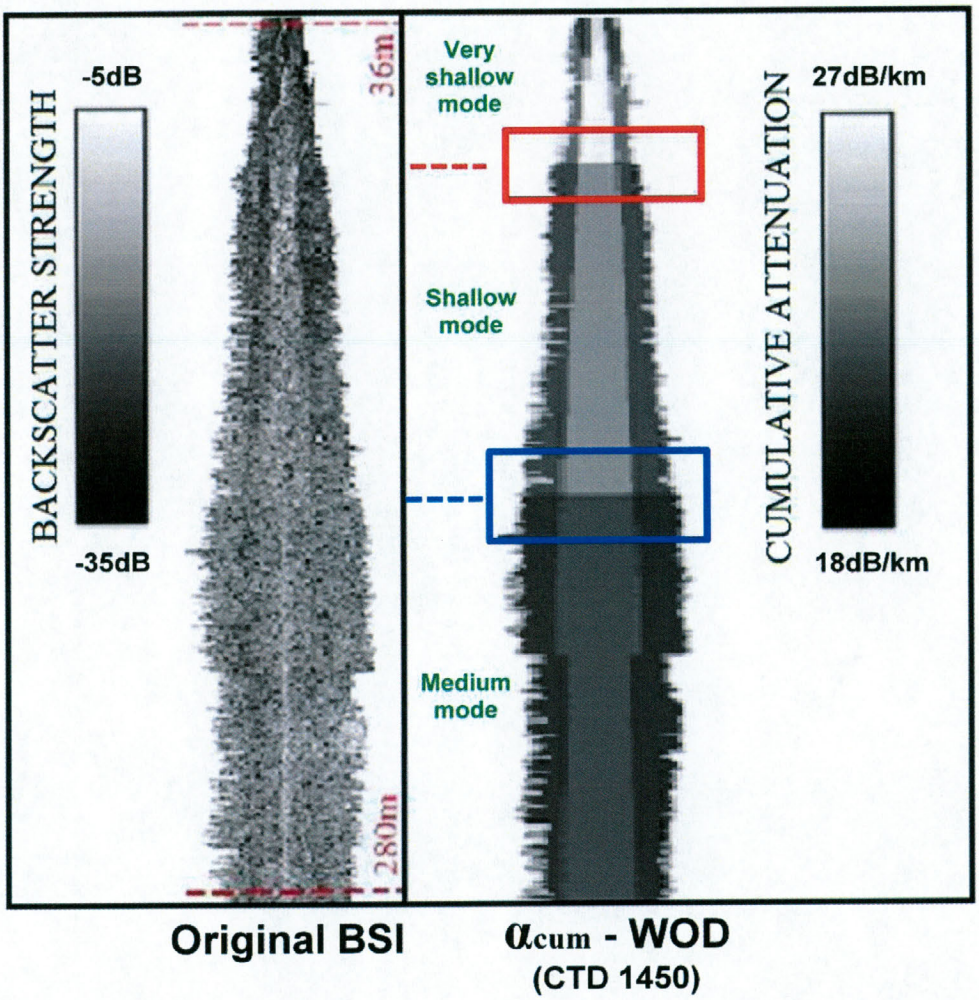

Figure 6.2 - EM710 original BS image (left) and the cumulative attenuation image, calculated by the proposed model and based on CTD 1450 from WOD (right). Boxes indicate mode transitions where centre frequencies are changed.

Notice also in Figure 6.2 that besides the new cumulative attenuation values calculated by the proposed model, we can clearly notice when the system switches from very shallow mode (2-100m depth range) to shallow mode (100-200m depth range), represented by the red rectangle, and from shallow mode to medium mode (200-300m depth range), represented by the blue rectangle. This is due to the change in sector centre

frequencies related to each different mode, as shown earlier in Table 5.1 for EM710 operating in dual swath mode.

Although the new OMG attenuation correction software has been used on specific historical data reduced imperfectly for attenuation for MBES EM3002 and EM710 (Chapters 5 and 6), it can be used in other types of Kongsberg Maritime single sector single swath or multi-sector multi-frequency multi-swath multibeam echo sounders.

Chapter 7: FUTURE APPLICATION IN BRAZILIAN NAVY

The condition of Brazil as an Atlantic country situated in relative proximity to the Antarctic region (it is the seventh closest country), and the influences of natural phenomena that occur there on the national territory, justify the historical Brazilian interest on the southern continent. These circumstances, as well as strategic motivations of geopolitical and economic factors were decisive when the country joined the Antarctic Treaty in 1975, and initiated the Brazilian Antarctic Program (PROANTAR) in 1982. In that same year, the Brazilian Navy acquired the Danish polar ship "Thala Dan", suitable for work in polar regions, receiving the name of Oceanographic Support Vessel (NApOc) "Barão de Teffé", Figure 7.1 (left). Due to the growing demand of science in Antarctica, the Brazilian Navy decided to acquire in 1994, the Norwegian polar ship "Polar Queen", built in 1981, which received the name of NapOc "Ary Rongel", shown in Figure 7.1 (centre). In 2002, the Oceanographic Support Vessel "Barão de Teffé" was decommissioned. Later, on February 3, 2009, the Polar Ship "Admiral Maximiano" was incorporated into Brazilian Navy, shown in Figure 7.1 (right) [Brazilian Antarctic Program, 2012].

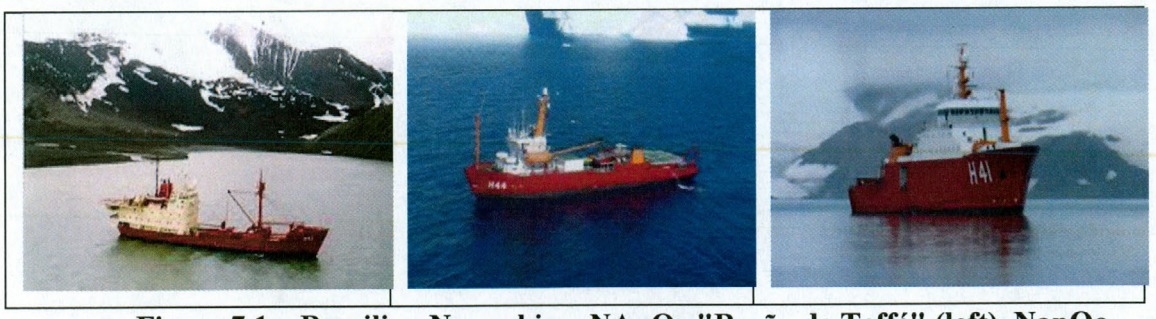

Figure 7.1 – Brazilian Navy ships: NApOc "Barão de Teffé" (left), NapOc "Ary Rongel" (centre) and Polar Ship "Admiral Maximiano" (right).

Since 1982, each year the Brazilian Navy conducts five to six months of Antarctic Operations involving their ships. Generally, the polar ships leave Rio de Janeiro (Brazil) in October/November towards the "White Continent" and returns in March/April of the following year. During that journey, each ship has two long transits from Brazil to Antarctica, as shown in Figure 7.2, with a great potential of collecting hydrographic and oceanographic data along the way.

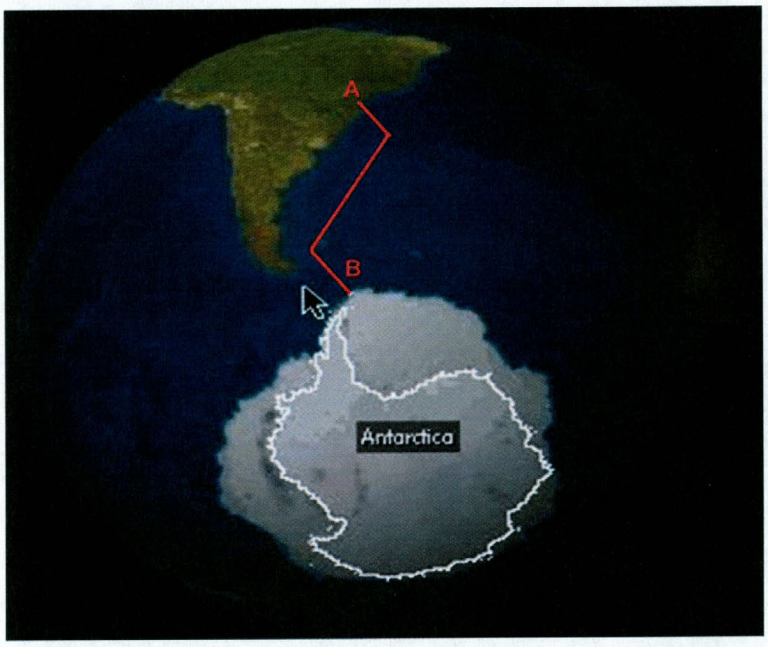

Figure 7.2 – Annual transit (red solid line) of Brazilian polar ships from Rio de Janeiro (A) until Antarctic Station "Comandante Ferraz" (B), Keller Peninsula, Admiralty Bay, King George Island, South Shetland Islands.

Previously, when the polar ships were equipped only with single beam echo sounders (SBES), bathymetric data were acquired during the transit and used in the composition of GEBCO (General Bathymetric Chart of the Oceans). On the other hand, considering that the Polar Ship "Admiral Maximiano" is currently equipped with 30 kHz Kongsberg-Simrad EM302 MBES, Brazilian Navy can expand the products collected

during those extensive transits, once MBES collect oblique soundings, allowing for a remarkable increase in seabed coverage compared to traditional downward looking SBES. Besides that, EM302 MBES can also record water column data and, if properly compensated, provide additional information about the nature of the seafloor, such as seabed type and bottom micro roughness, from backscatter strength images, as discussed in previous chapters.

Similarly to CCGS Amundsen in the ArcticNet Program [Beaudoin, 2010], the "Admiral Maximiano" is equipped with underway sound speed profile instrumentation, but, sometimes, it is not feasible to deploy the instrument while underway due to rough sea (Drake's Passage, between South of Chile and Antarctica Peninsula, is famous for the strong winds and rough seas caused by the intense cold fronts) or ice cover.

Due to the limited ability to systematically sample the water column while in transit, three dimensional gridded oceanographic climatologies of average temperature and salinity values, such as WOA, may be used to provide an average sound speed profile, depending on its sounding uncertainty [Beaudoin, 2010], which should meet the IHO specifications [IHO, 2008]. Besides that, the herein proposed attenuation model represents a post-processing tool to compensate backscatter strength data reduced imperfectly for attenuation using those oceanographic climatologies sources, which can improve the seafloor classification process. Once that process is improved, the number of seabed samples collected with box core, for example, which is ship time consuming, can be reduced, optimizing costs.

Thus, after some years running corridors during the long transits from Brazil to Antarctica with MBES, Brazilian Navy may have enough data for nautical charts,

backscatter strength mosaics and water column models of this remote, partially uncharted area.

The new algorithms developed in this thesis will significantly aid in maintaining the calibration of acoustic backscatter measurements made during transits through the South Atlantic.

Chapter 8: CONCLUSIONS

8.1 Summary

While an imperfect attenuation coefficient has no effect on bathymetry accuracy, it significantly reduces the value of the backscatter strength. As we move towards more precise calibration of backscatter strength to get additional information about the nature of the seafloor, such as bottom type or bottom micro roughness and their respective spatial and temporal homogeneity, the requirement for a precise attenuation coefficient is increasingly important.

The proposed model herein presented is a post processing tool that allows the MBES operator to utilize an attenuation coefficient from a more appropriate CTD, which is believed to be a better representation of the surveyed water mass in the area. The algorithms developed, automatically recognize the frequency, the sector, the swath, the mode, the range and the ray path, calculating the gain correction and applying it to each beam of the original backscatter data, minimizing the fluctuations caused by environmental controls on it, supporting the seafloor characterization process.

Distinguishing mud from rock is easy due to its large backscatter strength difference. However, the more typical challenge of distinguishing muddy sand from sandy mud is challenging as the backscatter strength difference between them is subtle. Similarly, distinguishing changes in surface sediments from winter to summer is usually difficult, because they may be masked by greater oceanographic variability. Thus, as we are particularly interested in monitoring seasonal changes in backscatter strength on the

seafloor of a fjord (Upper Howe Sound) with active turbidity currents, subtle variations of oceanographic properties are very important and must be taken into account [Hughes Clarke et al., 2011].

This thesis is one contribution toward better calibrated backscatter strength measurements. There are, however, other issues to correct, which I believe have a greater impact on backscatter strength images, such as the absolute sonar source level and problems in sectors related to transmitter and receiver beam pattern variations [Teng, 2012].

8.2 Limitations and Recommendations

In terms of oceanographic data collection, as the majority of operations today do not provide temperature and salinity structure, assumptions about these water properties have to be done, creating errors in absorption coefficients and ultimately in bottom backscatter strength. Particularly important for archived datasets, such as in Bay of Fundy surveys [Hughes Clarke et al., 2008] and in Brazilian shelf surveys done by hydrographic ship Taurus [Oliveira Jr., 2007]. This fact is actually a major constraint to determine a proper environmental reduction for attenuation for the new multi-sector multi-frequency multi-swath multibeam echo sounders nowadays.

Besides that, when the MBES operator, using the proposed model herein presented, chooses an oceanographic climatology as a CTD source, such as WOD, WOA or Generalized Digital Environmental Model (GDEM), their choice will depend on the availability of CTD profiles in the databases and on the data coverage of each

climatology for the area and the period of interest. This is the reason why we recommend sending the oceanographic data collected throughout the surveys done around the world annually, by governmental and nongovernmental institutions, to the several centres that control those databases, such as the U.S. National Oceanographic Data Centre (NODC) responsible for WOD and WOA. By increasing those databases, we also improve the data coverage and resolution, thus increasing the fidelity of the climatological mean fields.

On the other hand, once *in situ* measurements are preferable, the main recommendation is that people actually measure CTD profiles or sound velocity and temperature profiles (SV & T), minimizing attenuation errors and in turn backscatter strength errors (fluctuations).

8.3 Future Work

As we are moving toward more precise calibration of backscatter strength to get additional information about the nature of the seafloor, the next two big issues to address are the absolute sonar source level and problems in sectors related to transmitter and receiver beam pattern variations. This has partly been addressed by Teng [2012].

Although designed identically, the sensitivities of transducers and receivers slightly differ even for MBES hardware of the same model (discrepancies between the actual hardware performance and the design), causing apparent backscatter strength changes [Hughes Clarke et al., 2008]. Also grazing angle and ensonified area assumptions need to be removed. The OMG software has a tool called "***deTVG***" which does in part address that.

REFERENCES

Ainslie, M.A., and J.G. McColm (1998). "A simplified formula for viscous and chemical absorption in sea water." *Journal of the Acoustical Society of America*, 103 (3), pp. 1661-1662.

APL (1994). *APL-UW High Frequency Ocean Environmental Acoustic Models Handbook.* Applied Physics Laboratory - University of Washington TR 9407-AEAS 9501, Oct 1994. Seattle, Washington.

Beaudoin, J.D., J.E. Hughes Clarke, E.J.V.D. Ameele, and J.V. Gardner (2002). "Geometric and radiometric corrections of multibeam backscatter derived from Reson 8101 systems." *Proceedings of the Canadian Hydrographic Conference*, Toronto, Canada, 28-31 May, 2002.

Beaudoin, Jonathan (2010). *Estimation of Sounding Uncertainty from Measurements of Water Mass Variability.* Ph.D. dissertation, Department of Geodesy and Geomatics Engineering, Technical Report No. 271, University of New Brunswick, Fredericton, New Brunswick, Canada, 232 pp.

"Brazilian Antarctic Program." [On-line] 30 April 2012. https://www.mar.mil.br/secirm/proantar.htm#histo

Conkright, M. E., J. I. Antonov, O. Baranova, T. P. Boyer, H. E. Garcia, R. Gelfeld, D. Johnson, R. A. Locarnini, P. P. Murphy, T. D. O'Brien, I. Smolyar, C. Stephens, 2002: *World Ocean Database 2001, Volume 1: Introduction.* S. Levitus, Ed., NOAA Atlas NESDIS 42, U.S. Government Printing Office, Wash., D.C., 167 pp., CD-ROMs.

deMoustier, C. (2011). "Fundamentals of Sonar." UNB OMG/UNH CCOM 55th Multibeam Sonar Training Course, Lecture Notes No. 4, New Orleans, United States, 3-8 January, 2011.

Francois, R.E., and G.R. Garrison (1982a). "Sound absorption based on ocean measurements. Part I: Pure water and magnesium sulfate contributions." *Journal of the Acoustical Society of America*, 72 (3), pp. 896-907.

Francois, R.E., and G.R. Garrison (1982b). "Sound absorption based on ocean measurements. Part II: Boric acid contribution and equation for total absorption." *Journal of the Acoustical Society of America*, 72 (6), pp. 1879-1890.

Hammerstad, E. (2000). "EM Technical Note: Backscattering and Seabed Image Reflectivity." Kongsberg Technical Documentation.

"Hawaii Ocean Timeseries." [On-line] 24 July 2011. http://www.soest.hawaii.edu/HOT_WOCE/ctd.html

"Howe Sound." [On-line] 31 March 2012. http://www.britishcolumbia.com

"Howe Sound." [On-line] 31 March 2012. http://en.wikipedia.org/wiki/Howe_Sound

Hughes Clarke, J.E., Danforth, B.W. and Valentine, P. (1997). "Areal seabed classification using backscatter angular response at 95 kHz." *Proceedings of the NATO SACLANTCEN Conference CP-45*, High Frequency Acoustics in Shallow Water, p.243-250.

Hughes Clarke, J.E., Iwanowska, K.K., Parrott, R., Duffy, G., Lamplugh, M. and Griffin, J. (2008). "Inter-calibrating multi-source, multi-platform backscatter data sets to

assist in compiling regional sediment type maps: Bay of Fundy." Paper 8-2, *Proceedings of the Canadian Hydrographic Conference and National Surveyors Conference*, Victoria, BC.

Hughes Clarke, J.E. (2011a). "Acoustic backscatter data interpretation." UNB OMG/UNH CCOM 55th Multibeam Sonar Training Course, Lecture Notes No. 20, New Orleans, United States, 3-8 January, 2011.

Hughes Clarke, J.E. (2011b). "Sea bottom imaging with swath sonars." UNB OMG/ UNH CCOM 55th Multibeam Sonar Training Course, Lecture Notes No. 11, New Orleans, United States, 3-8 January, 2011.

Hughes Clarke, J.E. (2011c). Lecture notes of "Imaging and Mapping II" and "Marine Geophysics", Department of Geodesy and Geomatics Engineering, University of New Brunswick, Fredericton, N.B., Canada.

Hughes Clarke et al. (2011). "The Squamish Delta Repetitive Survey Program: A simultaneous investigation of prodeltaic sedimentation and integrated system accuracy." U.S. Hydrographic Conference 2011. http://www.thsoa.org

IHO (2008). "IHO Standards for Hydrographic Surveys – Special Publication No.44." 5th.ed. February 2008. International Hydrographic Organization, Monaco.

Jackson, D.R., D.P. Winebrenner, and A. Ishimaru (1986). "Application of the composite roughness model to high-frequency bottom backscattering." *Journal of the Acoustical Society of America*, 79 (5), pp. 1410-1422.

Kongsberg Maritime, (2006a). "EM302: 30 kHz multibeam echo sounder." Horten, Norway.

Kongsberg Maritime, (2006b). "EM122: 12 kHz multibeam echo sounder." Horten, Norway.

Kongsberg Maritime, (2009a). "Seafloor Information System – Operator Manual." Horten, Norway.

Kongsberg Maritime, (2009b). "EM Series Multibeam echo sounders – Datagram formats - Instruction Manual." Horten, Norway.

Kongsberg Maritime, (2010a). "Reference Manual for SIS with EM710." Horten, Norway.

Kongsberg Maritime, (2010b). "EM 710 Short Spec." Horten, Norway.

Kongsberg Maritime, (2010c). "EM 2040 Short Spec." Horten, Norway.

Kongsberg Maritime, (2010d). "EM 302 Short Spec." Horten, Norway.

Kongsberg Maritime, (2010e). "EM 122 Short Spec." Horten, Norway.

Kongsberg Maritime, (2011a). "EM710: Multibeam echo sounder." Horten, Norway.

Kongsberg Maritime, (2011b). "EM2040: Multibeam echo sounder." Horten, Norway.

"Multibeam Echo Sounders." [On-line] 9 January 2012. http://www.kongsberg.com/

Oliveira Jr., A.M (2007). *Maximizing the Coverage and Utility of Multibeam Backscatter for Seafloor Classification.* M.Sc.E. thesis, Department of Geodesy and Geomatics Engineering, University of New Brunswick, Fredericton, NB, Canada.

Raven, John et al. (2005). "Ocean acidification due to increasing atmospheric carbon dioxide." The Royal Society. [On-line] 28 February 2012. http://royalsociety.org/uploadedFiles/Royal_Society_Content/policy/publications/2005/9634.pdf

Stephens, C., J.I. Antonov, T.P. Boyer, M.E. Conkright, R.A. Locarnini, T.D. O'Brien, and H.E. Garcia, 2002: *World Ocean Atlas 2001, Volume 1: Temperature.* S. Levitus, Ed., NOAA Atlas NESDIS 49, U.S. Government Printing Office, Wash., D.C., 176 pp.

Teng, Y. (2012). *Sector-specific Beam Pattern Compensation for Multi-sector and Multi-swath Multibeam Sonars.* M.Sc.E. thesis, Department of Geodesy and Geomatics Engineering, University of New Brunswick, Fredericton, NB, Canada.

Urick, R.J. (1983). *Principles of Underwater Sound.* 3rd. ed. New York, McGraw-Hill.

CURRICULUM VITAE

Candidate's full name: Rodrigo de Campos Carvalho

Universities attended: University of New Brunswick
Fredericton, NB, Canada
September 2010 – August 2012
M.Sc.E. Geodesy and Geomatics Engineering

Directorate of Hydrography and Navigation
Niterói, RJ, Brazil
January 2003 – December 2003
Extension Hydrography Cat. A (IHO)

Naval Academy
Rio de Janeiro, RJ, Brazil
January 1996 – December 1999
B.Sc.E Electronics

Conference Papers:

Carvalho, R.C, and J.E. Hughes Clarke (2012). "Proper Environmental Reduction for Attenuation in Multi-sector Sonars." *Canadian Hydrographic Conference 2012*, Niagara Falls, ON, Canada, 15-17 May 2012.